CORROSION BEHAVIOR OF GALVANIZED STEEL REINFORCEMENTS IN MSE WALLS IN THE PRESENCE OF SOIL ORGANICS

by

Claudia Aide Soriano Vazquez

B. Sc., Universidad Nacional Autonoma de Mexico, 2009

A THESIS SUBMITTED IN PARTIAL FULFILLMENT OF

THE REQUIREMENTS FOR THE DEGREE OF

MASTER OF APPLIED SCIENCES

in

THE FACULTY OF GRADUATE AND POSTDOCTORAL STUDIES

(Materials Engineering)

THE UNIVERSITY OF BRITISH COLUMBIA

(Vancouver)

November 2014

Abstract

Mechanically Stabilized Earth is a civil infrastructure technology that is widely used in retaining walls. Although the structures are designed for a service life of 75 years, early distress has been reported. Corrosion of the galvanized steel reinforcements has been pointed as one of the major causes that jeopardize their long-term performance.

The corrosion behavior of galvanized steel in the presence of organics found in soil is studied through electrochemical techniques as PDP, EIS and LPR in two types of solutions at various concentrations below 1 wt%. The first type of solutions aims to determine the corrosion behavior in the presence of individual organic reagents: humic acid, dextrose, citric acid and oxalic acid. The second type of solutions is prepared with a system that combines the organic reagents in proportions that simulate the typical composition of organic matter in soil and is called Simulated Soil Organic Matter (SSOM). Subsequently, the surface is analyzed using SEM and EDX.

The data shows that the corrosion effect of organic matter on galvanized steel depends on its composition. The comparison of the highest current density produced by the individual organics, allows ranging them in terms of their aggressiveness on galvanized steel in the following order: citric acid > oxalic acid > humic acid > dextrose. The Simulated Soil Organic Matter was able to corrode the zinc coating and the base steel.

Preface

I was responsible for designing the experimental program presented in this thesis, conducting all electrochemical tests and surface characterization, and analyzing the results. Professor Akram Alfantazi supervised the progress of the research.

Results from this research work were presented in conferences as follow:

1. Soriano, C., Alfantazi, A. (2014). Individual effect of organics in soil on the corrosion of galvanized steel reinforcements in MSE walls. Student Poster at SAMPE[1] Seattle Conference.
2. Soriano, C., Alfantazi, A. (2014). Effect of soil organic matter on the corrosion of galvanized steel reinforcements in MSE walls. Conference paper A20 and presentation at NACE[2] International East Asia Pacific Rim Area Conference & Expo 2014.

[1] Society for the Advancement of Materials and Process Engineering, 1161 Park View Drive, Suite 200 Covina, CA 91724-3759, USA.
[2] National Association of Corrosion Engineers, 15835 Park Ten Place, Houston, Texas, 77084, USA.

Table of Contents

List of Tables

List of Figures

List of Symbols

a	Atomic weight
β_a	Anodic Tafel slope (V/dec)
β_c	Cathodic Tafel slope (V/dec)
c	Proportionality constant
D	Density
E	Measured potential (V)
E_b	Breaking potential (V)
E_{corr}	Corrosion potential (V)
E_{pp}	Primary passive potential (V)
E_{trans}	Transpassive potential
E_{Zn}^{o}	Standard potential of zinc
F	Faraday's constant (≈ 96500 C/mole)
i	Current density ($\mu A/cm^2$)
i_{corr}	Corrosion current density (A/cm^2)
i_{crit}	Critical current density (A/cm^2)
i_{pass}	Passivation current density
M	Molar concentration
Me	Metal
n	Number of equivalents exchanges in oxidation-reduction reactions
η	Overpotential

X	Radical
R	Gas constant (8.314 J/(mole.K))
R_P	Polarization resistance
R_s	Solution resistance
Re	Resistance of the electrolyte inside a pore
Q1	Capacitance of the porous layer
Q2	Capacitance of the double layer

List of Abbreviations

AASHTO	American Association of State Highway and Transportation Officials
ASTM	American Society for Testing and Materials
DOT	State Department of Transportation
EDX	Energy Dispersive X-ray Spectroscopy
EIS	Electrochemical Impedance Spectroscopy
FHWA	Federal Highway Administration
GS	Galvanized steel
HA	Humic acid
LMWOA	Low molecular weight organic acids
LPR	Linear Polarization Resistance
MIC	Microbially-Influenced Corrosion
MSE	Mechanically Stabilized Earth
NBS	National Bureau of Standards
OCP	Open Circuit Potential
PDP	Potentiodynamic Polarization Resistance
SCE	Saturated Calomel Electrode
SEM	Scanning Electron Microscope
SOM	Soil Organic Matter
SHE	Standard Hydrogen Electrode
TAI	Terre Armée Internationale

Glossary

Abutment	A substructure that supports the end of a superstructure and retains some or all of the bridge approach fill
Design life	Period of time specified by the owner during which a structure is intended to remain in service
Gabion	A wire mesh basket that is filled with stone or broken rock or concrete and forms part of a larger unit used for slope stability, erosion control, or related purposes
Ligand	Organic components capable of forming complexes with metals
Retaining wall	Structure designed to hold back masses of earth. Retaining walls include footings and pilings supporting the walls

Acknowledgements

I would like to express my sincere gratitude to my supervisor, Professor Akram Alfantazi, for introducing me to the world of knowledge of Corrosion Engineering but, most importantly, for guiding me and challenging me to improve my research, presentation, and instructional skills. I will take with me this invaluable learning.

Also, I would like to acknowledge the financial support provided by the British Columbia Ministry of Transportation and Infrastructure (BC MOTI), Atlantic Industries Limited (ALI) and Mitacs Accelerate. Special thanks are owed to Kevin Baskin, Ian Sturrock and Daryl Finlayson from the BC MOTI for sharing their experience and providing the questions and tools to apply my knowledge in field applications.

I owe thanks to my fellow students of the Corrosion Group for their continuous help and insight during my research. In particular, I offer my enduring gratitude to V. Padilla, whose answers always helped me to improve my work.

I also want to thank the staff of the Materials Engineering Department for their support during my work: Fiona Webster, Mary Jansepar, Norma, Michelle Tierney, Glenn Smith, and Jacob Kabel.

Finally, I want to express my recognition to my parents, who have supported me in countless ways throughout my lifetime and always encouraged and supported me in my years of education.

To:

My Mom, for her everlasting memory

My Dad, for his unconditional support

Chapter 1: Introduction

1.1 Mechanically Stabilized Earth walls

Mechanically Stabilized Earth (MSE) is a construction technology of retaining walls that was originally developed in France in the 1960s by Terre Armée Internationale[3]. The technology was introduced in North America in the early 1970s with the support of the Federal Highway Administration (FHWA) of the US (RECo, 2011). Although the main use of MSE was for retaining walls, the applicability of the technology was extended to other heavily-loaded structures such as highway bridges, railway and industrial structures (Anderson & Brabant, 2010). At the beginning, only a few dozen MSE abutments were built each year. However, given the advantages that MSE walls offered in front of the traditional cast-in place concrete structures, such as more rapid construction, better aesthetics and cost effectiveness (Holtz *et al*., 1995), after 1990 the construction rate increased to approximately 600 abutments per year, i.e. 300 bridges (Anderson *et al.*, 2012).

MSE walls have three main structural components (Chen, 2000): (i) the level pad, (ii) the vertical face element, and (iii) the soil reinforcement. The third component combines the tensile strength of horizontal reinforcements with the compressive and shear strengths of the backfill soil (Anderson *et al*., 2012). The reinforcements can be of two types depending on the material they

[3] Terre Armée Internationale (TAI) developed the Reinforced Earth® technology, which was the original denomination, but since it was a proprietary name of TAI, the generic name MSE was adopted. Later TAI changed its name to Reinforced Earth Company (RECo).

are made of: geosynthetic, called extensible; or metallic, called inextensible. In both cases, to build the MSE wall, the reinforcements are placed at specific heights in between layers of backfill soil according to the customary design. The inextensible reinforcements are made of hot-dip galvanized steel, which may be in the form of welded wire mesh or ribbed strips.

Figure 1-1: Components of an MSE wall: 1) Level pad; 2) Vertical face element; 3) Backfill soil; 4) Reinforcements

The components of an MSE wall can be observed in Figure 1-1 in two photographs that were taken at a site under construction located on Sneena Road, in West Kelowna, B.C. The picture on the left points the level pad and the concrete slabs that form the facing wall with labels 1 and 2, respectively, which will be the only components visible from outside upon completion of the abutment. The picture on the right illustrates how the galvanized steel mats (4) are placed on alternated layers of backfill soil (3) and anchored to the facing wall. These two components will be inaccessible once the construction is completed.

In addition, Figure 1-2 shows a diagram of the cross-section of an MSE wall, where it can be observed how the components will be integrated once the wall is completed. The vertical face element will appear as a wall that can be seen from the road. Behind the layers of backfill soil and galvanized steel reinforcements will lay horizontally, and the reinforcements will be anchored to the concrete slabs.

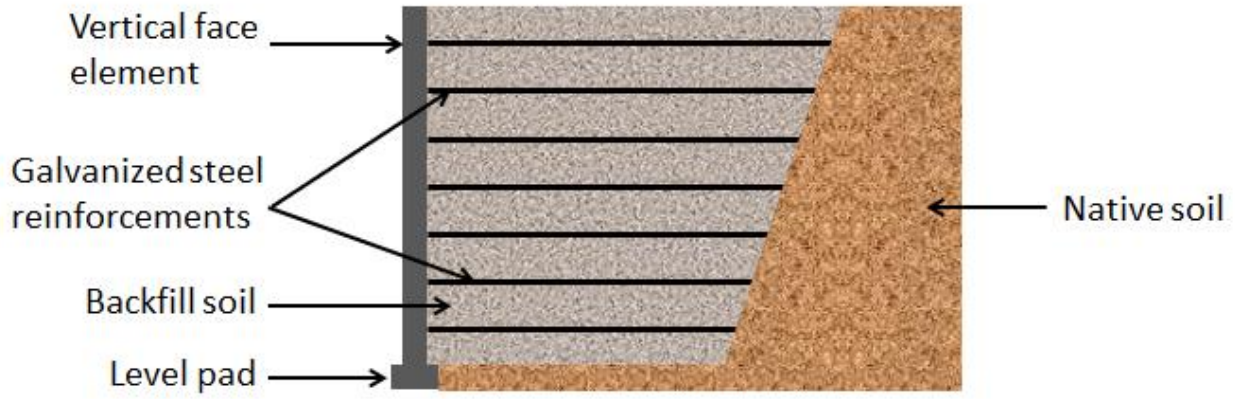

Figure 1-2: Cross-sectional diagram of a MSE wall

Furthermore, it is important to highlight that the soil used as backfill soil does not correspond to the foundation soil retrieved at the site of construction. Instead, the backfill soil is extracted from specific pits where it is known that the soil will meet the technical specifications required. Another remark about the materials used in this technology is that the steel in the reinforcements is of structural type. This implies that the steel will exhibit higher yield strength and tensile strength than carbon steel designed for other type of applications. The ASTM standards A36 and A709 provide the specifications for structural steel. The chemical composition will depend on the grade of the steel. For example, a structural steel of grade 36 will have a yield strength of 250 MPa, and for a rebar thickness over ¾ and below 1½ in (included), the maximum elemental composition is 0.27% C, 0.90% Mn, 0.04% P, 0.05% S, 0.40% Si, and 0.20% Cu. However, the

composition varies according to the grade, and the required grade for each wall will vary case by case according to the general design of the structure.

1.2 MSE walls in British Columbia

It is estimated that in British Columbia alone, there are over 1100 MSE walls (Padilla, 2013). This is an important inventory of infrastructure assets that the British Columbia Ministry of Transportation and Infrastructure (BC-MOTI) is interested in managing to ensure that they perform as expected (CSA, 2006).

The several factors that influence the long term performance of MSE walls, closely associated with the metal loss of the galvanized steel rebars due to corrosion, have been considered in the design specifications that provide the electrochemical characteristics that should be met by the backfill soil, as will be described in chapter 2. However, those specifications were developed based on environmental conditions that are not necessarily the same as the ones in British Columbia. For this reason, there is an interest in understanding how the variables that are specific to this province may affect the corrosion behavior of the galvanized steel reinforcements. For instance, the increase of sulfate and chloride concentrations in the backfill soil due to the use of de-icing salts on the roads during the winter season has been addressed in a collaboration work between BC-MOTI and UBC (Padilla & Alfantazi, 2013; Padilla *et al.*, 2013a). In 2012, several sites were visited by a PhD student from the University of British Columbia and personnel from the BC-MOTI to evaluate the current state of MSE walls.

Superficial soil samples were taken from 34 sites and sent to the laboratory to determine if the backfill soil characteristics were in compliance with the specifications after variable years in service. As a result, a numerical model was developed whose key innovating feature was the possibility to provide variable values of the electrochemical parameters of the soil as input to estimate the remaining service life of the reinforcements. Although various electrochemical parameters were incorporated, the organic content was not part of them. Therefore, a study that focused on this component was still required to complete the model (Padilla *et al.*, 2013b).

From the information gathered on the field work performed in 2012, the soil analysis revealed that only in 8 sites, the organic content was within the established limit of 1% whereas, in the rest of the sites, the organic content was 2.22 ± 1.24%. Given the results, the immediate question was: Does the higher organic content in the backfill soil have an impact on the corrosion of the galvanized steel reinforcements? By visual inspection of the visited walls, it became evident that the low percentages of organic content in the backfill soil were sufficient to provide nutrients for vegetation in a number of sites. The most severe case is shown in Figure 1-3, where a growing tree is already damaging the concrete slabs on the facing wall. Similarly, in another wall (Figure 1-4), the organic content was enough to promote plant growth at the same time that the red stains on the concrete revealed that corrosion had reached the base steel of the reinforcements.

Figure 1-3: Growing tree on an MSE wall in B.C.

Figure 1-4: Evidence of corrosion of steel and plant growth

This research aims to determine the corrosion behavior of galvanized steel due, exclusively, to the presence of soil organics typically and to establish the path to find an equation that relates the content of organic matter with the polarization resistance that can be used to incorporate a new variable to the numerical model.

Chapter 2: Literature review

2.1 Corrosion

Corrosion is the degradation of a material due to its interaction with the environment. Four fundamental elements are required for corrosion to take place: (i) an anode, (ii) a cathode, (iii) an electronic path, and (iv) an ionic path. In the case of a civil infrastructure reinforced with steel, the reinforcements themselves provide the electronic path, while the medium into which they are embedded, either concrete or soil, provide the ionic path. The anode and the cathode are different regions of the steel reinforcements that act as one electrode or the other due to differences in the surrounding electrolyte that induce the formation of corrosion cells. At the anode, the metal dissolves and ions are released and the surface is negatively charged. At the cathode, ions are reduced and deposited on the surface. (Asgari *et al.*, 2009)

2.1.1 Corrosion protection of steel by galvanizing

Galvanizing is the process through which steel is coated with zinc. During hot-dip galvanizing, zinc-iron alloy layers are formed with different compositions depending on their proximity to the base metal, with the highest content of pure zinc found on the surface. The zinc coating improves the corrosion resistance of the steel reinforcements in two ways: (i) acting as physical barrier and (ii) providing galvanic protection (Asgari *et al.*, 2009). The physical barrier isolates the steel from the environment, first by the layer of zinc and, second, by the zinc corrosion products layer.

The galvanic protection means that even if the steel substrate gets exposed, the zinc layer will corrode preferentially (Yadav *et al.*, 2004a).

2.1.2 Corrosion process of galvanized steel

The corrosion of galvanized steel can be described as a three-stage process (El-Mahdy *et al.*, 2000; Padilla *et al.*, 2013b; Yadav *et al.*, 2004b). In the first stage, solid zinc corrodes near its standard potential (E_{Zn}^{o}) releasing divalent ions, according to Eq. 2-1.

$$Zn \rightarrow Zn^{2+} + 2e^{-} \quad \textbf{Eq. 2-1}$$

The zinc corrosion products, composed mainly of zinc oxide (ZnO), have a very low solubility and precipitate forming a semi-compact, adherent, porous layer that has a characteristic white color (Thebault *et al.*, 2008; Zhang, 1996). The galvanic protection that zinc provides to steel occurs in this stage within a limited distance from the coating (Thebault et al., 2008; Thebault *et al.*, 2011).

In the second stage, the layer of corrosion products grows until zinc is depleted and a thick, porous, soluble and non-protective layer of corrosion products is formed. The main components of this layer are $Zn(OH)_2$ and $ZnCl_2 \cdot 4Zn(OH)_2$. It is in this stage, that the corrosion front reaches the Zn-Fe alloy layer and the galvanized steel experiences a shift of its corrosion potential to more noble values. In the third stage, corrosion of steel initiates and iron ions are released, according to Eq. 2-2. The corrosion products from steel become visible as red rust.

$$Fe \rightarrow Fe^{2+} + 2e^{-} \quad \textbf{Eq. 2-2}$$

2.1.3 Factors that influence the corrosion of galvanized steel in soil

Soil is the naturally-occurring, unconsolidated, mineral or organic material at the earth's surface (Soil Classification Working Group, 1998). Seen as a corrosive environment, soil is highly inhomogeneous and exhibits a wider range of chemical and physical properties compared to atmospheric and aquatic environments, due to the large number of chemical compounds that can be found in soils. Various properties have a synergistic influence on the corrosion rates of metals in soil, including pH, soil resistivity, moisture content, aeration, temperature, and soluble salt concentration.

For instance, the range of pH values that can be found in soils is wide, ranging from 2.6 to 10.2 (Soil Survey Division Staff, 1993). The soil resistivity itself depends on other factors such as particle size, porosity, and temperature. The size of the particles determines the specific surface area (i.e. total surface area per unit of mass). Soils with smaller particles have bigger specific surface areas and therefore exhibit higher conductivity at the surface than soils with coarse particles of the same mineralogy. For this reason, the fine fraction in backfill soil is limited to only 15% passing the 200 sieve. Porosity also affects resistivity because the distribution and geometry of the voids influences the proportion of air and water than can be retained in the soil. Finally, the day-night and seasonal temperature cycles may also have an effect con corrosion because an increase in temperature decreases the viscosity of water and increases the ion agitation resulting in a decrease of resistivity (Andrade *et al.,* 2002). Therefore, comparison of soil resistivity measurements requires the value expressed at the standardized temperature of 25°C (Campbell *et al.,* 1948; Samouelian *et al.,* 2005). The American Association of State

Highway and Transportation Officials (AASHTO) of the US classifies the types of soil used in the construction of highways in different levels of corrosion aggressiveness in terms of their resistivity as follows:

Table 2-1: AASHTO classification of aggressiveness of soils in terms of resistivity

Aggressiveness of the soil	**Resistivity ($\Omega \cdot cm$)**
Very corrosive	R < 700
Corrosive	700 < R < 2,000
Moderately corrosive	2000 < R < 5000
Mildly corrosive	5000 < R < 10000
Non-corrosive	R > 10000

The moisture content also plays an important role in the corrosion of metals because higher moisture contents facilitate the transport of dissolved electrolytes in soil, whereas higher aeration levels increase the availability of oxygen that can participate in reduction reactions. The color of the soil provides an indication of the degree of aeration of the soil. Red, yellow and brown soils are typical of aerated soils, due to the presence of oxidized forms of iron; whereas gray soils are characteristic of poorly-aerated soils, where reduced forms of iron are predominant (Zhang, 1996).

The electrode potential of zinc and steel has been measured in 12 different soils. The value for zinc varied from -0.8 V to -0.97 V, whereas for steel, the values ranged from -0.54 V to -0.66 V versus the Saturated Calomel Electrode (SCE) (Romanoff, 1957).

2.1.4 Deterioration of MSE walls due to corrosion

The design life of MSE walls is 75 years for general applications and 100 years in bridges (AASHTO, 2002; AASHTO, 2010; CSA, 2006). At forty years from the introduction of the MSE technology, information gathered from numerous state departments of transportation (DOTs), 39 from US and 5 from Canada, revealed that the DOTs consider corrosion of the reinforcements as one of the three major factors that compromise the long-term performance of MSE walls, along with drainage and global stability (Gerber, 2012). The concern about corrosion is that it reduces the cross sectional area of the reinforcements and, as a consequence, their tensile strength is also reduced, jeopardizing the internal stability of the structure.

Naturally, several efforts have been done to understand the variables involved in the corrosion of galvanized steel reinforcements in soil in order to predict accurately the loss of material. When the MSE technology was developed, the first predictions of the metal loss of the reinforcements were based on data from the US National Bureau of Standards (NBS) that conducted corrosion investigations over a period of 45 years, motivated by the economic losses in the pipeline industry (Romanoff, 1957). Subsequently, more specific research was conducted on the corrosion of galvanized steel reinforcements in MSE applications in periods that ranged from 8 to 10 years (Darbin *et al.*, 1986). As a result, it was recommended to limit the content of chlorides in the backfill soil to 100 ppm and that of sulfates to 200 ppm (LCPC -SETRA, 1979). These recommendations were incorporated in the electrochemical parameters of the backfill soil given in the AASHTO specifications (AASHTO, 2002; AASHTO, 2010) and are shown in Table 2-2.

Table 2-2: Electrochemical characteristics of backfill soil

Characteristic	Accepted value
pH	5 - 10
Resistivity	R ≥ 3000 $\Omega \cdot cm$
Chloride concentration	≤ 100 ppm
Sulfate concentration	≤ 200 ppm
Organic content	≤ 1%

AASHTO developed its own model of metal loss (Table 2-3), according to which, provided the backfill soil specifications are met, it is estimated that the layer of zinc will corrode at a rate of 15 μm/year during the first two years after construction and then corrosion will continue at a lower rate of 4 μm/year until depletion of zinc, which is expected to occur after 16 years. After that, steel will corrode at a rate of 12 μm/year and lose thickness during 59 years to reach a design life of 75 years in service. Using these predictions, sacrificial thickness of steel can be calculated and added to the dimensions of the rebars to guarantee that the tensile resistance of the reinforcements will be sufficient through the design life (Gerber & Billings, 2010).

Table 2-3: AASHTO model of metal loss

Corroding material	Period of time	Rate of loss of material
Zinc	First 2 years	15 μm/year
Zinc	From year 2 until depletion of zinc (approx. 16 years)	4 μm/year
Steel	From initiation of corrosion of steel (approx. year 16) until end of service life (year 75)	12 μm/year

Even though, the electrochemical parameters of the backfill soil and the metal loss model are based on extensive research, there is still a disagreement on the accuracy of the predictions of the

model. On one hand, (Gladstone *et al.*, 2006; Gladstone *et al.*, 2008) consider that the AASHTO model is too conservative because they claim that the zinc coating can protect the steel rebar for as long as 30 years, i.e. 14 more years than predicted by AASHTO. On the other hand, some cases have been reported where high levels of corrosion of the reinforcements were accidentally discovered (Thornley & Siddharthan, 2010; Thornley *et al.*, 2010). The dissent may lay on the general assumption of the AASHTO model that the electrochemical conditions of the soil will remain constant through the entire service life of the structures or in the fact that some MSE walls were built according to early specifications that are no longer accepted by AASHTO.

2.1.5 The organic content in backfill soil

One specific electrochemical parameter of the backfill soil to which very little attention has been paid is the organic content in soil. It has generally been assumed that the only mechanism through which it affects the corrosion of galvanized steel is by providing food to bacteria that participate in the Microbially-Influenced Corrosion (MIC) process (Elias *et al.*, 1990; Uhlig & Revie, 2000). But the role of organics, themselves, on the corrosion of galvanized steel in soil has been neglected.

2.2 Soil organic matter

An extensive research of the type of organics that could be found in soil was essential in order to select the reagents that would be used in the electrochemical experiments to study the corrosion

behavior of galvanized steel in the presence of typical soil organics. This section summarizes the investigation.

2.2.1 Definition and composition

The presence of organics is what distinguishes soil from decomposed rock. Soil Organic Matter (SOM) is the whole of organic materials in soil, which includes both, living and non-living organisms. Figure 2-1 depicts the typical composition of organic matter in soils (Bohn *et al.*, 2001; Schnitzer & Khan, 1978; Stevenson, 1994).

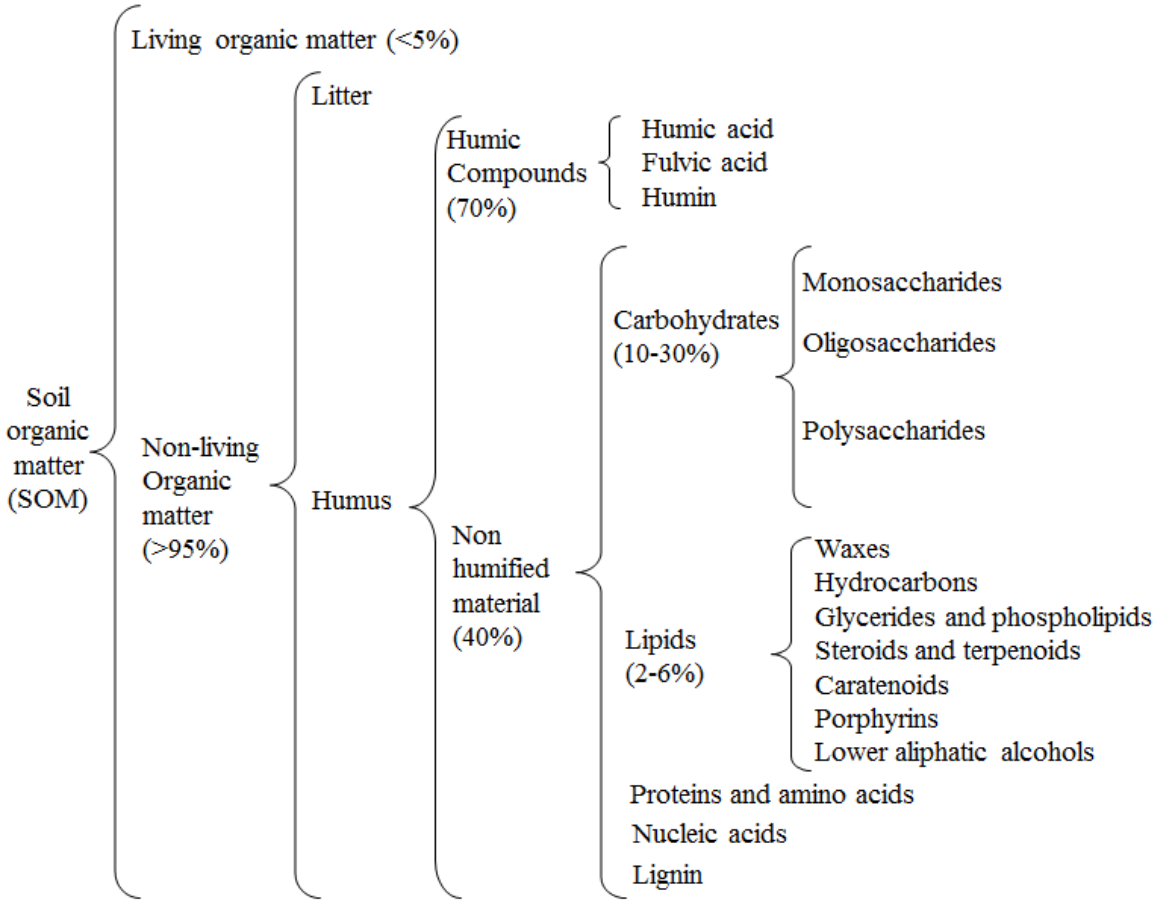

Figure 2-1: Composition of organic matter in soil

The living fraction represents less than 5% of the total SOM, while the non-living organic matter accounts for 95% or more of the total organic content in soils and is more important for the soil chemistry (Bohn *et al.*, 2001). The living organic matter includes bacteria, fungi, algae, plant roots, soil fauna and un-decomposed debris derived from plants or animals. The non-living organic matter is an accumulation of dead plant and animal residues at different stages of decomposition. It can be divided into litter and humus. The former is partially-decayed products that still conserve a visible anatomy and are susceptible to further decomposition; whereas the latter is completely decomposed material that will not break down further and may remain as it is for centuries.

Humus is classified into humic compounds and non-humified material. Humic compounds are those that no longer exhibit specific chemical characteristics. They represent the bulk of humus, accounting for up to 70% of it and can be classified into humic acid, fulvic acid and humin according to their solubility characteristics: humic acid is the fraction soluble in alkali (pH > 2); fulvic acid is soluble in both alkali and acid solution; and humin is the insoluble fraction (Yasakau *et al.*, 2008). Both, humic acid and humin, are considered passive humus because they are stable complexes that will not decompose further, whereas fulvic acid is the active fraction.

The non-humified material is the remaining fraction of humus that still exhibits recognizable physical and chemical characteristics, e.g. melting point and elemental composition. Its major components are carbohydrates and lipids that represent, respectively, from 10 to 30% and from 2 to 6% of humus (Huang *et al.*, 2009; Schnitzer & Khan, 1978). The rest of humus is a combination of various types of organics that are present in minute amounts such as organic acids, fatty acids, waxes, proteins, nucleic acids, and lignin.

2.2.2 Characteristics of humic substances

Humic compounds are acidic, dark-colored amorphous polymers that are responsible for the yellow to brown color of soil (Schulten & Schnitzer, 1993). These macromolecules have reached a point of stability through a process called humification where partially-decomposed plant and animal residues are synthetized by microbial activity and chemical reactions. The molecular weights of these structures vary from a few hundreds to 10^5 Daltons[4] (Yasakau *et al.*, 2008).

Humic compounds are composed of carbon and oxygen as major elements and smaller percentages of hydrogen, nitrogen, and sulfur. In humic acids, the proportions of carbon and oxygen are about 55% and 33%, respectively; whereas for fulvic acids, they are approximately 41% and 48%. Then nitrogen and hydrogen represent about 2-5% each, followed by less than 2% of sulfur.

Humic substances control various physical and chemical properties of soil. For example, they facilitate the warming of the soil and their hydrophilic nature is responsible for their capability to retain up to 20 times their weight in water. Also, they exhibit a buffer capacity. It has been reported that the pH range in which they act as a buffer goes from 5.5 to 8 (Pertusatti & Prado, 2007). Furthermore, humic substances contain a broad range of functional groups that allow them to participate as electron donors or acceptors. In particular, their high content of acidic functional groups facilitates metal binding and transport. The number of stable complexes that

[4] Dalton is the unified atomic mass unit that is usually used in molecular chemistry and corresponds to one twelfth of the mass of an unbound atom of carbon 12. It is approximately equal to 1.66×10^{-27} kg.

they can form with metal ions is almost infinite (Livens, 1991), but the interactions of humic substances with metal ions can be mainly of three types: oxidation-reduction reactions, surface adsorption, and chelation.

2.2.2.1 Oxidation-reduction reactions

The oxygen-containing functional groups, which retain about 80% of the total oxygen in humic compounds, are of particular interest to this research for their role in oxidation-reduction reactions (Struyk & Sposito, 2001). The functional groups of this type are hydroxyl (-OH), carbonyl ($-C=O$) and carboxyl (-COOH). They are shown in Figure 2-2, where the X represents a radical that may be any atom or group of atoms. The hydroxyl group (Figure 2-2a) is formed by an oxygen atom bonded to a hydrogen atom. The carbonyl group (Figure 2-2b) consists of a carbon atom double bonded to an oxygen atom. The carboxyl group (Figure 2-2c) is formed when the hydroxyl group is bonded to the carbon of the carbonyl group. This carboxyl group is the functional group that characterizes the carboxylic acids, also named organic acids.

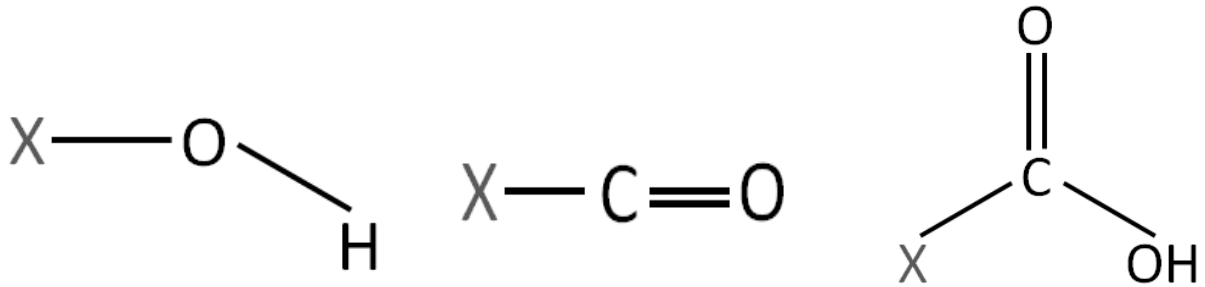

a) Hydroxyl group b) Carbonyl group c) Carboxyl group

Figure 2-2: Oxygen containing functional groups in humic acid: a) hydroxyl, b) carbonyl, c) carboxyl

The hydroxyl and carboxyl group provide an aprotic character to organics i.e. ability to readily provide protons because they self-dissociate as described in equation 2-3 where X represents any radical (Heitz, 1974).

$$HX + HX \leftrightarrow HXH^+ + X^- \qquad \textbf{Eq. 2-3}$$

The negatively-charged sites provide humic substances the ability to form complexes with metal cations.

The role of the carboxyl group in the corrosion process of metals is explained using formic acid (HCOOH) for simplification purposes because it only contains one carboxyl group (El-Maksoud, 2008). At the cathode, the reactions are given by Eq. 2-4 and Eq. 2-5, where Me is any metal:

$$Me + HCOOH + e^- \rightarrow MeH_{ads} + HCOO^- \qquad \textbf{Eq. 2-4}$$

$$MeH_{ads} + MeH_{ads} \rightarrow H_2 + 2Me \qquad \textbf{Eq. 2-5}$$

As a prerequisite for the anodic dissolution, the formate ions ($HCOO^-$) need to be adsorbed on the surface. The reactions at the anode are given for the case of the corrosion of mild steel:

$$Fe + HCOO^- \rightarrow [Fe(HCOO)]_{ads} + e^- \qquad \textbf{Eq. 2-6}$$

$$[Fe(HCOO)]_{ads} \rightarrow [Fe(HCOO)]^+ + e^- \qquad \textbf{Eq. 2-7}$$

$$[Fe(HCOO)]^+ + H^+ \leftrightarrow Fe^{2+} + HCOOH \qquad \textbf{Eq. 2-8}$$

2.2.2.2 Surface adsorption

It is believed that adsorption of humic substances on metal surfaces is due to the interaction of the carboxylic functional group with hydroxylated oxide sites (Korshin *et al.*, 1997). Additionally, organic compounds containing oxygen, sulfur, and nitrogen are well known as corrosion inhibitors of zinc because they can be adsorbed on the surface and block the active sites (El-Sherbini *et al.*, 2005). Since these elements also are also components of humic substances, they may provide them adsorption capabilities.

2.2.2.3 Chelation

Chelation is the process of metal-organic complexation. The organic components capable of forming complexes with metals are referred to as ligands. Chelation occurs when two or more coordinate positions of a metal ion are occupied by groups of a single ligand and a ring structure is formed. If the chelating agent forms two bonds with the metal ion it is said to be bidentate. Similarly, terdentate, tetradentate, and pentadentate complexes are possible.

It has been determined that over a wide range of pH values, fulvic acids form complexes with Zn, according to the reaction described in equation 2-9, in which *a* moles of a cation Me^{x+} react with *b* moles of a ligand L^{y}.

$$aMe^{x+} + bL^{y-} \leftrightarrow Me_aL_b{}^{ax-by} \qquad \textbf{Eq. 2-9}$$

The stability constant is given by:

$$K = \frac{(Me_aL_b)^{ax-by}}{(Me^{x+})^a(L^{y-})^b} \qquad \textbf{Eq. 2-10}$$

The value of the stability constant of zinc fulvates increases with increasing the pH values. Reported values are (log K) = 1.7 at pH 3.5 and 2.3 at pH 5, but also (log K) = 2.3 at pH 3 and 3.6 at pH 5 (Stevenson, 1994). Some authors proposed that the stability of the metal-organic complexes with humic acids is as follows: $Pb^{2+} > Cu^{2+} > Ni^{2+} > Co^{2+} > Zn^{2+} > Cd^{2+} > Fe^{2+} > Mn^{2+} > Mg^{2+}$. Others determined that the affinity of humic substances with metal ions decreases in this order: $Fe^{3+} > Al^{3+} > Cu^{2+} > Ni^{2+} > Pb^{2+} > Co^{2+} > Zn^{2+} > Fe^{2+} > Mn^{2+} > Ca^{2+} > Mg^{2+}$ (Dick & Rodrigues, 2006).

2.2.3 Carbohydrates in soil

Carbohydrates are the second most significant component of SOM, accounting for up to 30% of it. The main source of soil carbohydrates is plant residues, given that they represent between 50 and 70% of the dry weight of plants. Carbohydrates are sugars with the general formula $C_n(H_2O)_m$. They are classified into monosaccharides, oligosaccharides, and polysaccharides. Monosaccharides are water-soluble, simple sugars that cannot be decomposed into smaller molecules. The most common monosaccharides in soil are fructose $(C_6H_{12}O_6)$ and glucose $(C_6H_{12}O_6)$, which are classified as hexoses because they contain 6 carbon atoms. Oligosaccharides are compound sugars that can yield from 2 to 6 molecules of monosaccharides when hydrolysed. Polysaccharides are water-insoluble, complex carbohydrates. Some examples of polysaccharides are hemicellulose, cellulose, and plant starches.

Carbohydrates in soil may occur in three forms: free sugars, polysaccharides, and polymeric molecules. The free sugars that have been identified in a variety of mineral and organic soils are glucose, galactose, mannose, fructose, arabinose, xylose, fucose, and ribose (McLaren & Peterson, 1967). Polysaccharides are the most common form of carbohydrates found in soil. They are insoluble in water and have molecular weights from 200,000 to 2 million. They may be decomposed into simpler sugars by microbial attack. Finally, the polymeric molecules in soil are strongly attached to clay colloids and are difficult to isolate.

2.2.4 Characteristics of organic acids

The most corrosive organic species are organic acids. They are ubiquitous in soil in concentrations that range from 10^{-2} to 5mM (Schwab *et al.,* 2008; Stevenson, 1994). More than a dozen high molecular weight organic acids have been isolated from soil, but low molecular weight organic acids (LMWOA) are also normal constituents of mineral soils. LMWOA are exuded by plant roots, produced by microorganisms, or decomposed from plant and animal residues. They may also be incorporated into the soil by precipitations, which carry from 0.6 μM of them in remote areas to 80 μM in urban areas (Graedel *et al.*, 1986). LMWOA are capable of forming complexes with metals due to their hydroxyl derivatives (Renella *et al.*, 2004). The most common types of organic acids are carboxylic acids, which are classified according to the number of carboxyl groups that they contain into carboxylic, dicarboxylic, tricarboxylic, etc.

The feasibility of the complexation between organic acids and metal ions has widely been studied (Zaleckas *et al.*, 2013). Although a dependence between the corrosion rates of SS41 steel and the concentration of formic and acetic acid has been demonstrated (Sekine & Senoo, 1984), it has been determined that they do not form as stable complexes with metals as citric and oxalic acids do (Kim *et al.*, 2013). The capability of citric, acetic and oxalic acid to complex with Zn ions in soil was compared and it was found that citric acid exhibits the best binding capacity (Zaleckas *et al.*, 2013).

Chapter 3: Objectives

The goal of this research is to quantify the corrosion behavior of hot-dip galvanized steel in the presence of selected organic reagents that represent the major organic components of soil.

3.1 Key technical objectives

1. Determine the electrochemical corrosion behavior of galvanized steel in solutions with additions of 0.01wt%, 0.02wt%, 0.1wt%, 0.25wt%, 0.5wt%, and 1.0wt% of three organic acids:
    a. Humic acid
    b. Oxalic acid
    c. Citric acid
2. Determine the electrochemical corrosion behavior of galvanized steel in solutions with additions of 0.1wt%, 0.25wt%, 0.5wt%, and 1.0wt% of glucose.
3. Characterize the surface of the galvanized steel after accelerated corrosion tests in order to determine the morphology of the corrosion products and the extent of corrosion due to each organic.
4. Determine the corrosion behavior of galvanized steel in solutions with additions of 0.1wt%, 0.25wt%, 0.5wt%, 0.75wt%, and 1.0wt% of simulated soil organics that combine the four reagents following typical compositions in soil using various electrochemical methods.

5. Characterize the surface of the galvanized steel after accelerated corrosion tests in simulated soil organic solutions.

Chapter 4: Approach and methodology

The purpose of conducting these experiments was to quantify the corrosion behavior of galvanized steel in the presence of organic reagents that represent the main components of SOM. In this chapter, the selection of materials, their preparation, and the electrochemical and surface characterization methods are discussed.

4.1 Materials selection

4.1.1 Galvanized steel

The electrochemical tests were performed using galvanized steel samples with an exposed area of 1 cm^2. The samples were cut from an as-received, low carbon, cold-rolled galvanized steel sheet that was fabricated according to ASTM A653 standard, with a bath composition for the hot-dip coating of 99.96wt% zinc and 0.04wt% Al, without a chromate finish. The sheet thickness was 0.03cm and the coating thickness approximately 20 μm ± 2 μm. All samples were cleaned with ethyl alcohol and dried prior to immersion in the test solution.

4.1.2 Organic reagents

In literature review, previous corrosion experiments of the behavior of metals due to soil organics were found to be non-existent. Therefore, the selection of the organic reagents herein described is proposed as synthetic soil organics for electrochemical studies. Four organic

reagents were chosen to prepare the solutions for the electrochemical tests. The reasoning behind the selection was based on the information gathered in the literature review regarding the composition of soil organics that is applicable to all types of soils. Two of the organic reagents were chosen to represent the two major components of SOM: humic acid to represent the humic substances, and dextrose (D-glucose) to represent the carbohydrates. The other two organic reagents were oxalic acid ($C_2H_2O_4$) and citric acid ($C_6H_8O_7$). They were chosen to account for the effect of the most corrosive organic species that are ubiquitous in minute amounts (less than 5 mM): organic acids.

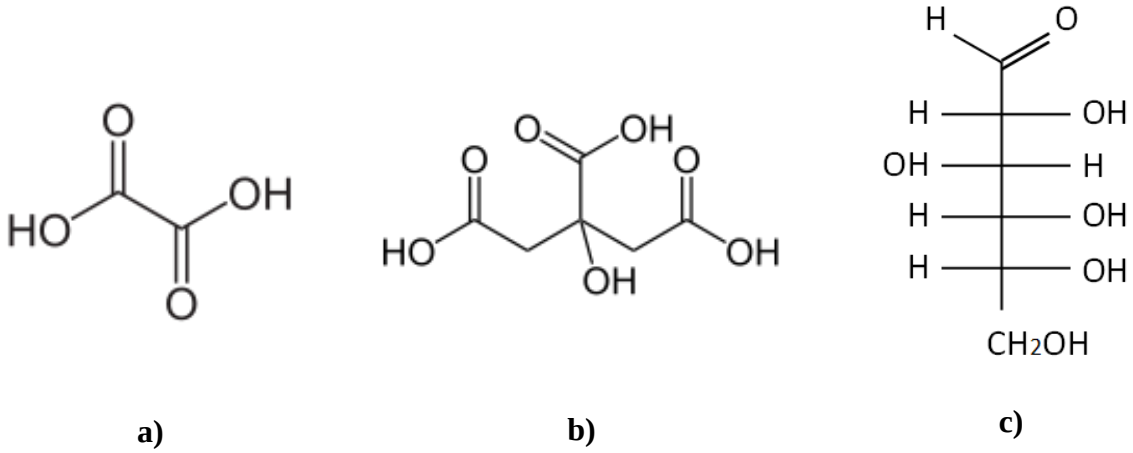

a) **b)** **c)**

Figure 4-1: Model of selected organics: a) oxalic acid, b) citric acid, and c) dextrose in open-chain form

Oxalic acid (Figure 4-1a) is a dicarboxylic acid (it contains two carboxylic groups), citric acid (Figure 4-1b) is a tricarboxylic acid (it contains three carboxylic groups), and dextrose (Figure 4-1c) contains five hydroxyl groups.

4.2 Preparation of solutions

Two types of solutions were used. In the first type, solutions of each individual organic reagent were prepared separately. In the second type, the four organics were combined in solution in proportions that simulated the typical composition of soil organic matter. Such combination is referred to as Simulated Soil Organic Matter (SSOM) in this thesis.

4.2.1 Solutions with individual organics

Commercial humic acid sodium salt was purchased from Acros Organics. The other three reagents were ACS certified and supplied by Fisher Scientific as Dextrose Anhydrous, Citric Acid Anhydrous and Oxalic Acid Dihydrate. For each organic reagent, six solutions were prepared at the concentrations presented in Table 4-1.

Table 4-1: Concentrations of solutions prepared for each organic

Organic	Concentration (wt%)					
Humic acid	0.01	0.05	0.10	0.25	0.50	1.00
Citri acid	0.01	0.02	0.10	0.25	0.50	1.00
Oxalic acid	0.01	0.07	0.10	0.25	0.50	1.00
Glucose			0.10	0.25	0.50	1.00

4.2.2 Simulated soil organic solutions

The second set of solutions was prepared with SSOM at four concentrations: 0.25 wt%, 0.50 wt%, 0.75 wt%, and 0.91 wt%. For each concentration, the percentage that was added to each individual organic reagent, mimicking the typical composition of SOM, is detailed in Table 4-2.

Table 4-2: Composition of simulated soil organics by weight percent in 1L solution

Typical SOM composition	70% Humic substances	30% Carbohydrates	≤ 5 mM Organic acids	

Solution No.	Total concentration of simulated soil organics	Individual concentration of organics (wt%)			
		Humic acid	Dextrose	Citric acid	Oxalic acid
1	0.25 wt%	0.147	0.063	0.02	0.02
2	0.50 wt%	0.311	0.133	0.03	0.025
3	0.75 wt%	0.483	0.207	0.03	0.03
4	0.91 wt%	0.6	0.255	0.03	0.03

4.3 Electrochemical tests

To study the corrosion behavior of galvanized steel in the presence of soil organics, three accelerated corrosion tests were selected: Potentiodynamic Polarization Resistance (PDP), Linear Polarization Resistance (LPR), and Electrochemical Impedance Spectroscopy (EIS). To ensure that the samples had reached a stable state, the Open Circuit Potential (OCP) was measured prior to each test. To ensure repeatability of the results, each electrochemical test was performed three times for each solution described in section 4.3. For each run, a fresh solution and a fresh galvanized steel sample were used. The parameters applied for each electrochemical test are described here.

4.3.1 Open Circuit Potential

The Open Circuit Potential (OCP) was monitored through time. In most solutions, a stable value was obtained within 1 hour of immersion, but for some solutions it was necessary to wait longer before a steady state potential was reached.

4.3.2 Potentiodynamic Polarization Resistance

Potentiodynamic Polarization Resistance (PDP) tests were performed in all solutions from -0.250 V Ag/AgCl to +1.00 V Ag/AgCl with respect to the OCP, with a scan rate of 0.166 mV/s. The PDP curves presented in this thesis were selected from the three runs performed to simplify the visualization. With this test it was possible to obtain the corrosion potential (E_{corr}) and the corrosion current densities (i_{corr}), as well as to identify passive behaviors. The i_{corr} values were obtained by the intersection of the Tafel slopes from the anodic (β_a) and cathodic (β_b) branches, where the conditions of the Tafel behavior was met. In the cases where the Tafel criteria were not met, a least square regression analysis was used to fit the Butler-Volmer equation (Eq. 4-1) to the measured values on the cathodic and anodic branches at 100 mV from the E_{corr}. The squared error between the measurements and the calculated values was minimized by modifying the Tafel slopes and the i_{corr} (V. Padilla *et al.*, 2013a).

$$i = i_{corr}\left(\exp\left(\frac{\alpha_a nF\eta}{RT}\right) - \exp\left(-\frac{\alpha_c nF\eta}{RT}\right)\right) \quad \textbf{Eq. 4-1: Butler-Volmer equation}$$

The method used to determine i_{corr} values from PDP curves is always a potential source of error.

An example of the repeatability of the three PDP test performed on galvanized steel in 1wt% humic acid solution is presented in Figure 4-2. A result is said to be repeatable when the shape of the curve and the Ecorr values are similar between the different runs of a test in identic experimental conditions.

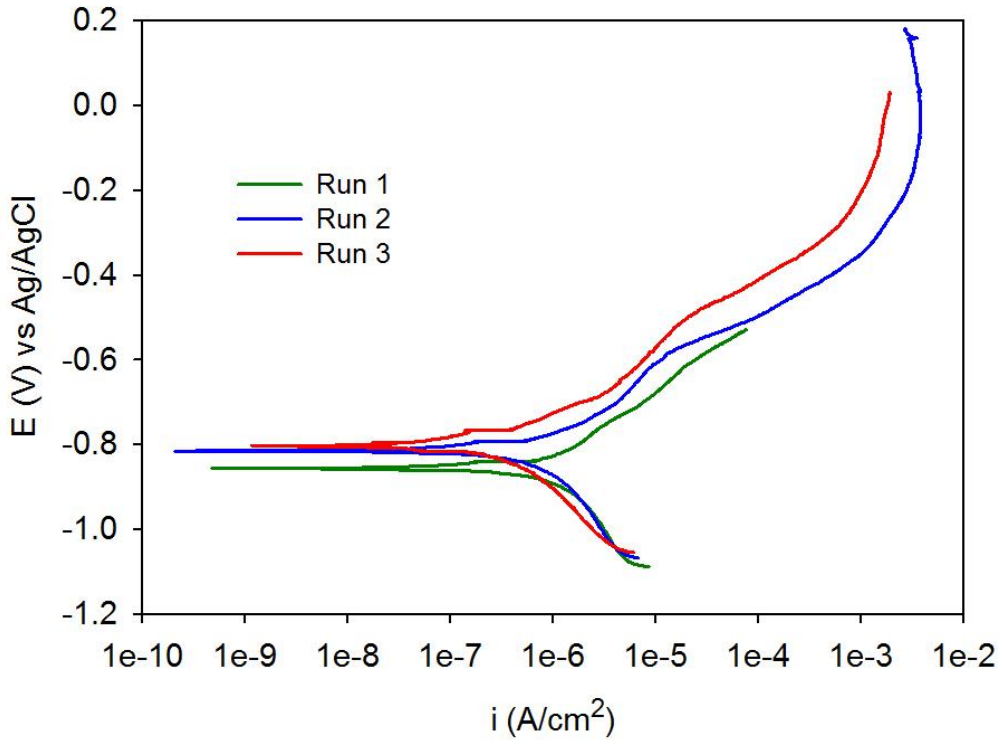

Figure 4-2: Three repeatable results after performing PDP test in galvanized steel in 1.00 wt% humic acid solution.

4.3.3 Linear Polarization Resistance

Linear Polarization Resistance (LPR) was used for the samples in SSOM solutions. The potential was varied from -0.20 mV Ag/AgCl to +0.20 mV Ag/AgCl with respect to OCP with a potential

sweep rate of 0.166 mV/s. From the plots obtained of current versus potential, the polarization resistance (R_P) was determined.

4.3.4 Electrochemical Impedance Spectroscopy

Electrochemical Impedance Spectroscopy (EIS) was performed for the samples in SSOM solutions. The measurements were taken in the frequency range of 0.01 to 10,000 Hz, with an amplitude of 10 mV and a sampling rate of 10 points per decade. The results were analyzed with ZSim software to find the equivalent electronic circuit that best represented the response of the system. The response of the circuit had a chi-square value in the order of 10^{-4} with respect to the experimental results.

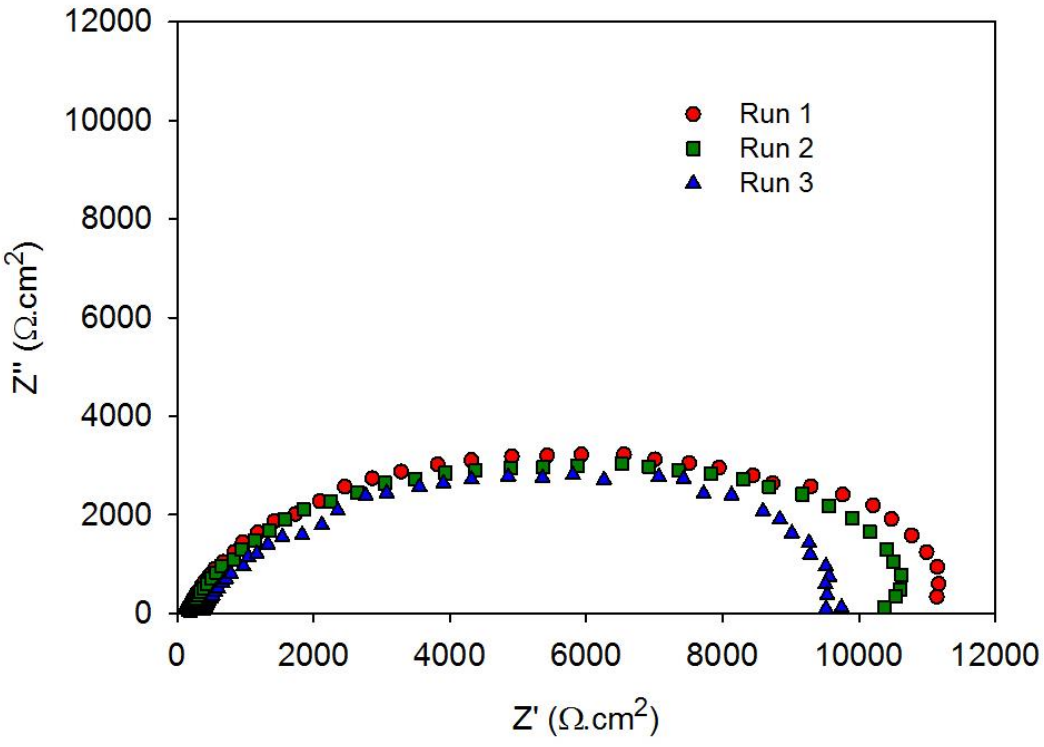

Figure 4-3: Three repeatable results of EIS test performed on galvanized steel in 0.05 wt% SSOM solution.

Figure 4-3 presents an example of the repeatability of three EIS test performed on galvanized steel in 0.50 wt% SSOM solutions. In EIS, results are said to be repeatable, for example in the Nyquist plot, when the same number of time constants are observed as revealed by the number of semicircles and when the real and imaginary values of the total impedance are similar.

4.4 Equipment

The electrochemical corrosion tests were carried out in a conventional three-electrode corrosion cell, as shown in Figure 4-4. Each galvanized steel sample, the working electrode, was held in place by a sample holder, the counter electrode was a graphite rod and the reference electrode was Ag/AgCl ($[Cl^-]$ = 4M). The cell was placed on a magnetic stirrer with a rotating speed of 300rpm to produce a vortex at the electrode. The temperature of the cell was maintained constant at 25°C using a VWR water bath. The measurements were taken with a Princeton Applied Research VersaStat 4 potentiostat.

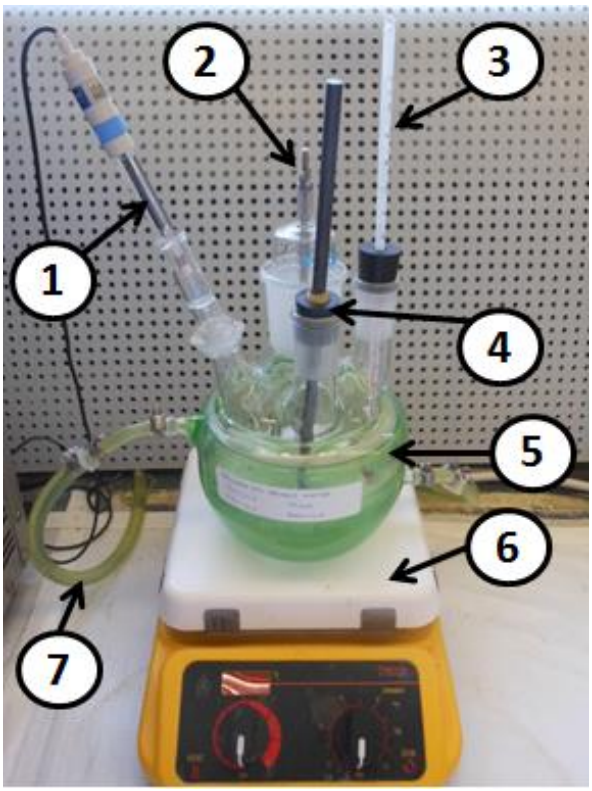

Figure 4-4: Experimental set-up of a standard electrochemical cell: 1. Reference electrode; 2. Sample holder; 3. Thermometer; 4. Counter electrode; 5. Corrosion cell; 6. Magnetic stirrer; 7. Water bath.

A detail of the sample holder is shown in Figure 4-5. The body (1) of the sample holder is composed of a white polymer case with a cylindrical space to place the sample. The inner part of the case is of metallic material and is in contact with a rod that allows connecting electrically the potentiostat with the sample, while remaining isolated from the solution by a glass cylindrical shield. The bottom side of the case has a circular orifice that has an area of 1 cm^2. Before putting the sample in the body, a flat O-ring (2) is put in place to prevent the solution from filtering and getting in contact with a bigger are of the sample (3). A metallic lid (4) is screwed into the cylinder so that the sample is not loose. Finally, the ensemble is locked from the solution

on the open side of the case by a polymer lid that also has an O-ring to avoid filtrations of solution.

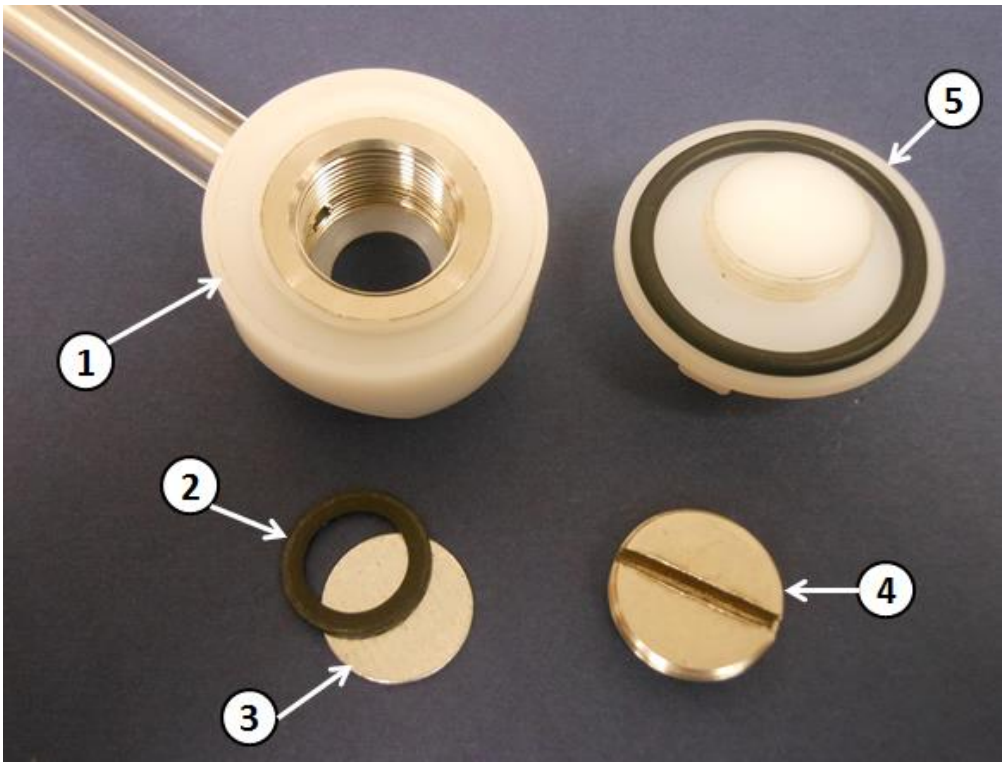

Figure 4-5: Components of the sample holder: 1. Body; 2. Flat O-ring; 3. Galvanized steel sample; 4. Metallic lid; 5. Polymer lid with O-ring

4.5 Surface characterization

The surface of the samples was characterized after PDP tests by means of two methods.

4.5.1 Scanning Electron Microscope

After the electrochemical tests, the samples were extracted from the solution, rinsed with deionized water, and dried. The morphology of the surface and the corrosion products were observed with the Scanning Electron Microscope (SEM).

4.5.2 Energy Dispersive X-ray Spectroscopy

The Energy Dispersive X-ray Spectroscopy (EDX) technique was used to determine the elemental composition of different areas of the surface. This method helped to confirm the extent of corrosion.

Chapter 5: Corrosion of galvanized steel due to individual organics

This chapter presents the corrosion performance of galvanized steel (GS) exposed to four different organic reagents at different concentrations below 1.00 wt%, a solution containing 100 ppm of chlorides, and a solution containing 200 ppm of sulfates. The kinetic parameters were obtained from PDP tests and the surface of the samples was characterized by SEM and EDX.

5.1 Properties of organic solutions

5.1.1 pH

The pH of the solutions of humic acid (HA), glucose, citric acid and oxalic acid were measured prior to the beginning of the electrochemical tests. The values are presented in Table 5-1. HA solutions were alkaline with pH values around 10. Glucose solutions were rather neutral with slight increases in pH as the concentration increased, from 6.2 to 7.4. As expected, solutions of citric and oxalic acid exhibited the lowest pH values, with oxalic acid solutions being the most acidic. Citric acid solutions had pH values between 2.9 and 2.6, while oxalic acid solutions had pH values between 2.4 and 2.

Table 5-1: pH of four organic solutions at four concentrations from 0.1 wt% to 1.0 wt%

	pH			
wt%	HA	Dextrose	Citric acid	Oxalic acid
0.10	10.1 ± 0.29	6.6 ± 0.98	2.9 ± 0.04	2.4 ± 0.14
0.25	10.1 ± 0.19	6.2 ± 0.58	2.9 ± 0.14	2.1 ± 0.42
0.50	10.2 ± 0.29	6.9 ± 0.58	2.7 ± 0.12	1.9 ± 0.21
1.00	10.3 ± 0.31	7.4 ± 0.76	2.6 ± 0.08	2.0 ± 0.03

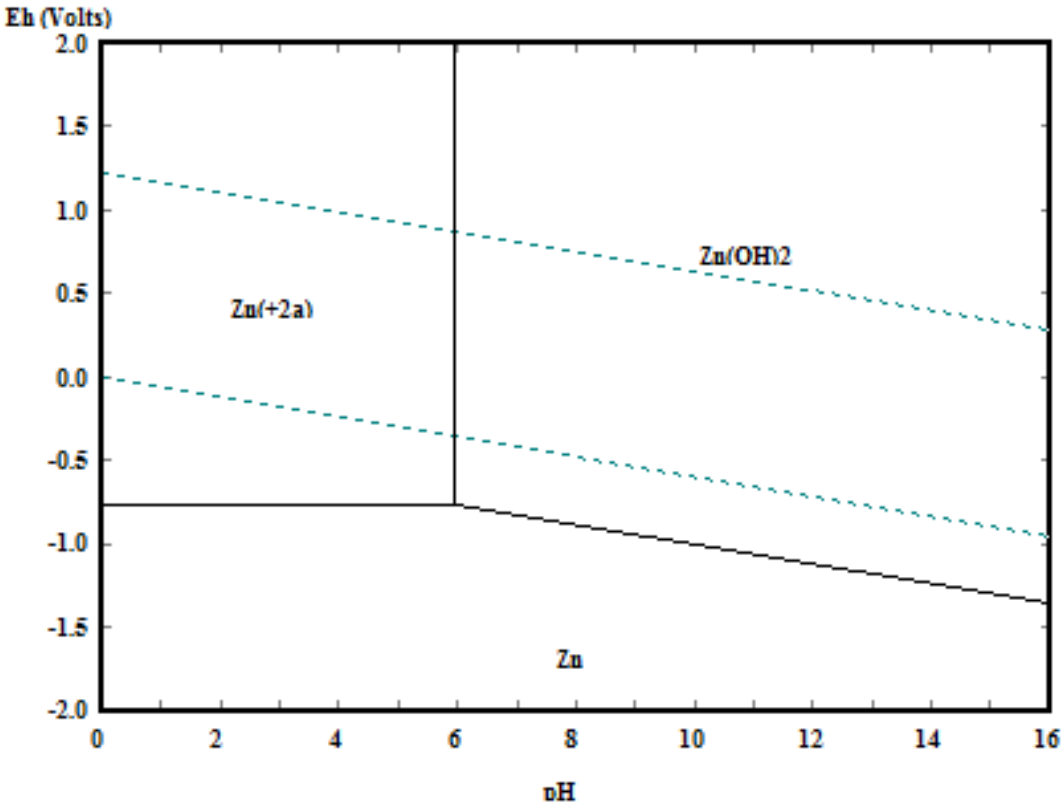

Figure 5-1: E-pH diagram of the zinc-water system at 25 °C

The potential-pH diagram of zinc in water (Figure 5-1) provides an indication of the expected corrosion behavior of zinc. However, the diagram should be used with caution because it refers to a system that is not identical to the ones studied in this chapter. For humic acid and glucose solutions that exhibited pH values higher than 6, it was expected that they promoted the formation of zinc hydroxide ($Zn(OH)_2$) as the potential was increased in the PDP tests. In the case of citric and oxalic acid which produce lower pH values than 6, it was expected that they promoted the formation of zinc cations (Zn^{2+}).

5.1.2 Conductivity

The influence of the concentration of the organic species on the conductivity of the solution is shown in Figure 5-2. The corresponding numeric values are given in the following sections of this chapter. The measurement of the conductivity shows that, while the conductivity of the glucose solutions remained constant at all concentrations (0.3 ± 0.2 µS), it increased linearly with increasing concentrations of humic, citric, and oxalic acids. The conductivity in HA solutions increases from 0.8±0.1 µS at 0.01 wt% to 65±2.3 µS at 1 wt%. Citric acid increased it from 3.5±0.5 µS at 0.1 wt% to 39.5±1.3 µS at 1 wt%. The conductivity of humic acid solutions was higher than citric acid solutions at most concentrations. In oxalic acid solutions at 0.001 wt%, the conductivity was 7.5±0.1 µS, which was higher than the conductivity of 0.1 wt% citric acid solution. At 1.0 wt%, the conductivity of the oxalic acid solution was as high as 530±7.2 µS.

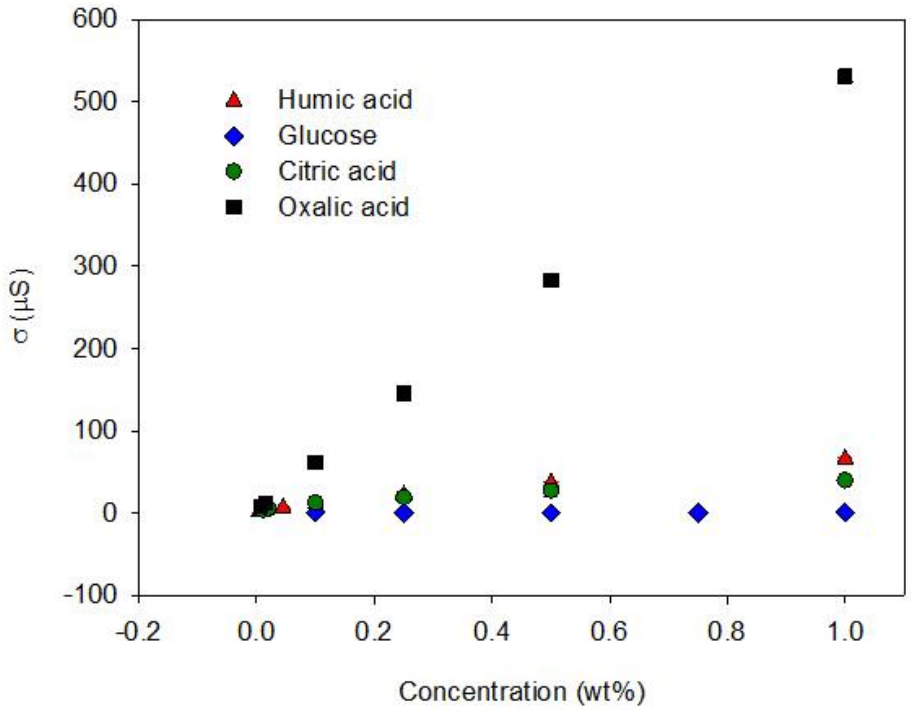

Figure 5-2: Variation in conductivity of four organic solutions as a function of concentration

5.2 Control sample

The surface of a galvanized steel control sample that was not exposed to any electrochemical test was characterized by SEM and EDX. The purpose of this characterization was to provide a reference of the morphology and composition to which the surface of samples exposed to organic solutions could be compared. The SEM image of the control sample (Figure 5-3) is mostly of one color and the characteristic grain boundaries formed during hot dip galvanizing steel can be observed.

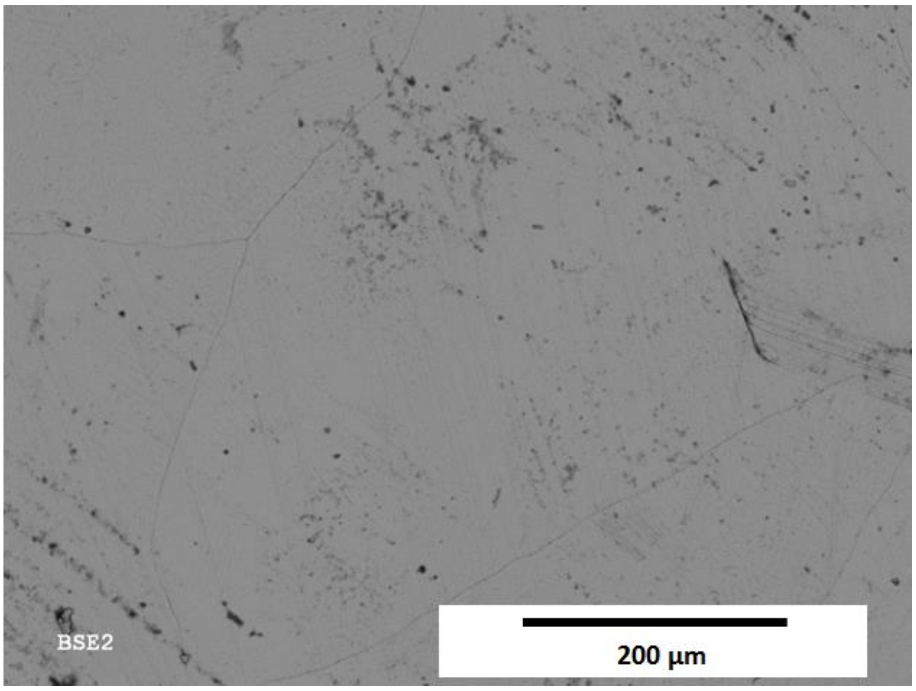

Figure 5-3: SEM image of control sample of galvanized steel

The EDX performed on the surface (Figure 5-4) reveals that zinc is the main component on the surface. Oxygen and iron are also detected but they are present in insignificant amounts.

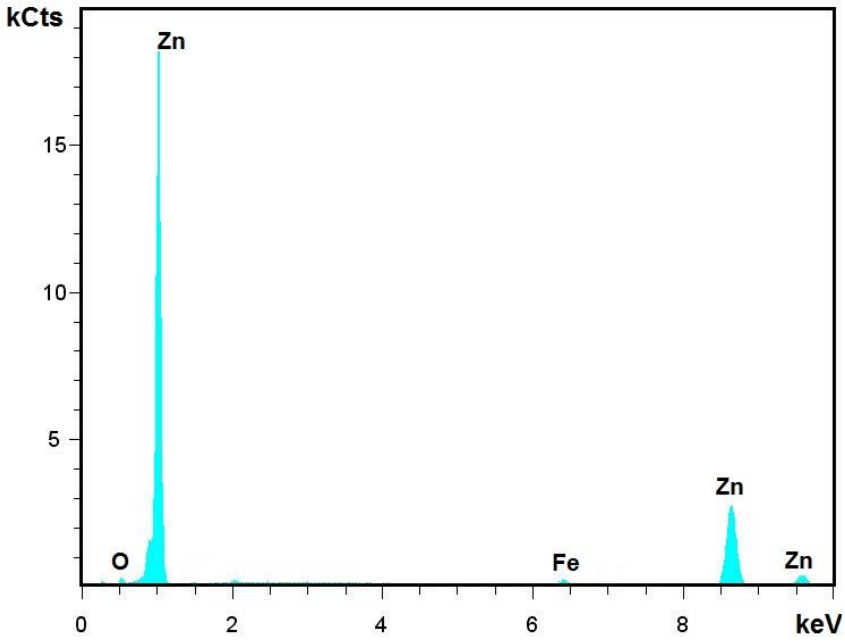

Figure 5-4: EDX analysis of control sample of galvanized steel

5.3 Humic acid

5.3.1 Electrochemical tests in humic acid solutions

The open circuit potential (OCP) was measured prior to each PDP test until a stable potential was reached, which for humic acid solutions, occurred within one hour after immersion (Figure 5-5). In all cases, the open circuit potential shifted towards more noble values as the immersion time increased from zero to one hour. Although no specific reference was found about the behavior of galvanized steel or zinc in the presence of humic acid, it has been proposed that zinc spontaneously develops an oxide/hydroxide film whose structure and protective properties

depend on the specific conditions of the corrosive environment (Sziraki, Szocs, Pilbath, Papp, & Kalman, 2001). This offers a plausible explanation for the increase of the potential.

Considering the final open circuit potential, no particular trend was observed on the measured value for concentrations between 0.005 wt% and 0.5 wt%. Only when the concentration was 1.0 wt% a significant shift towards more negative potentials was observed in comparison to all smaller concentrations. Moreover, the difference between the final open circuit potential and the potential measured immediately after immersion was smaller at 1.0 wt% concentration than the difference between the first and final OCP values at 0.005 wt%.

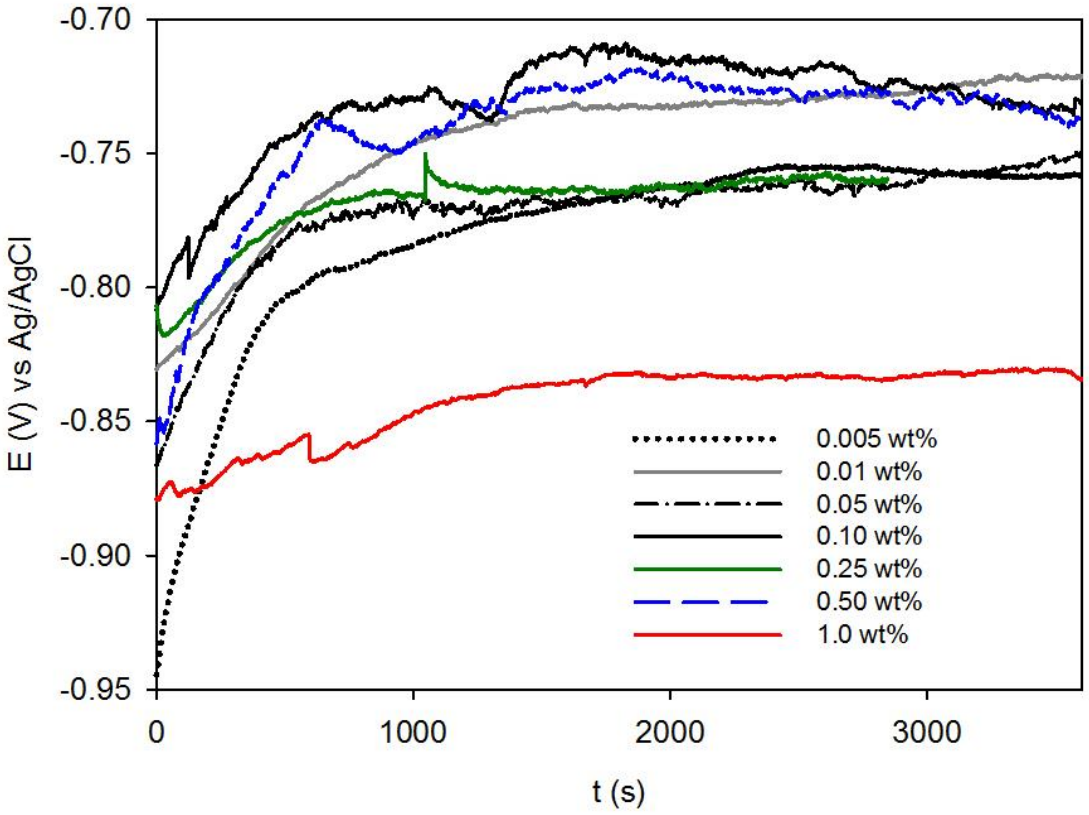

Figure 5-5: Measurement of open circuit potential of galvanized steel in humic acid solutions at different concentrations at pH 10 and 25°C

The PDP curves of galvanized steel in HA solutions at concentrations of 0.005, 0.01, and 0.05 wt% are presented in Figure 5-6. The shape of the cathodic branch confirms that the cathodic process was controlled by diffusion. The limiting current density (i_L) increased slightly as the concentration was increased with values of 3.6, 4 and 7.5 $\mu A/cm^2$ respectively. The shape of the anodic branches shows that the anodic process is controlled by activation. The E_{corr} of these solutions oscillated around -660 mV. For concentrations of 0.005 wt% and 0.01 wt%, the slope of the anodic branch in the vicinity of E_{corr} was approximately 20mV per decade, however at current density of 10^{-4} $\mu A/cm^2$ the slope became bigger, with an increase in potential of more than 60mV is less than one decade. In the case of 0.05 wt%, the anodic slope was smaller and the sudden increase was not observed.

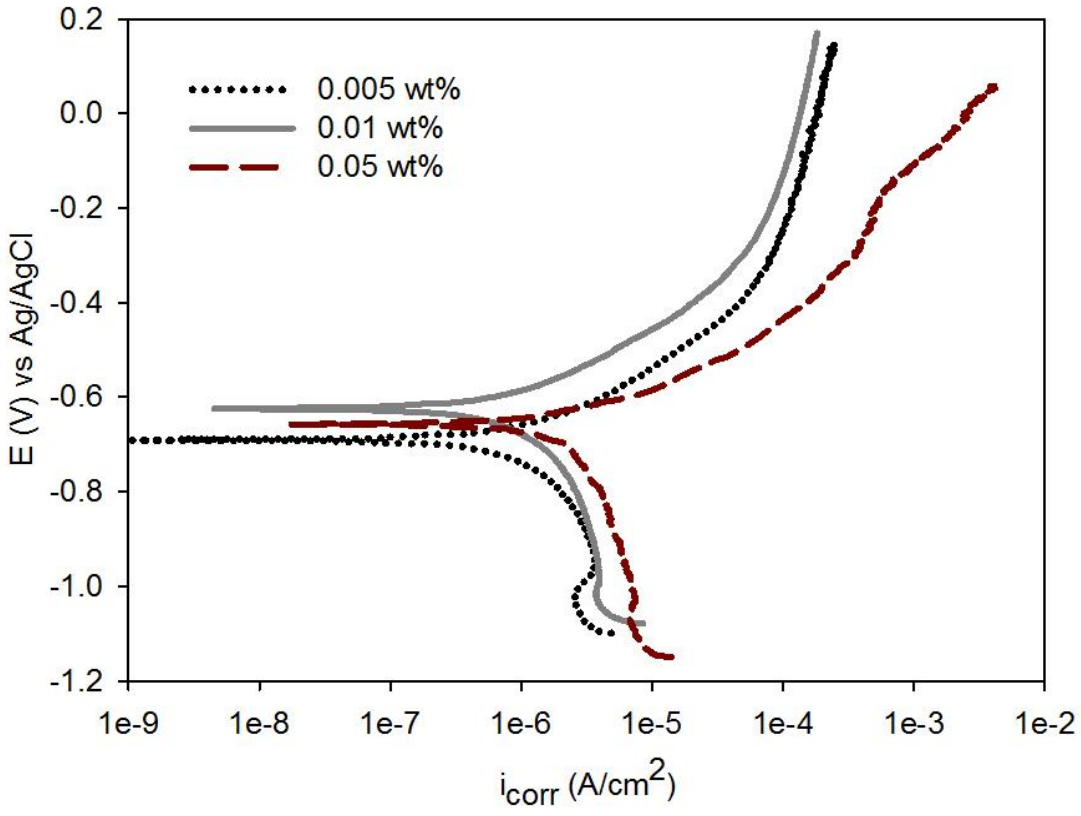

Figure 5-6: Potentiodynamic curves of galvanized steel immersed in humic acid solutions at concentrations below 0.1 wt% at pH 10 and 25°C

Figure 5-7 presents the PDP curves for GS in HA solutions at concentrations 0.10 wt%, 0.25 wt%, 0.50wt%, and 1.00 wt%. The diffusion process in the cathodic branch became less apparent. The slope in the anodic branch was similar than for smaller concentrations, i.e. approximately 20mV/dec. However, this slope was maintained until a current density of $10^{-3}\ \mu A/cm^2$, after which a high increase in the slope was observed. Furthermore, the E_{corr} measurements at concentrations 0.10 wt%, 0.25 wt%, and 0.50 wt% were close to each other, in the order of -781 mV. At the highest concentration of 1.0 wt%, the lowest E_{corr} was obtained with a value of -824 mV.

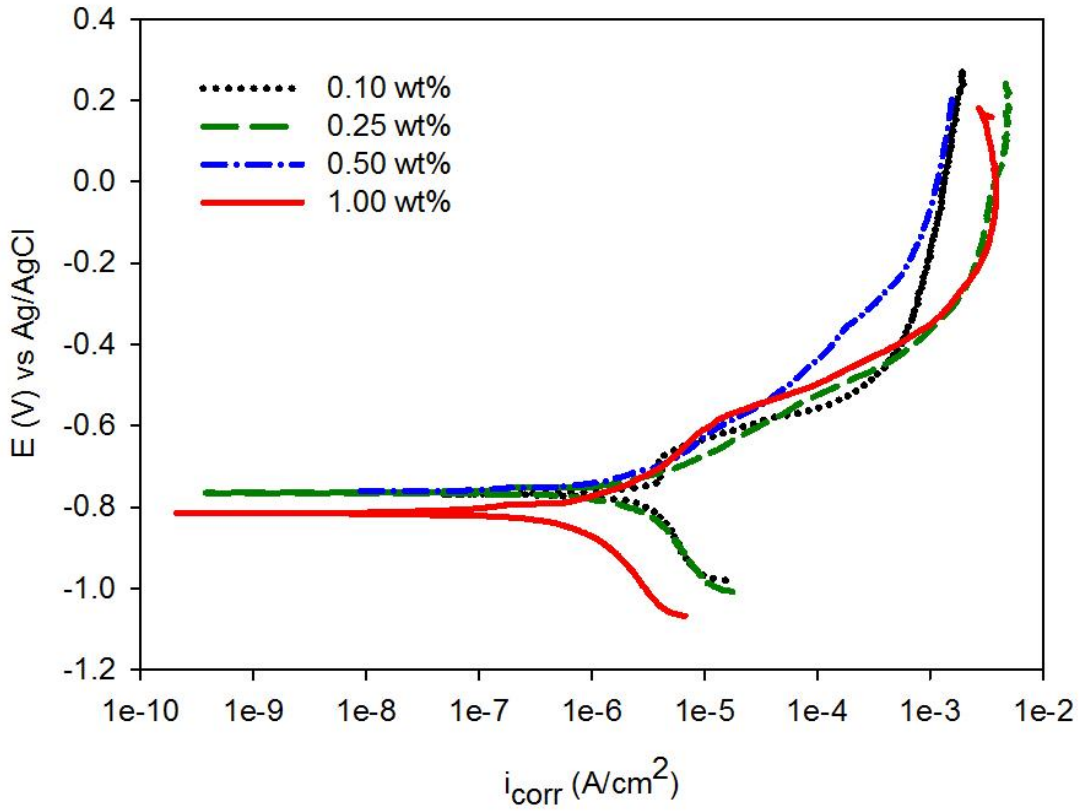

Figure 5-7: Potentiodynamic curves of galvanized steel immersed in humic acid solutions at concentrations between 0.1 wt% and 1.00 wt% pH 10 at 25°C

Table 5-2 summarizes the E_{corr} and i_{corr} values obtained from PDP measurements. In general, as the concentration of HA increased, the E_{corr} shifted towards more negative values. The same trend was not true for i_{corr}. The maximum values of i_{corr} were reached at 0.01 wt%, however, the maximum most stable value was obtained at 0.05 wt%. After this concentration the i_{corr} decreased gradually until at 1.0 wt% the value was comparable to that obtained at 0.005 wt%.

Table 5-2: Conductivity of solutions and kinetic parameters from PDP measurements for galvanized steel in humic acid solutions at concentrations ranging from 0.005 wt% to 1.0 wt% at pH 10 and 25°C

wt%	σ (µS)	E_{corr} (mV)	i_{corr} ($\mu A/cm^2$)
0.005	0.9 ± 0.1	-681 ± 22	2.9 ± 1.3
0.01	1.9 ± 0.4	-674 ± 54	18.8 ± 14.9
0.05	6.6 ± 0.1	-638 ± 28	15.3 ± 0.3
0.10	10.7 ± 0.0	-767 ± 5	10.7 ± 3.2
0.25	21.3 ± 0.5	-793 ± 52	9.7 ± 4.6
0.50	36.9 ± 0.1	-784 ± 32	4.9 ± 4.8
1.00	65.4 ± 2.3	-824 ± 28	3.0 ± 1.4

5.3.2 Surface characterization of galvanized steel in humic acid solutions

It was observed that, independently of the concentration, when the galvanized steel samples were extracted from the solution immediately after the PDP tests, the exposed area appeared completely covered by a very thick layer (about 2mm) of dark deposits that could not be removed by rinsing the sample. However, those deposits were easier to remove using the same method after drying the layer at ambient temperature. The surface of the sample appeared to be non-uniformly covered by dark brown deposits in some regions (labeled with number 2 in Figure 5-8), while other areas seemed to be metallic (labeled with number 1 in Figure 5-8).

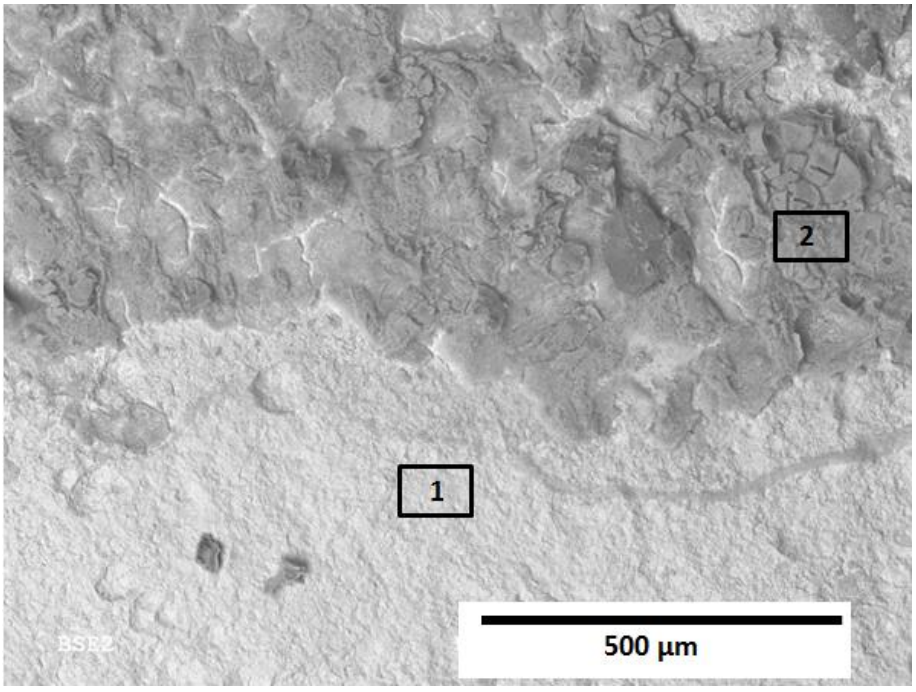

Figure 5-8: SEM image of galvanized steel after PDP in 0.25wt% humic acid solution

EDX confirmed that in region 1, humic acid at 0.25 wt% was able to corrode the zinc layer and reach the base steel (Figure 5-9). The feasibility of the interaction between humic acid and zinc has been studied in various contexts and the formation of humic acid-zinc complexes has been confirmed in various studies (Baker & Khalili, 2005; Gungor & Let, 2010; Li *et al.*, 2010; Prado *et al.*, 2006; Yang & Van, 2009; Yip *et al.*, 2010).

The dark brown deposits had an elemental composition that contained carbon, oxygen, iron, zinc, and aluminum (Figure 5-10). The presence of aluminum can be explained because it is an alloying element that is typically incorporated in the zinc bath in hot-dip galvanizing to further improve the corrosion resistance of the material by promoting the formation of a continuous layer of Al_2O_3 (Marder, 2000). The high counts of iron and oxygen may indicate that iron

corrosion products have been formed. It has been reported in the past that humic acid is capable of promoting corrosion of API 5LX65 steel in soil (Dick & Rodrigues, 2006) and carbon steel in natural freshwaters (Jiang *et al.*, 2008). These corrosion products could be any of the ones that have been identified for galvanized steel: FeO, Fe_3O_4, Fe_2O_3, $Fe(OH)_2$, and $Fe(OH)_3$ (Pantazopoulou & Papoulia, 2001). The appearance of carbon in the EDX results is normal for two reasons: first, carbon is an alloying element of steel (Markham, 1913); second, humic acid contains up to 50% carbon (Schnitzer & Khan, 1978) and can be strongly complexed with iron (Szilagyi, 1971).

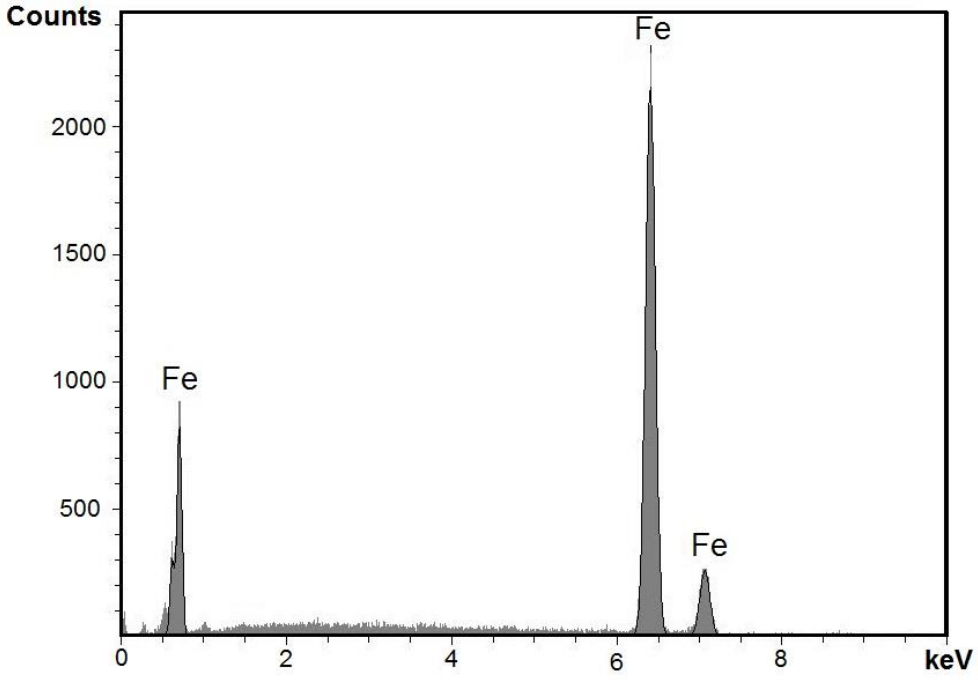

Figure 5-9: EDX analysis of region 1 of Figure 5-8

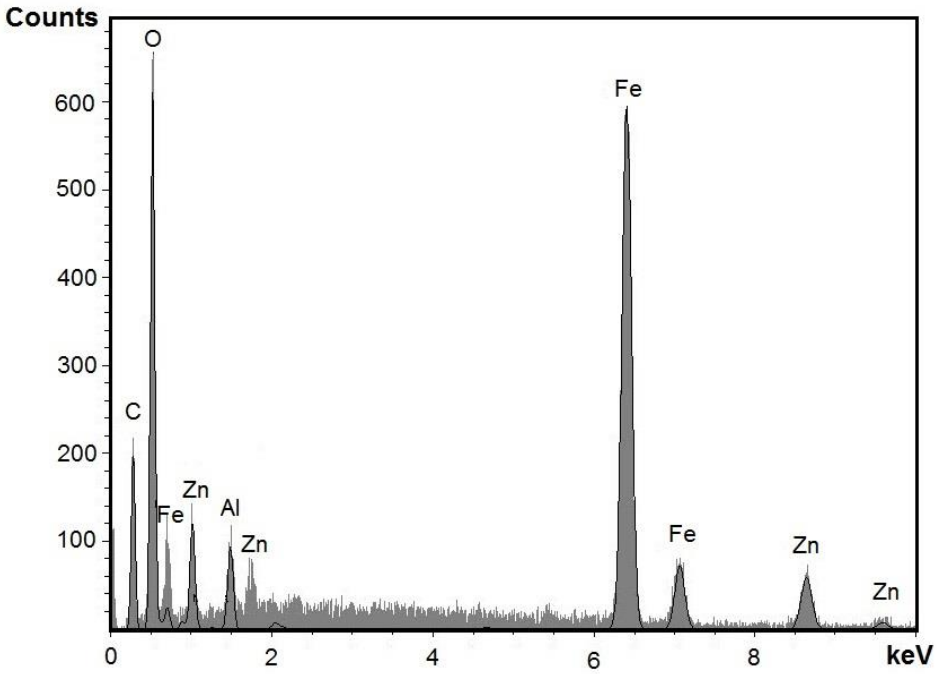

Figure 5-10: EDX analysis of region 2 of Figure 5-8

5.4 Dextrose

5.4.1 Electrochemical tests in dextrose solutions

The OCP was measured before performing the PDP test until a stable potential was reached (Figure 5-11). For concentrations of 0.10 wt% and 0.25 wt% the stability was reached in one hour. Nevertheless, solutions with higher concentrations of 0.50 and 1.0 wt% required an extra half an hour before stabilizing. At all concentrations, two changes in the potential were observed. First, the potential shifted towards more negative values during the first 1000 seconds and then the potential moved towards more noble values.

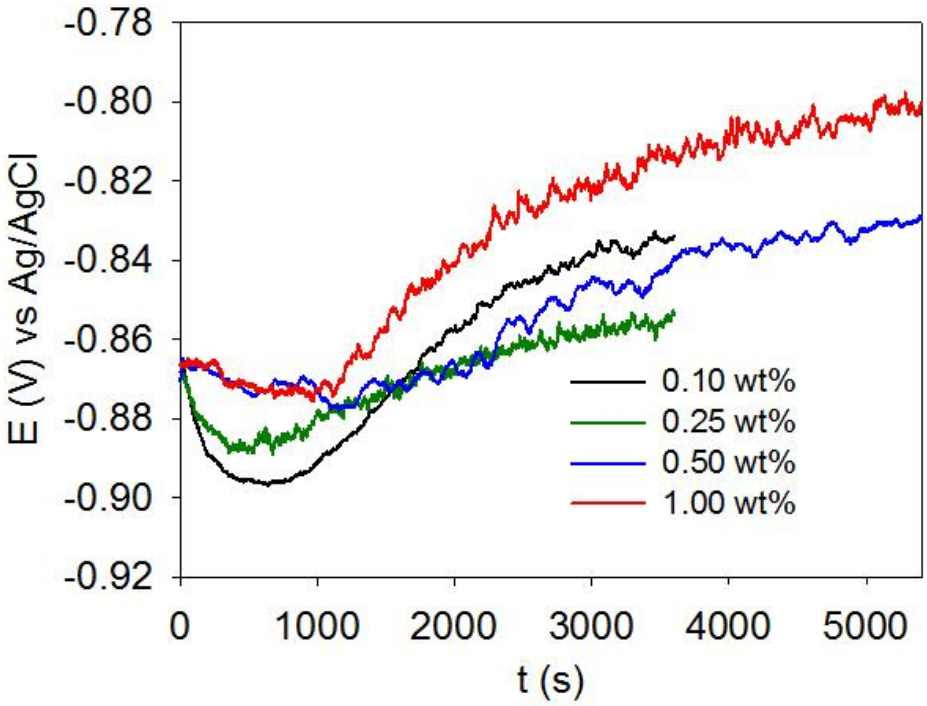

Figure 5-11: Measurement of open circuit potential of galvanized steel in dextrose solutions at different concentrations at pH 7 and 25°C

It was also observed that as the concentration increased, the difference between the stable potential and the potential immediately after immersion was higher than for lower concentrations. This difference was approximately of 60, 20, 20 and 10 mV for 1.0, 0.5, 0.25, and 0.1 wt% respectively. In Figure 5-12, the PDP curves of galvanized steel in 0.1, 0.25, 0.5, and 1.0 wt% dextrose solutions are presented. In the cathodic branch, the cathodic process was controlled by diffusion. The limiting current density (i_L) for 0.1, 0.25, 0.5, and 1.0 wt% concentrations was, respectively, 4.7, 3.4, 2, and 0.7 $\mu A/cm^2$, thus i_L decreased as the concentration increased. In the anodic branch, the process was controlled by activation and the slope at all concentrations was small for potentials near E_{corr}. This slope was smaller than 50

mV/dec for only one decade. After the current density of $10^{-5} A/cm^2$, the slope became sharply bigger, approaching 90 mV/dec.

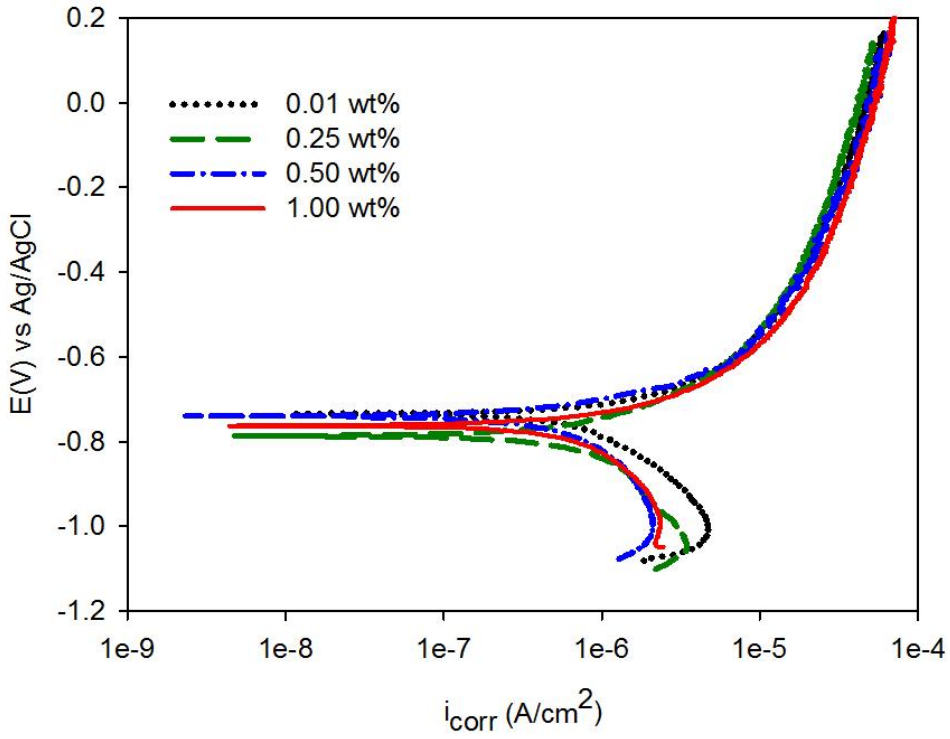

Figure 5-12: Potentiodynamic curves of galvanized steel immersed in dextrose solutions at different concentrations at pH 7 and 25°C

Table 5-3 summarizes the conductivity, E_{corr} and i_{corr} values obtained experimentally for galvanized steel in dextrose solutions.

Table 5-3: Conductivity of solutions and kinetic parameters from PDP measurements of galvanized steel in dextrose solutions at concentrations ranging from 0.10 wt% to 1.0 wt% at pH 7 and 25°C

wt%	σ (µS)	E_{corr} (mV)	i_{corr} ($\mu A/cm^2$)
0.10	0.5 ± 0.53	-740 ± 19	2.8 ± 0.3
0.25	0.5 ± 0.51	-793 ± 44	1.7 ± 0.8
0.50	0.2 ± 0.01	-743 ± 4	2.4 ± 1.7
1.00	0.2 ± 0.02	-748 ± 20	2.7 ± 2.1

Overall, the E_{corr} did not appear to be affected by the concentration as this potential oscillated around -756 mV with standard deviations of less than 44 mV at concentrations between 0.10 wt% and 1.0 wt%. Similarly, the concentration did not have a significant effect on i_{corr} values, which were all between 1.7 and 2.8 $\mu A/cm^2$ in the same concentration range.

5.4.2 Surface characterization in dextrose solutions

Figure 5-13 shows a selected SEM image of a galvanized steel sample after PDP test in 1.0 wt% dextrose solution. A few randomly distributed black spots were observed and are pointed with number 2. The EDX analysis (Figure 5-14) performed on them indicates the presence of zinc and oxygen, which may correspond to zinc corrosion products. On the rest of the surface, in light gray shade in Figure 5-13, the grain boundaries of grains that measure about 0.7mm in length were observed. These large grains are formed during the hot-dip galvanizing process and are visible to the naked eye as spangles, that are a characteristic feature of galvanized steel (A. P. Yadav *et al.*, 2004b). EDX performed on region 1 of Figure 5-15 only identified zinc (Figure 5-15). This means that the zinc coating remained intact.

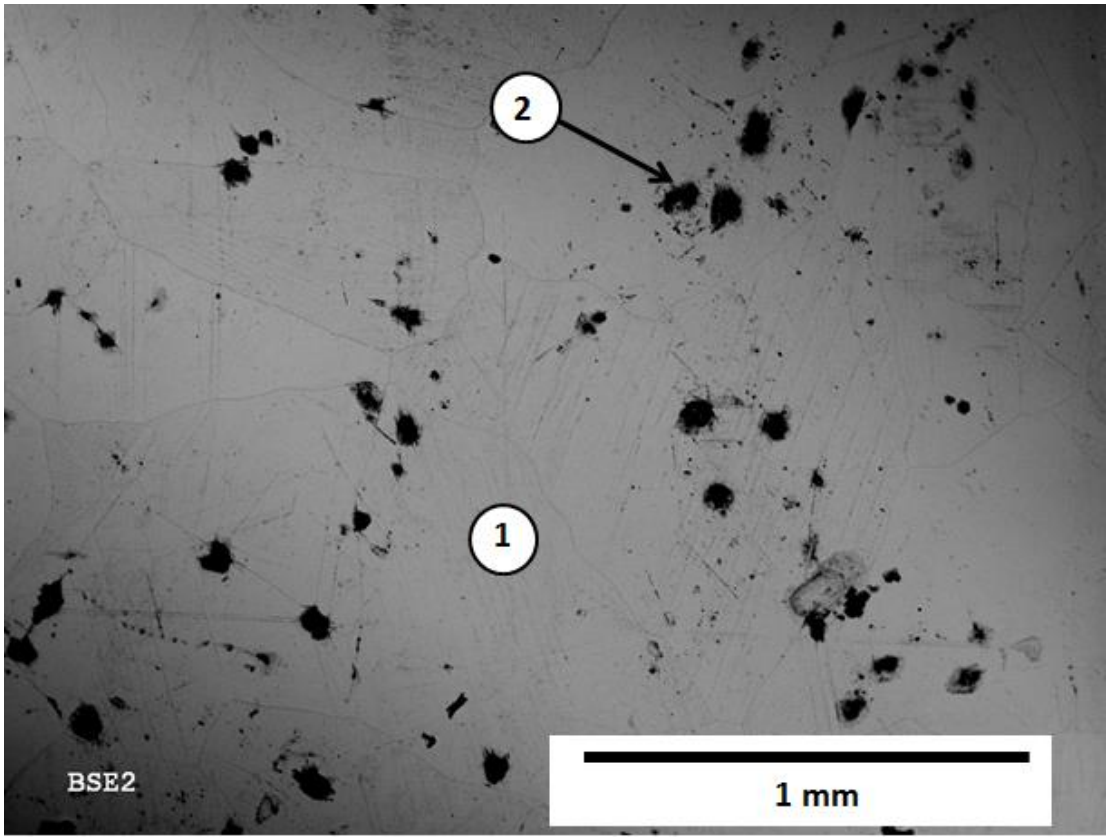

Figure 5-13: SEM image of galvanized steel after PDP in 1wt% dextrose solution

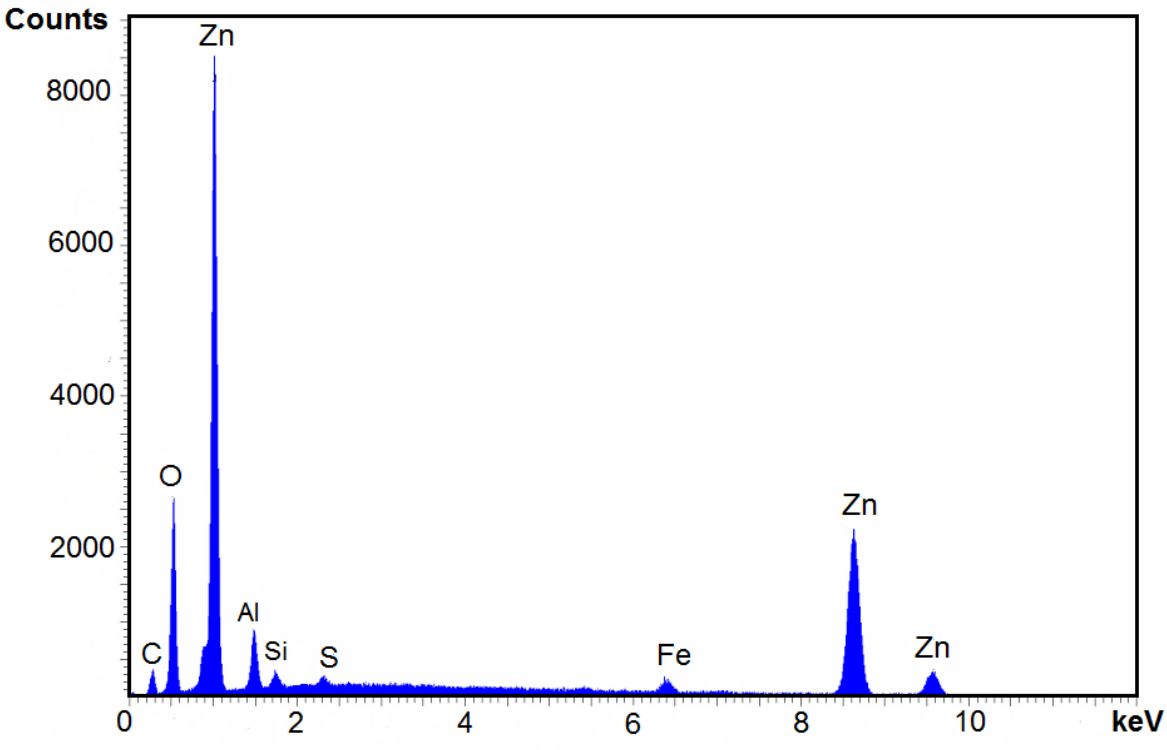

Figure 5-14: EDX analysis of region 2of Figure 5-13

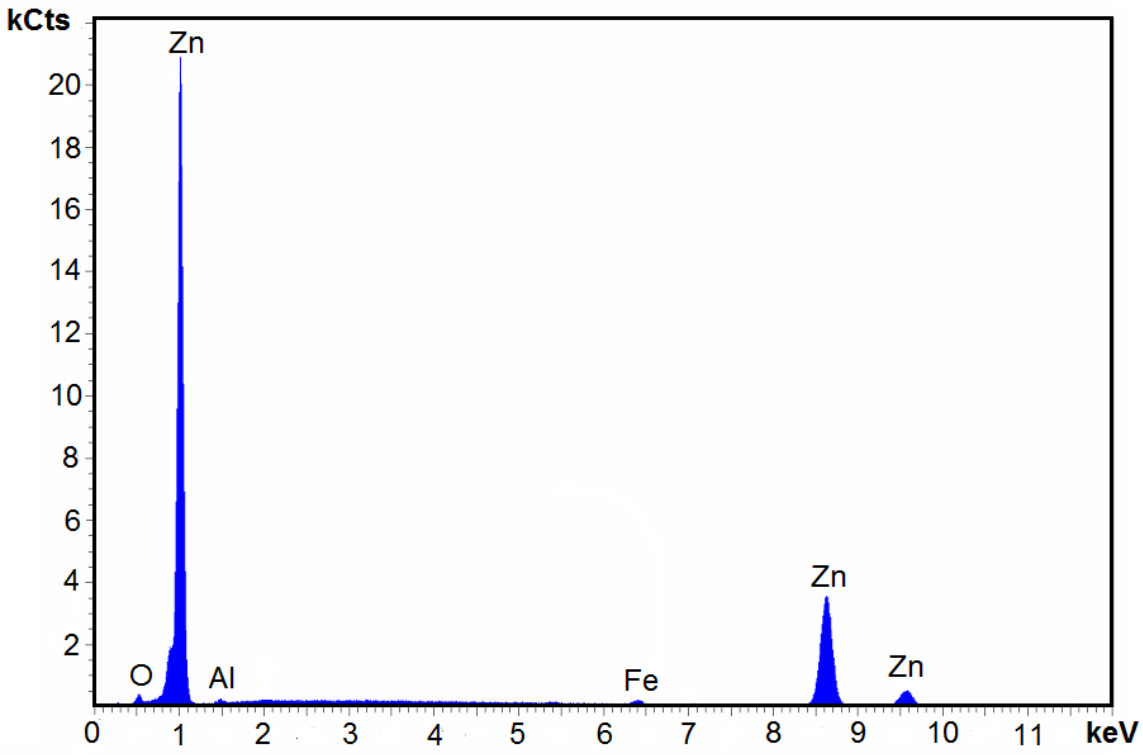

Figure 5-15: EDX analysis of region 1 of Figure 5-13

5.5 Citric acid

5.5.1 Electrochemical tests in citric acid solutions

Previous to the PDP test, the OCP of solutions with 0.01, 0.02, 0.1, 0.25, 0.5, and 1.0 wt% concentrations of citric acid were recorded, as shown in Figure 5-14. The stable potential was reached for all solutions after 2000 seconds. Furthermore, the same trend of shifting gradually towards more negative potentials was exhibited at all concentrations, which is in agreement with the expected corrosion aggressiveness of citric acid. Although no apparent trend was observed in the final potential with regards to the concentration, it must be noted that the difference between all values was approximately 10 mV.

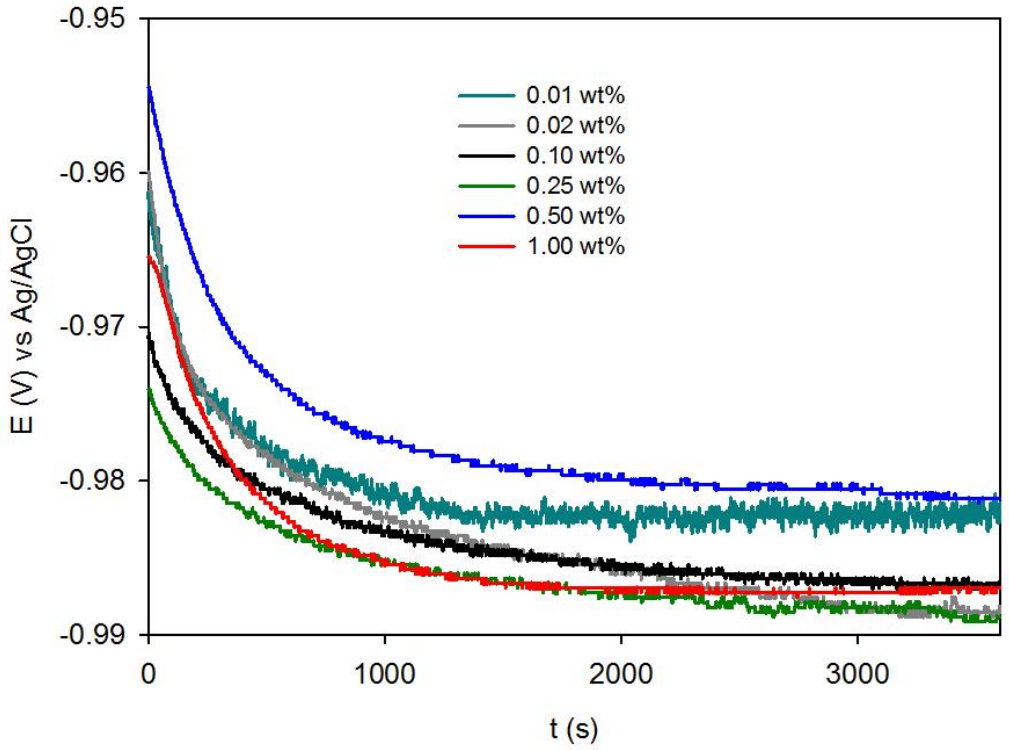

Figure 5-16: Measurement of open circuit potential of galvanized steel in Citric Acid solutions at different concentrations at pH 3 and 25°C

The PDP curves of the solutions of citric acid at six concentrations ranging from 0.01 to 1.0 wt% are presented in Figure 5-17. The shape of the PDP curves is similar at all concentrations. In particular, the PDP curves of 0.02 wt% and 0.1 wt% appeared overlapped. The E_{corr} was virtually the same at all concentrations of citric acid in the range 0.01 wt% to 1.00 wt% with a mean value of -982 mV. In the cathodic branch, a limiting current density was not easily identifiable within 25 mV below E_{corr}. The only evident effect of the increase of citric acid concentration on the corrosion behavior of galvanized steel was the increase in current density, which is detected visually by the displacement towards the right of both, the anodic and cathodic branches. Furthermore the slopes of the anodic branches were large compared to the slopes of PDP curves in humic acid and dextrose solutions, since they were higher than 80mV/dec.

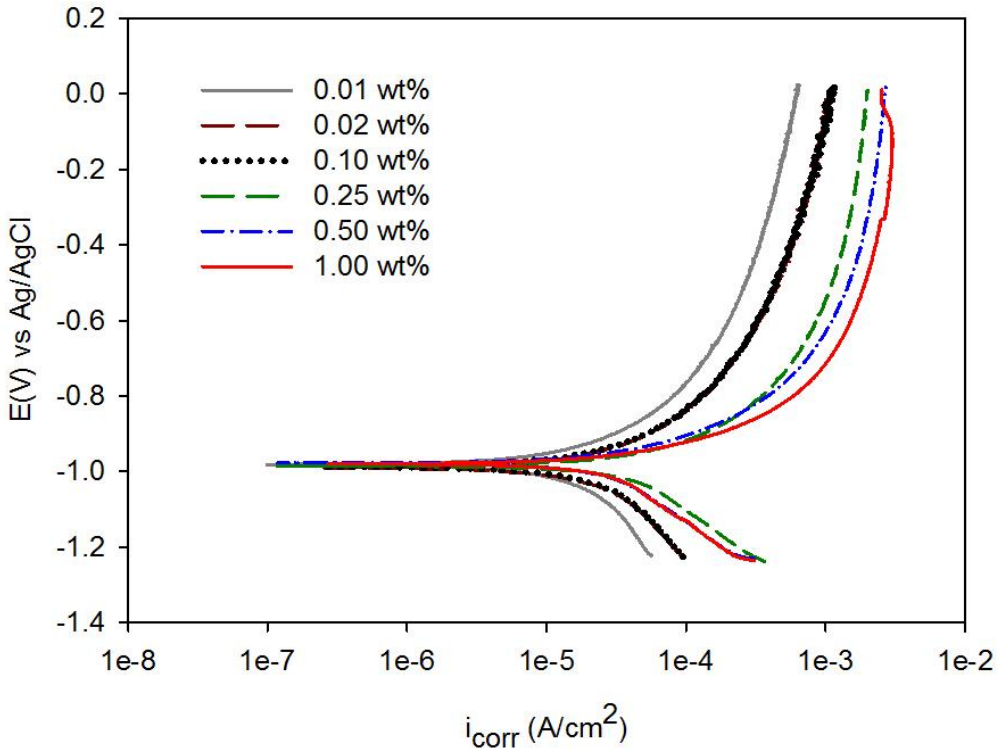

Figure 5-17: Potentiodynamic curves of galvanized steel immersed in citric acid solutions at different concentrations at 25°C

The conductivity and kinetic parameters at the different concentrations of citric acid are presented in Table 5-4.

Table 5-4: Conductivity of solutions and kinetic parameters from PDP measurements of galvanized steel in citric acid solutions at concentrations from 0.01 wt% to 1.0 wt% at pH 2 and 25°C

wt%	σ (µS)	E_{corr} (mV)	i_{corr} ($\mu A/cm^2$)
0.01	3.5 ± 0.5	-986 ± 13	55.0 ± 0.8
0.02	5.4 ± 0.3	-984 ± 6	53.2 ± 21.9
0.10	12.1 ± 0.4	-983 ± 4	72.4 ± 5.5
0.25	18.7 ± 0.1	-979 ± 16	108.0 ± 67.0
0.50	27.1 ± 7.2	-980 ± 3	186.5 ± 155.3
1.00	39.5 ± 1.3	-982 ± 3	153.2 ± 100.4

The values of i_{corr} in Table 5-4 confirmed that as the concentration increased, the current densities also increased. This same tendency in the current densities as the concentration of citric is increased has also been reported on steel and tin (Gouda *et al.*, 1980; Gouda *et al.*, 1981; Sekine *et al.*, 1990). In general, the corrosive effect of citric acid has been recognized on various metals, including bronze, iron and tin (Abdel Rehim *et al.*, 2003; Jafarian *et al.*, 2008; Li *et al.*, 2014; Ying *et al.*, 2003; Zerfaoui *et al.*, 2004). However, a maximum i_{corr} was obtained at 0.50 wt%, after which higher concentration produced a lower current density than this maximum value.

The electrochemical tests do not provide information about the complexes formed between zinc or iron with citric acid. However, in order to determine the nature of the complexes that would be formed at a given potential and pH, a speciation diagram was created for each of these metals

with citrate using the MEDUSA[5] software. The diagrams are presented in Figure 5-18 and Figure 5-19. For instance, considering the pH of the experimental conditions which is 3, zinc is expected to form stable complexes (Zn(Hcit)) at potentials above -1.00 V. However, zinc becomes leachable at neutral pH in a range that goes from 4 to 10, as indicated by the ionic form $Zn(cit)^{-}$.

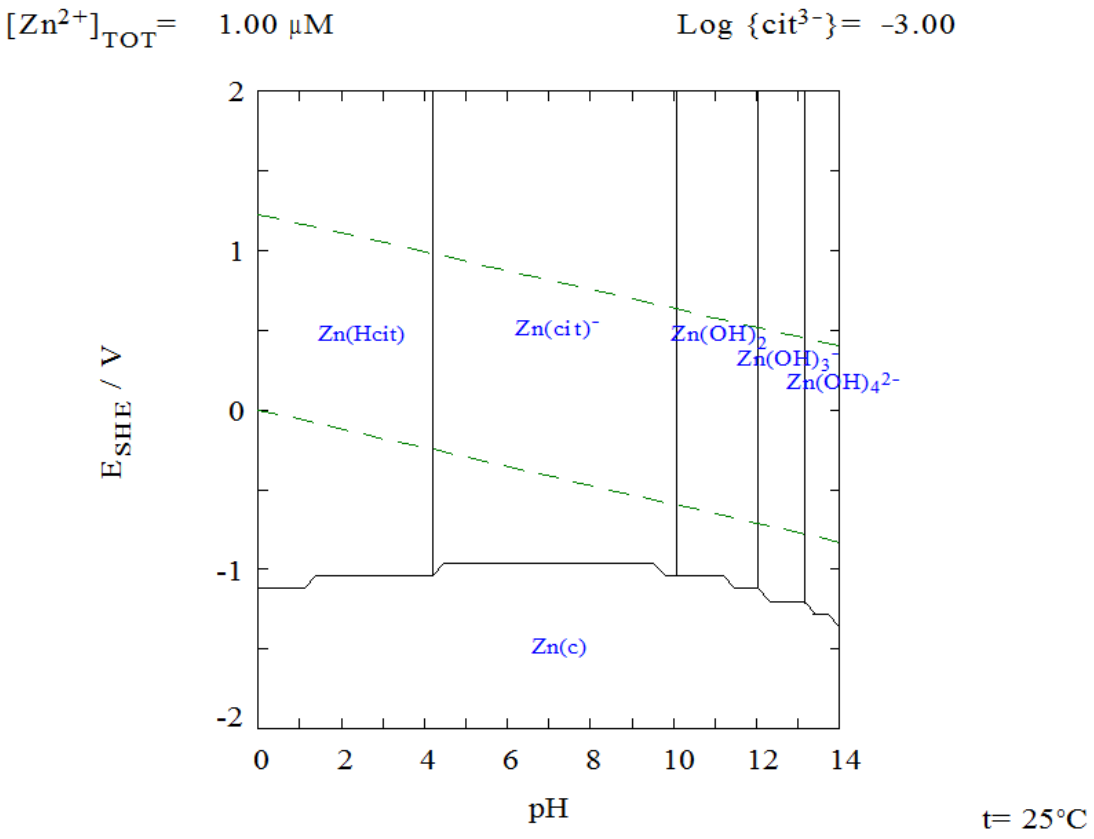

Figure 5-18: Predominance area diagram of zinc-citrate complexes in aqueous solutions.

Once the zinc layer is depleted and the base steel is exposed, at the same pH 3, the type of complexes that iron can form with citrate will depend on the potential. For potential values

[5] MEDUSA (Make Equilibrium Diagrams Using Sophisticated Algorithms), software developed by the School of Chemical Science and Engineering from the Royal Instute of Technology, 100 44 Stockholm, Sweden.

between -0.50 V and +1.0 V, the Fe^{2+} ions will be the predominant species, while at higher potentials, the predominant species will be stable complexes (Fe(cit)).

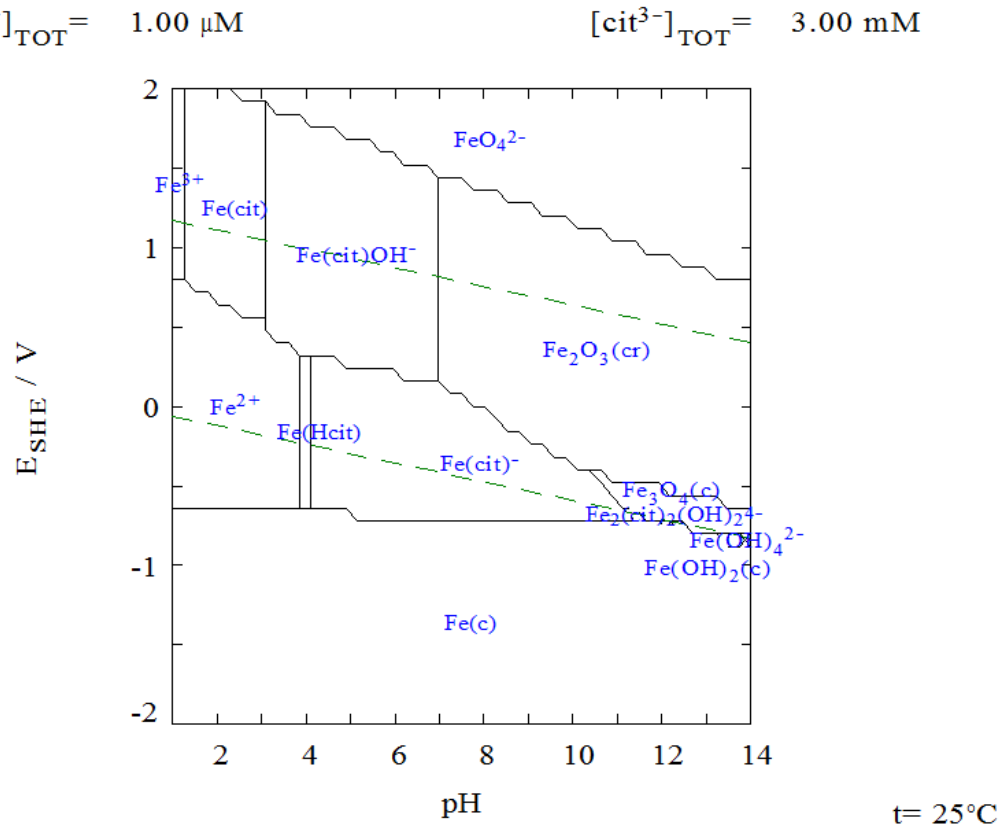

Figure 5-19: Predominance area diagram of iron-citrate complexes in aqueous solutions.

5.5.2 Surface characterization of galvanized steel in citric acid solutions

A representative SEM image of the galvanized steel samples surface after the PDP test is shown in Figure 5-20. The surface appeared to be covered in some areas by residual accumulations that seemed to be detached form the surface. By performing EDX analysis on the surface labeled as region 1 in Figure 5-20, it was determined that the galvanizing coating was completely corroded

by the citric acid solution at 0.25 wt%, leaving the base steel surface exposed to the environment, which was confirmed by the high counts of iron in Figure 5-21. The elemental composition of the residues labeled with number 2 in Figure 5-20 was mainly Zn, Fe, and O, suggesting that most likely it was a form of zinc oxide as revealed by EDX results shown in Figure 5-22.

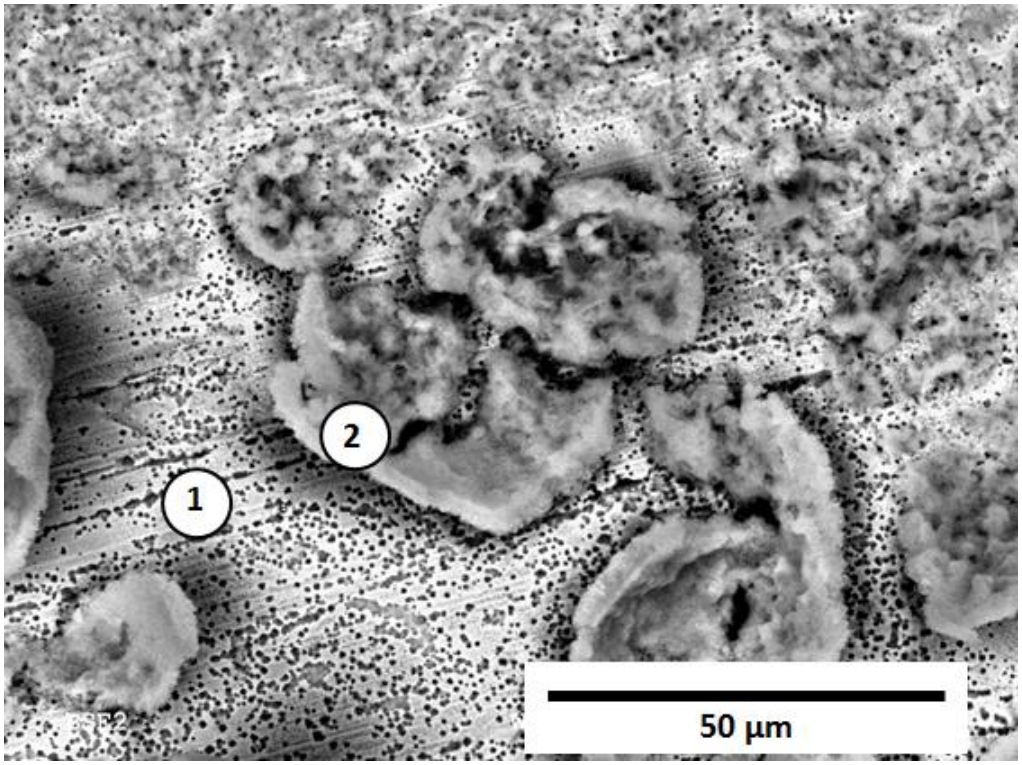

Figure 5-20: SEM image of galvanized steel after PDP in 0.25 wt% citric acid solution

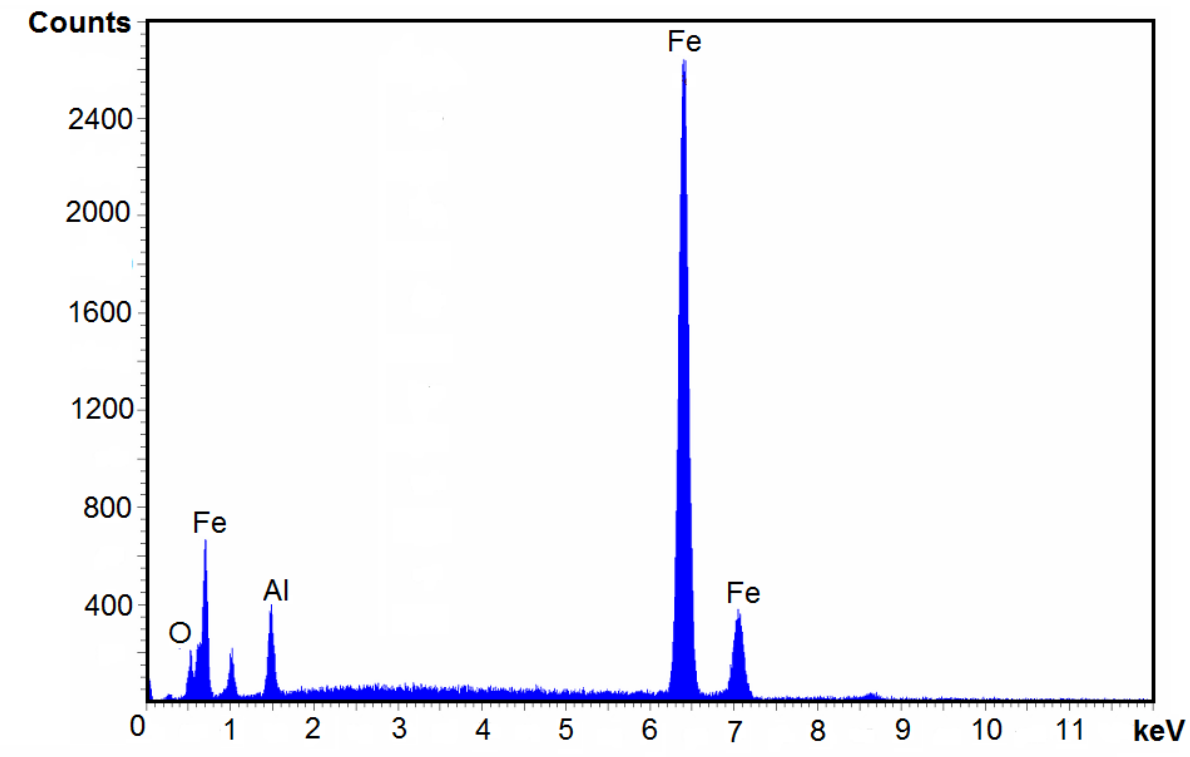

Figure 5-21: EDX analysis of region 1of Figure 5-20

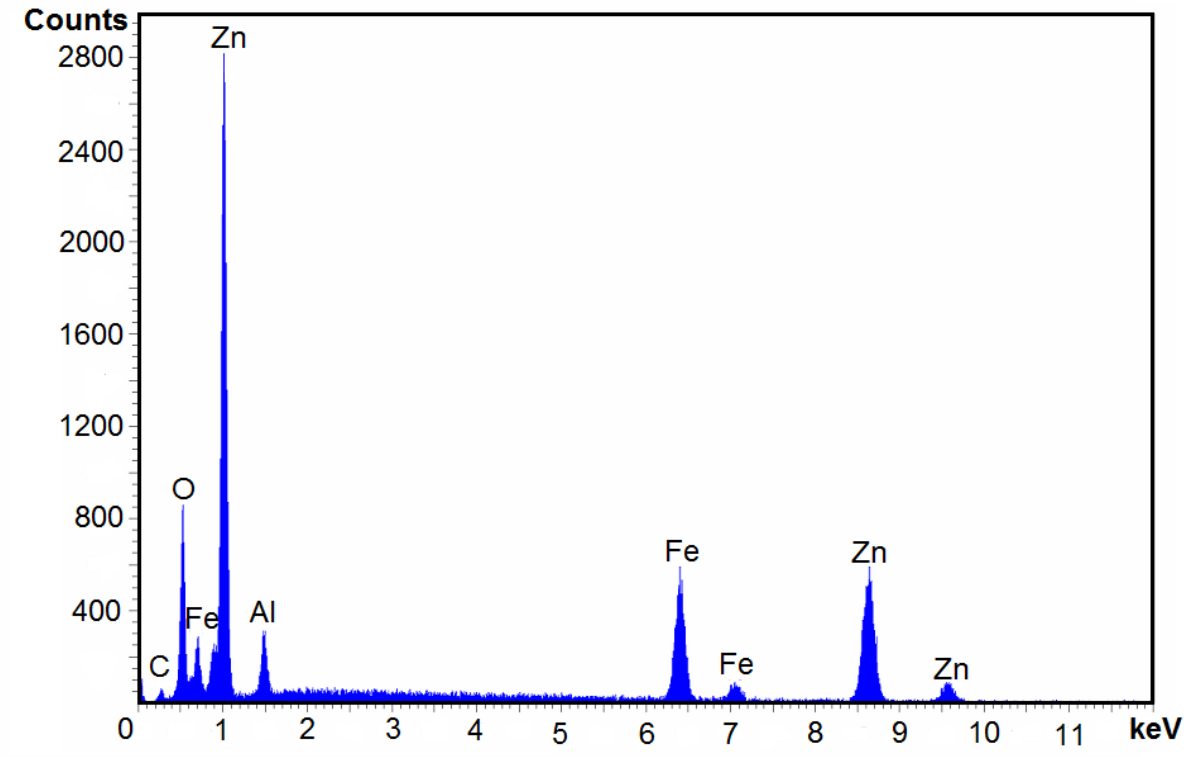

Figure 5-22: EDX analysis of region 2 of Figure 5-20

5.6 Oxalic acid

5.6.1 Electrochemical tests in oxalic acid solutions

The OCP of galvanized steel in solutions with different concentrations of oxalic acid was measured until a stable potential was reached. For solutions with concentrations of 0.10, 0.25, and 5.0 wt%, a stable potential was reached after 2000s (Figure 5-23). For these concentrations, the potential was between -0.94 V and -0.9 V.

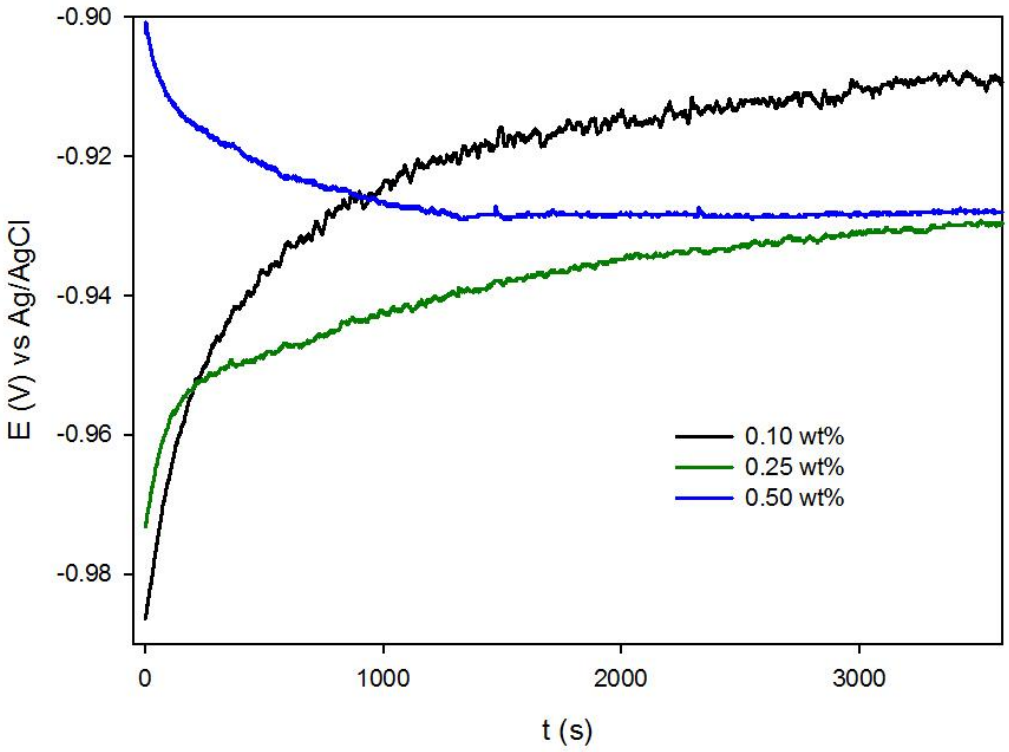

Figure 5-23: Measurement of open circuit potential of galvanized steel in 0.10, 0.25 and 0.50 wt% oxalic acid solutions at pH 2 and 25°C

However, for the solution with 1.0 wt% of oxalic acid, it was necessary to continue recording the potential for more than 8 hours before a stable potential could be observed (Figure 5-24). At this concentration, the final OCP value was more noble than for the smaller concentrations.

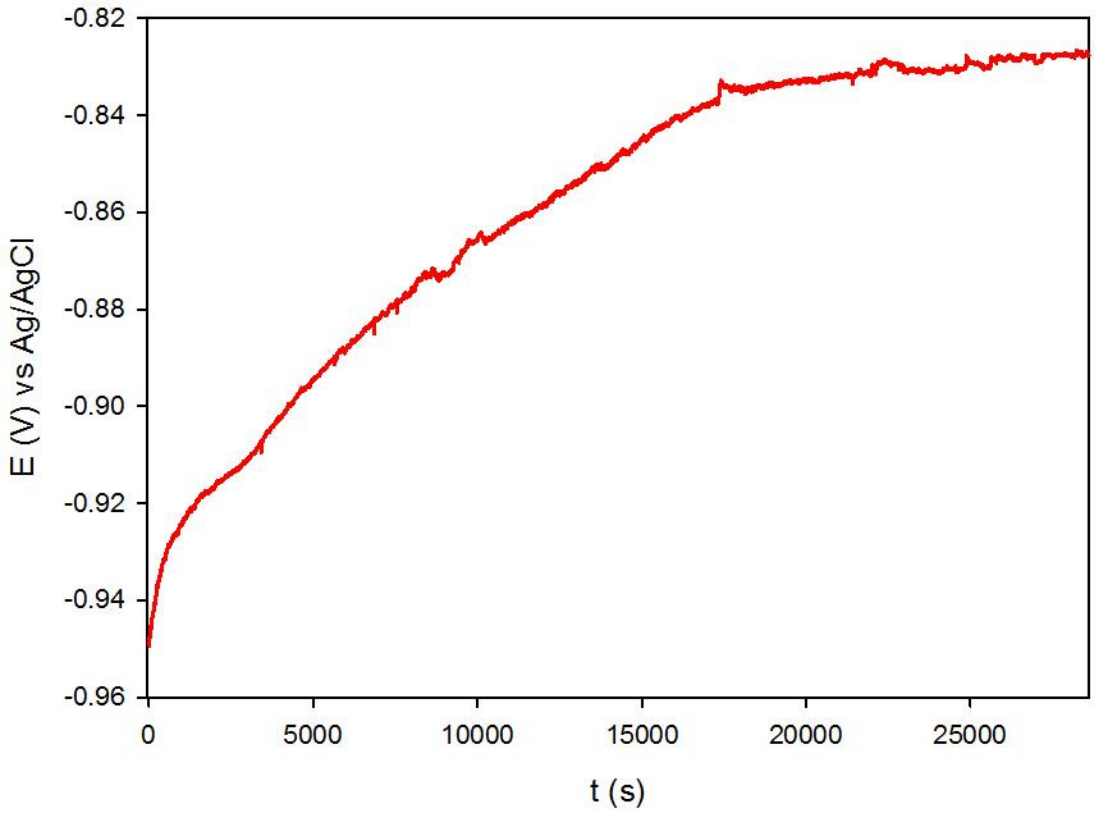

Figure 5-24: Measurement of open circuit potential of galvanized steel in 1.0 wt% oxalic acid solution at pH 2 and 25°C

For concentrations of 0.10, 0.25, and 1.0 wt%, it was noticed that during the stabilization of the potential, the measurements tended to shift towards more noble values. This trend was not observed at 0.50 wt%, where each OCP measurement exhibited a different behavior.

The PDP curves at concentrations below 0.10 wt% did not exhibit a consistent shape (Figure 5-25). At the smallest concentration of 0.01 wt%, linearity within a decade could not be observed. Then, at 0.015 wt%, a passive-like behavior was exhibited at a current density of 160 $\mu A/cm^2$. Finally, at concentration 0.07 wt%, passivation was observed by an inflection of the curve between potentials -1.0V and -0.7V. This could correspond to the formation of zinc corrosion products because the potential of the inflection corresponds to the potential of dissolution of zinc. Above this potential, active dissolution continued with a slope bigger than 80mV/dec in the anodic branch.

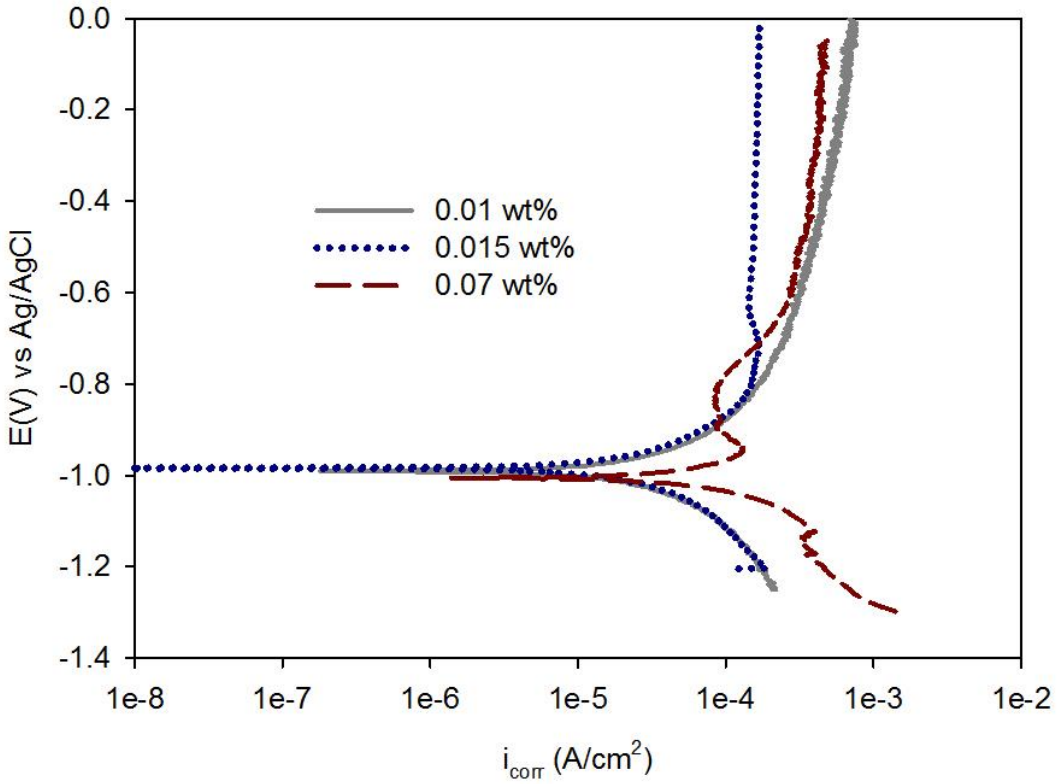

Figure 5-25: Potentiodynamic curves of galvanized steel immersed in oxalic acid solutions at concentrations below 0.1 wt% at pH 1 and 25°C

For concentrations of 0.1, 0.25, 0.5, and 1.0 wt%, the PDP curves did have a similar shape (Figure 5-26). In the anodic branches, slopes of about -10mV/dec were observed and a limiting current density could not be identified. In the anodic branch, a passive-like behavior became clearer with the vertical lines. At concentrations 0.25 wt% and 1.0 wt%, an inflection point to the right was observed that corresponded to the primary passive potentials (E_{pp}) and critical current (i_{crit}) densities after which the current decreased until the passivation current density (i_{pass}) was attained. For the 0.25 wt% solution, plotted in Figure 5-26, E_{pp} was about -0.650 V and i_{crit} 150 $\mu A/cm^2$. The corresponding values for 1.0 wt% were -0.360 V and 20 $\mu A/cm^2$. Moreover, the measured value of i_{pass} was 120 $\mu A/cm^2$ for 0.1wt%; 40 $\mu A/cm^2$ for 0.25 and 0.5 wt%; and 9 $\mu A/cm^2$for 1.0 wt%.

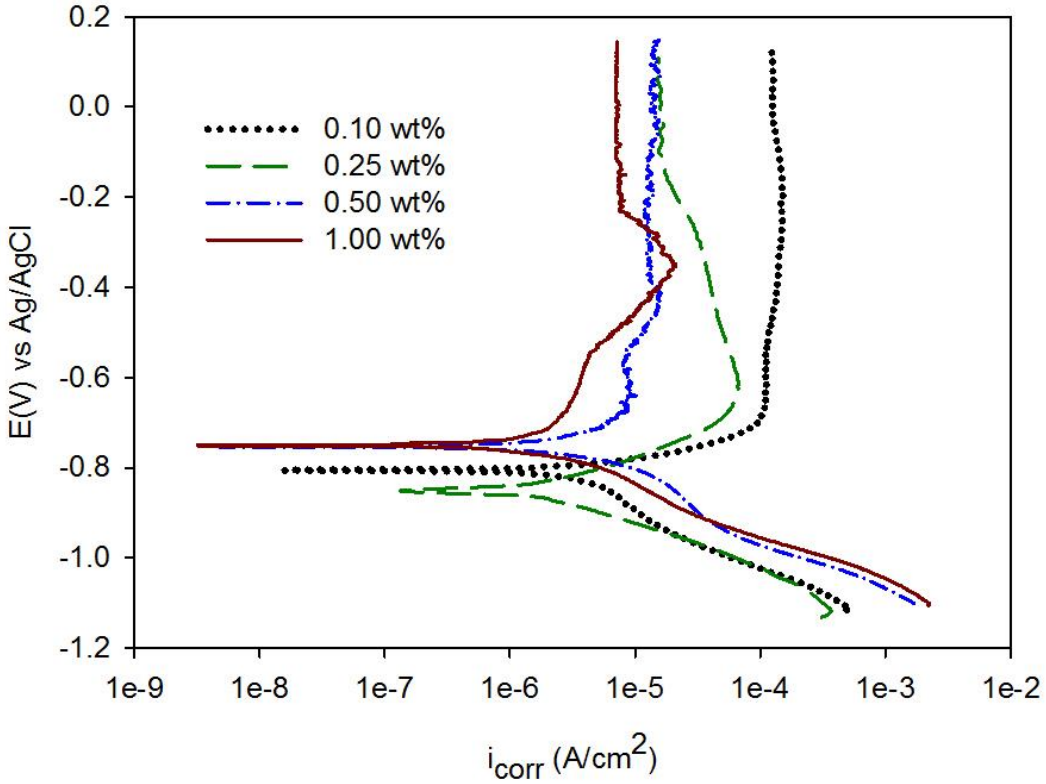

Figure 5-26: Potentiodynamic curves of galvanized steel immersed in oxalic acid solutions at concentrations between 0.1wt% and 1.0wt% at pH 1 and 25°C

The inhibition effect of oxalic acid has been reported on other metals. For example, oxalic acid has produced an inhibition of copper in dilute citric and concentrated propionic solutions at 30°C (Baah & Baah, 2000). In sulfuric acid solutions, additions of 10^{-7} to 10^{-3} M also had an inhibiting effect on carbon steel at room temperature (Giacomelli *et al.*, 2004). An increase of corrosion rates as the concentration of oxalic acid increased was observed only at the boiling point on ferritic stainless steels (Sekine & Okano, 1989).

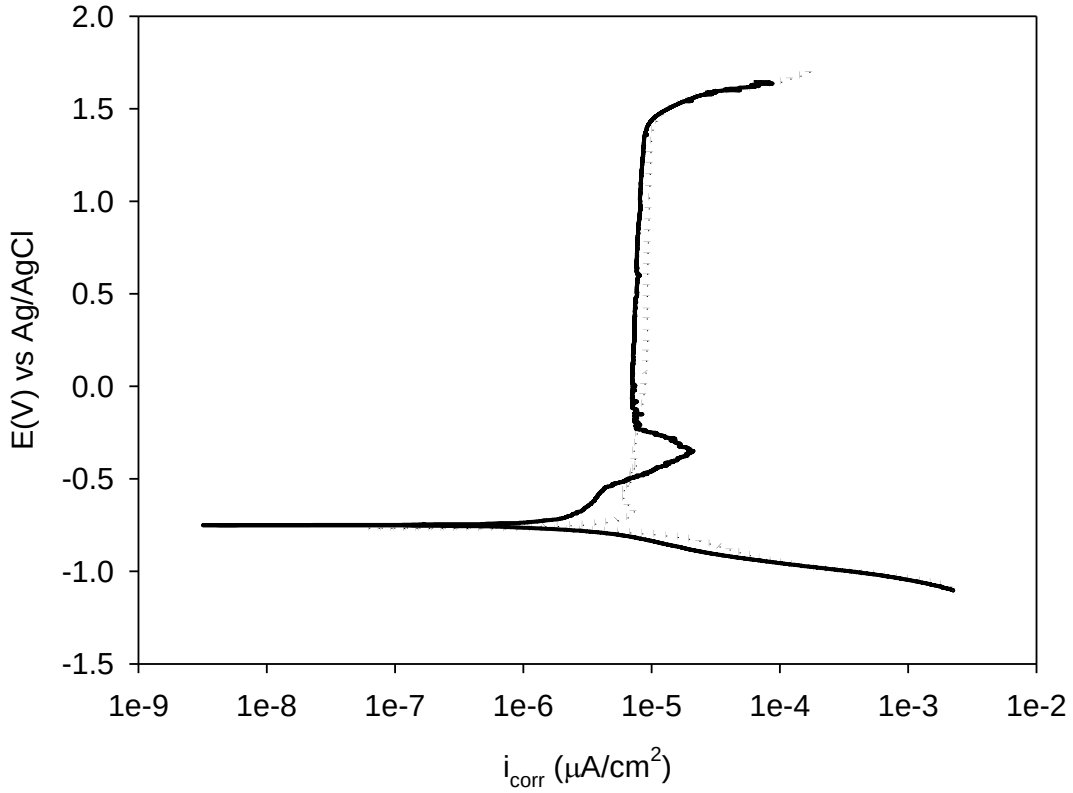

Figure 5-27: Passive-like behavior of galvanized steel immersed in 1.0wt% oxalic acid solution at pH 1 and 25°C

The passive-like behavior is desirable because it means that further corrosion of the material is being prevented. However, a risk associated with this condition is that if the passive region is trespassed and the trans-passive region is reached, pitting corrosion may occur. For this reason, additional experiments were carried out, aiming to determine the value of the breaking potential,

E_b, at which a sharp increase in the current density would be observed. Figure 5-27 shows the PDP results of two identical experiments. The sharp increase in current density was found at E_b= +1.5 V. At this potential, it is said that the material has reached the transpassive state. There are two possible explanations for the fast increase of current density. It is possible that the metal experienced severe dissolution or that another reaction took place, namely oxygen evolution (Zhang, 1996).

Table 5-5 summarizes the OCP measurements and kinetic parameters of GS in oxalic acid solutions. The increase of concentration between 0.01 and 1.0 wt% resulted in a shift of E_{corr} values towards more noble values. Three groups of corrosion potentials were observed. At concentrations below 0.1 wt%, the E_{corr}values were close to -1 V. At concentrations of 0.1 and 0.25 wt%, an increase of 100 to 150 mV was detected. Finally, at concentrations of 0.5 and 1.0 wt%, the corrosion potential values were in the order of -767 mV. The corrosion behavior in terms of current density was clear. As the concentration increased, i_{corr} decreased.

Table 5-5: Conductivity of solutions and kinetic parameters from PDP measurements of galvanized steel in oxalic acid solutions at different concentrations at pH 1 and 25°C

wt%	σ (µS)	E_{corr} (mV)	i_{corr} ($\mu A/cm^2$)
0.01	7.4 ± 0.1	-990 ± 5	73.5 ± 5.1
0.015	11.7 ± 0.3	-986 ± 2	75.3 ± 8.6
0.07	45.9 ± 1.2	-1007 ± 2	49.9 ± 43.1
0.10	61.4 ± 0.9	-847 ± 64	19.5 ± 4.4
0.25	145.7 ± 2.1	-924 ± 70	12.3 ± 9.0
0.50	282.3 ± 7.8	-757 ± 7	6.4 ± 0.5
1.00	531.0 ± 7.2	-778 ± 33	2.9 ± 0.7

5.6.2 Surface characterization of galvanized steel in oxalic acid solutions

All galvanized samples appeared covered by white deposits that could not be removed by rinsing the samples with distilled water. By visual inspection of the samples, the amount of white deposits on the surface seemed to be related to the concentration of oxalic acid in solution. SEM imaging confirmed that the surface was completely covered by a compact layer of deposits whose homogeneity was interrupted by randomly-distributed nests (Figure 5-28), which were filled with crystals that appeared to be loose (Figure 5-29). At longer exposure time, the platelets would eventually spread over the surface (Asgari *et al.*, 2009). Both the white compact layer and the nests, are characteristic of zinc corrosion products. It has been proposed that a membrane of colloidal oxyhydroxides is responsible for retaining the zinc corrosion products in the form of a compact layer and that diffusion of water into the layer, driven by high ionic strength of the solution, is responsible for bursting the membrane and forming the blisters (Weissenrieder *et al.*, 2004).

The elemental composition of the compact layer (Figure 5-30) and the crystals inside the nests (Figure 5-31) were examined by EDX. In both cases, the highest counts were found for zinc and oxygen. Therefore, the presence of zinc corrosion products was confirmed.

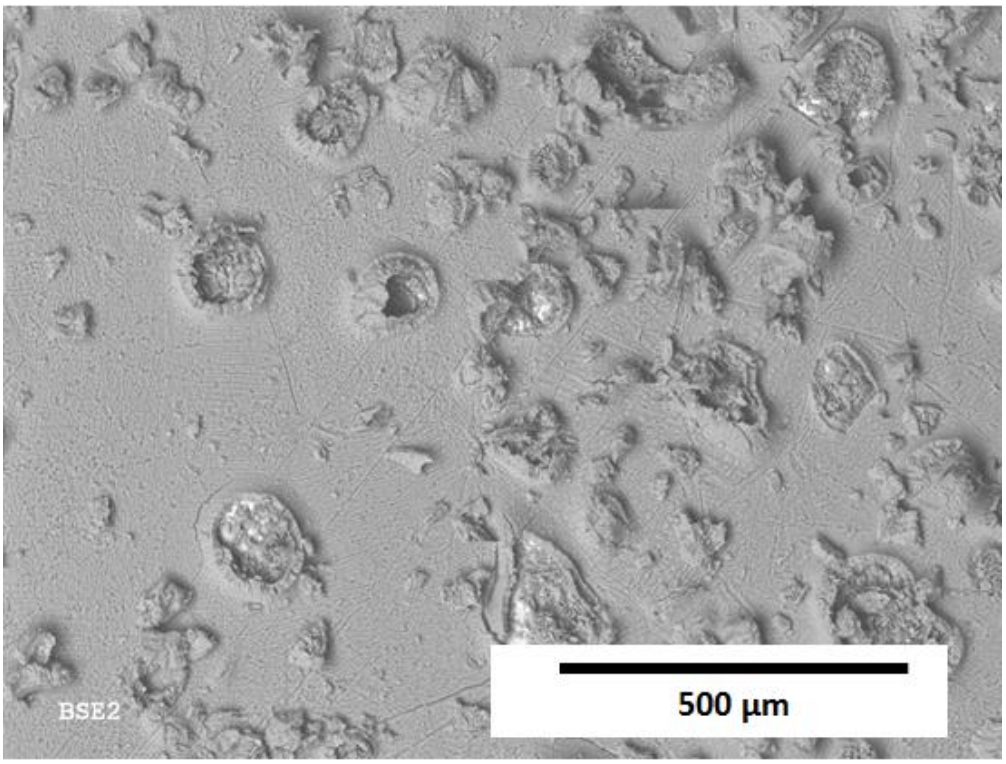

Figure 5-28: SEM image of galvanized steel after PDP in 0.25 wt% oxalic acid solution

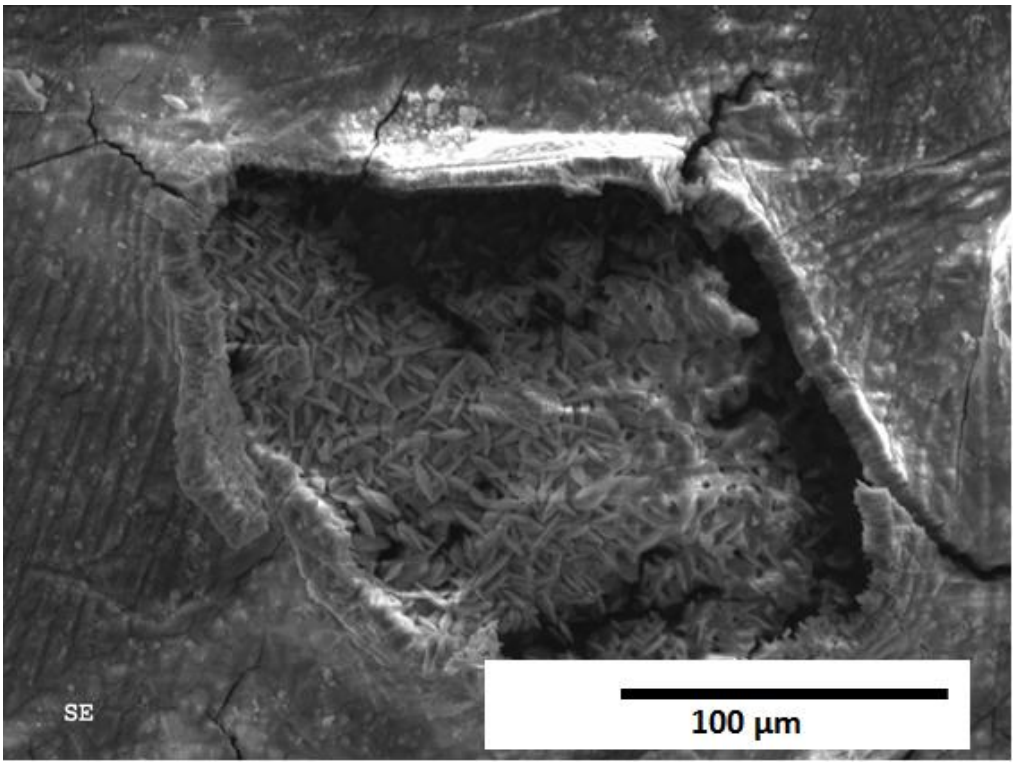

Figure 5-29: SEM image of crystals inside blisters

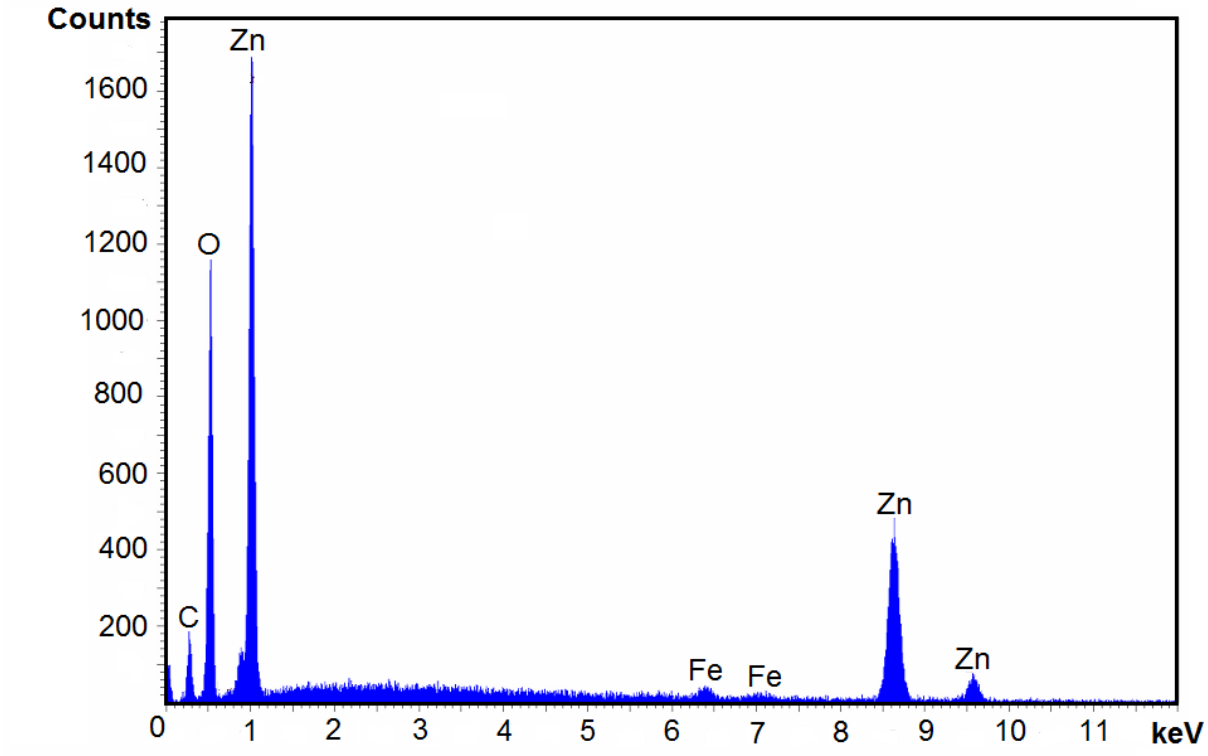

Figure 5-30: EDX analysis of compact layer

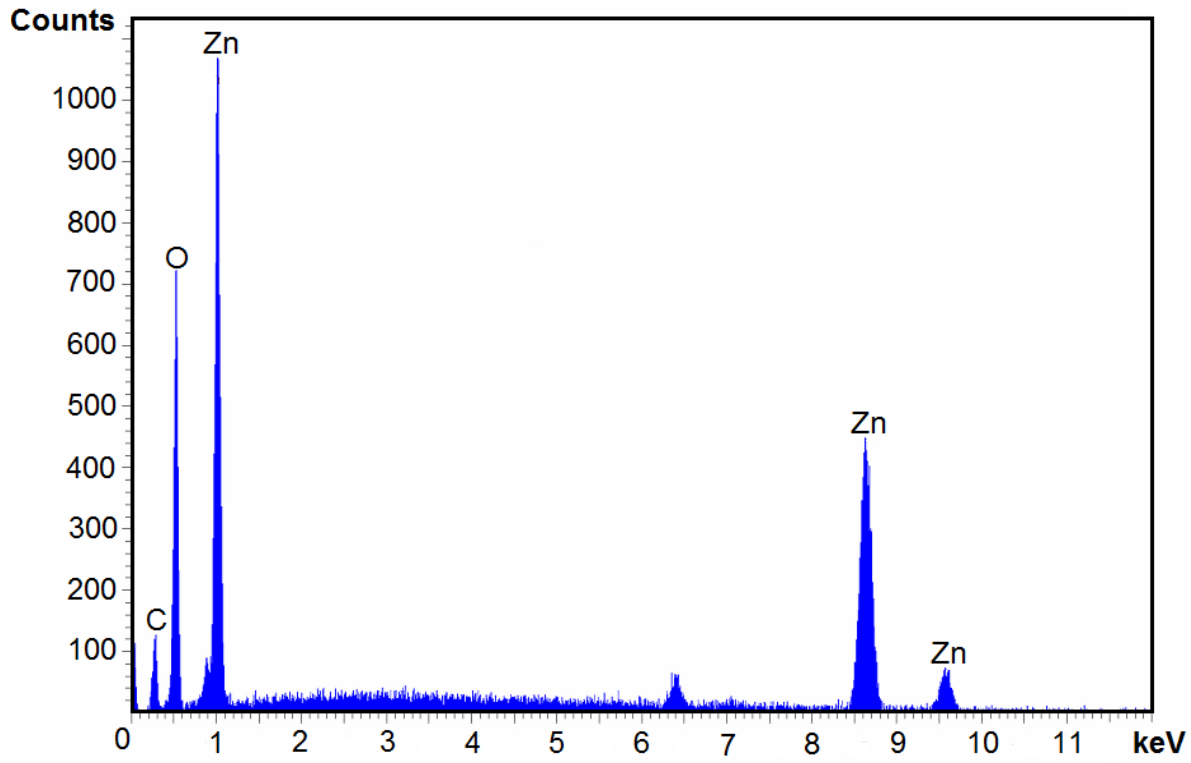

Figure 5-31: EDX of nests crystals

The ability of oxalic acid to readily dissociate into oxalates ($C_2O_4^{2-}$) and act as an excellent ligand is known and has been studied for its applicability in soil remediation (Kim *et al.*, 2013) and chemical cleaning of reactors (Borghi *et al.*, 1996). The possible pathway for the formation of metal complexes due to the interaction of oxalic acid and metal ions (Me^{a+}) has been described (Sekine *et al.*, 1990) as follows:

$$Me^{a+} + H_2C_2O_4 = MeC_2O_4^{a-2} + 2H^+ \qquad \textbf{Eq. 5-1}$$

$$MeC_2O_4^{a-2} + H_2C_2O_4 = [Me(C_2O_4)_2]^{a-4} + 2H^+ \qquad \textbf{Eq. 5-2}$$

$$[Me(C_2O_4)_2]^{a-4} + H_2C_2O_4 = [Me(C_2O_4)_3]^{a-6} + 2H^+ \qquad \textbf{Eq. 5-3}$$

Given the surface characterization, it can be concluded that the passive-like behavior observed on PDP curves of galvanized steel in oxalic acid solutions is not a passivation effect, but rather, a passive-like behavior due to the formation of a layer of zinc corrosion products that provides a physical barrier that isolates the steel from the corrosive environment, blocking the anodic and cathodic reactions. At the breaking potential, E_b, the film dissolves and the corrosion process of the metal continues.

5.7 Chlorides and sulfates

In order to provide a parameter to compare the corrosion current densities produced by the individual organics, the PDP test was also performed in solutions containing 100 ppm chlorides (0.01 wt%) and 200 ppm sulfates (0.02 wt%). As for previous solutions, OCP was also measured until a stable potential was reached. However, only the final value is reported in the summary table (Table 5-6). The curves obtained exhibited a clear limiting current density in the cathodic branch in the order of 20 to 40 $\mu A/cm^2$. In the anodic side, both had a slope of less than 50mV/dec with a sharp increase of about 600 mV in less than one decade when the current density values approached $1 mA/cm^2$. An example of the PDP curves is presented in Figure 5-32.

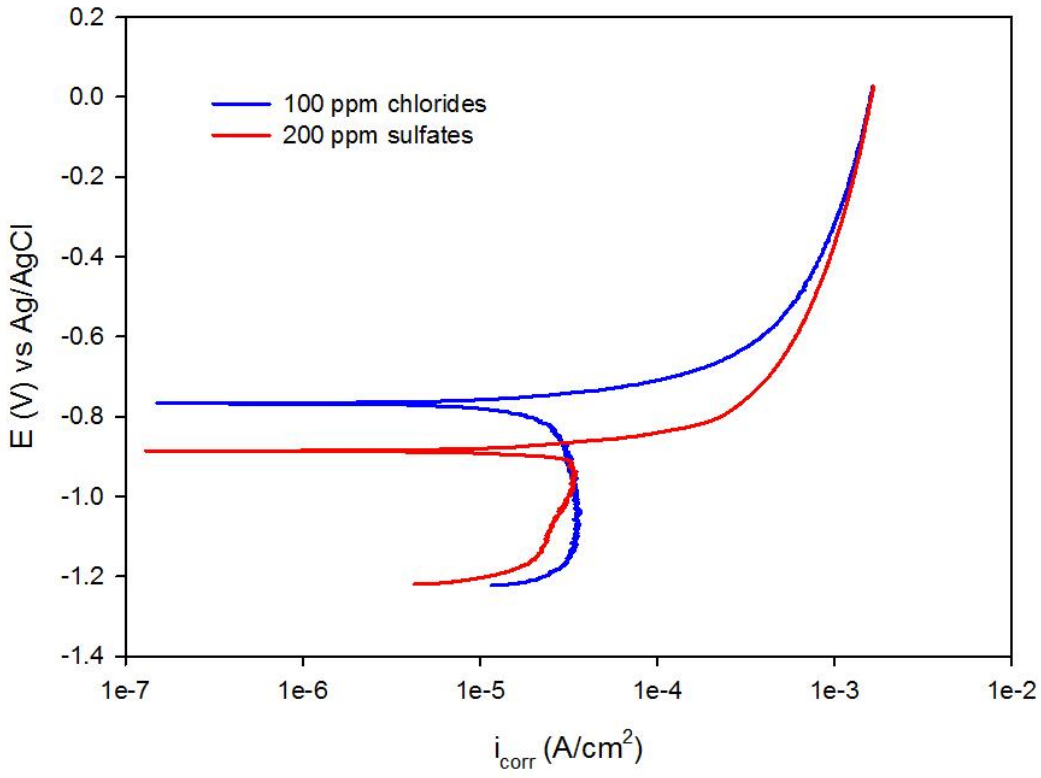

Figure 5-32: PDP curves of solutions with 100ppm chlorides and 200ppm sulfates at 25°C

All the parameters that were reported for organic solutions are also presented for these solutions in the following table. However, for comparison purposes, the i_{corr} values are of interest.

Table 5-6: Parameters of solutions with 100ppm chlorides and 200ppm sulfates and electrochemical measurements from PDP tests in 25°C

	pH	**σ (µS)**	**E_{corr} (mV)**	**i_{corr} ($\mu A/cm^2$)**
100ppm chlorides	6.6 ± 1.46	8.5 ± 0.9	-789 ± 31	30.6 ± 4.8
200 ppm sulfates	8.1 ± 3.08	10.1 ± 0.2	-872 ± 20	23.4 ± 3.1

5.8 Comparison of corrosion behavior of galvanized steel in four organic solutions

The PDP curves of galvanized steel in the four organic solutions at 1.00 wt% are compared in Figure 5-33. The samples in dextrose and oxalic acid solutions exhibited the most noble corrosion potential values of the organics studied, with similar values of -749 mV and -778 mV, respectively. In citric acid solutions the most negative corrosion potential values were measured at -982 mV. In humic acid solutions, E_{corr} was found at an intermediate potential of -824 mV. From this PDP plots, it can also be observed that, at 1.00 wt% concentration, the aggressiveness of the organics decreased in the following order: citric acid > oxalic acid > humic acid and dextrose. Also, the passive-like behavior produced by oxalic acid that was explained in section 5.5.1 is observed.

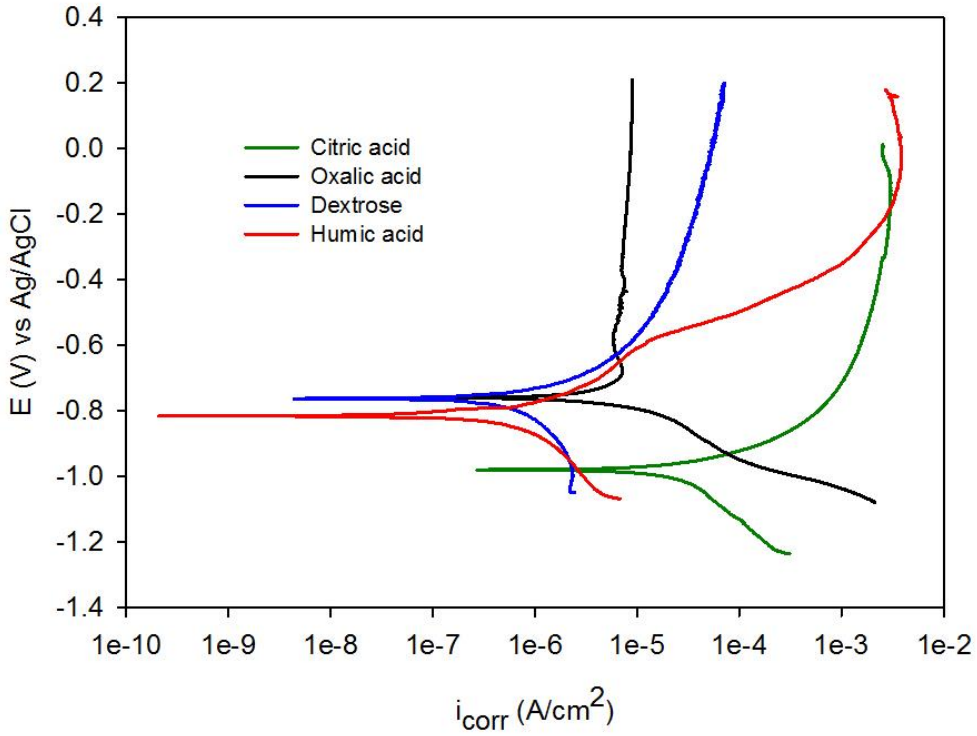

Figure 5-33: Comparison of potentiodynamic polarization resistance plots of galvanized steel immersed in 1 wt% organic solutions at 25°C

Figure 5-34 presents together the plots of the corrosion current densities (i_{corr}) produced by each organic on galvanized steel as a function of concentration for comparison purposes. It is observed that the current densities produced by dextrose do not change significantly with the concentration, as all values were inferior to 3 $\mu A/cm^2$. Humic acid produced higher current densities at low concentrations. The highest measured value with low variation was produced at 0.05 wt% with 15.3±0.3 ($\mu A/cm^2$). However, the current density decreased as the concentration increased. At 1.00 wt%, the corrosion effect was identical to that produced by dextrose. Oxalic acid produced considerably higher current densities, also at the lowest concentrations. The maximum peak was 75 $\mu A/cm^2$ reached in 0.015 wt% oxalic acid solution. At concentration

0.07 wt%, the variation in the readings was big and for higher concentrations the value of the measurements dropped with small variation.

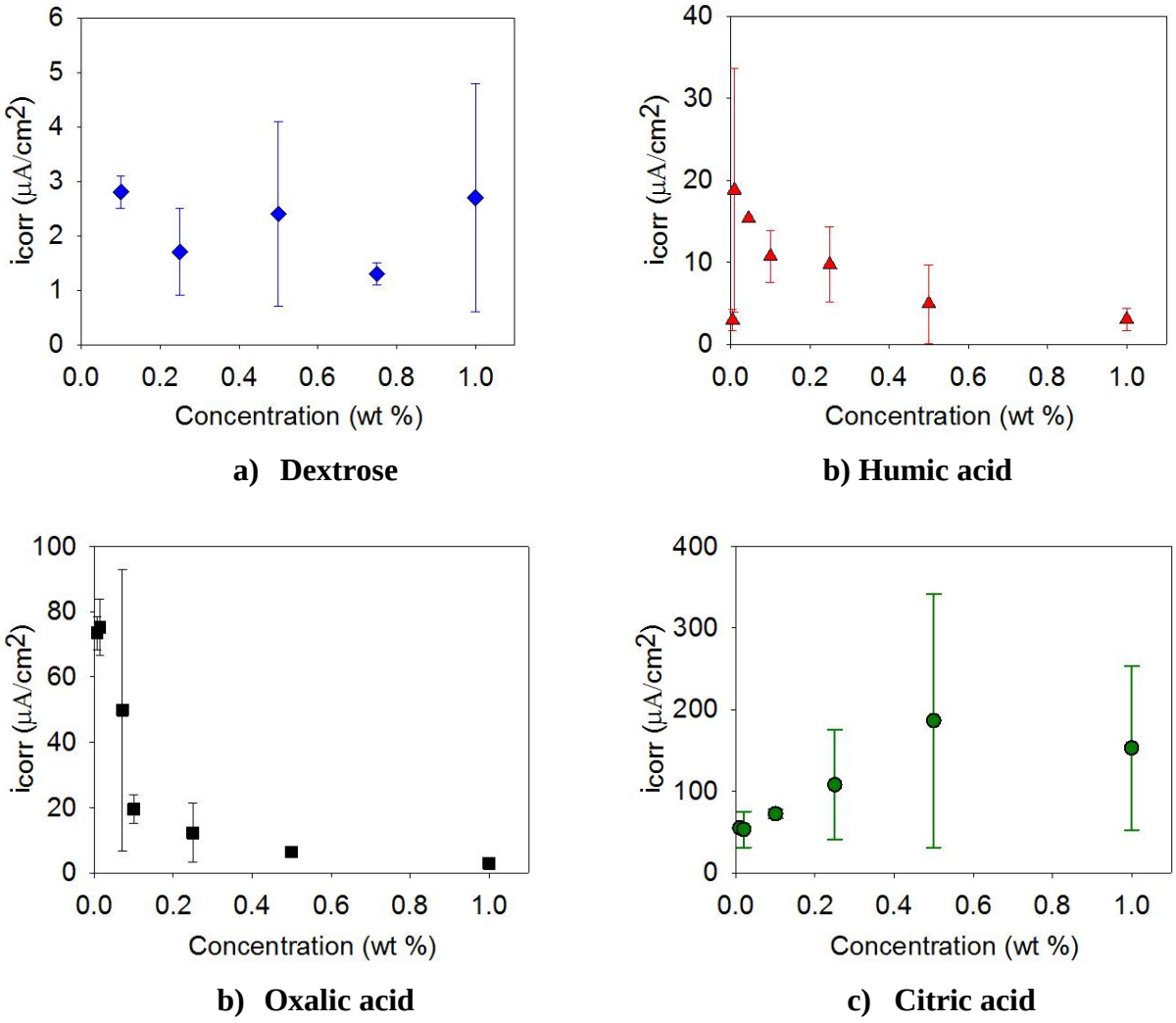

Figure 5-34: Comparison of corrosion current densities of galvanized steel as a function of concentration of individual organics in solutions at 25°C: a) dextrose; b) humic acid; c) oxalic acid; d) citric acid.

As discussed in section 5.5.2, the reason might be the formation of a compact layer of corrosion products. It is possible that the minimum concentration of oxalic acid that promotes the formation of zinc corrosion products on all the surfaces of the materials is between 0.015 wt%

and 0.10 wt%. Galvanized steel exhibited the highest current densities in citric acid solutions. Additions of citric acid resulted in an increase of the current density. The maximum value was observed at concentration 0.50 wt% that produced 187 $\mu A/cm^2$. Furthermore, comparing the current densities of organic solutions with those produced by 100 ppm chlorides and 200 ppm sulfates, it can be concluded that dextrose and humic acid are less aggressive. Nevertheless, oxalic acid can be more aggressive at concentrations lower than 0.07 wt%, while citric acid is more aggressive at all concentrations.

Given the corrosion current density, it is possible to determine the mass (*m*) that will be lost due to corrosion by Faraday's law (Eq. 5-4), where *i* is the current density, *a* is the atomic mass, *n* is the number of electrons transferred and *F* is Faraday's constant.

$$m = \frac{ia}{nF} \qquad \textbf{Eq. 5-4: Faraday's law}$$

From Faraday's law the following expression is obtained that directly relates the corrosion current densities to penetration rates (*r*), in which *c* is a conversion constant equal to 3.27 to obtain r in micrometers per year (μm/yr) and *D* is the density of the material in g/cm^3.

$$r = c\frac{a \cdot i_{corr}}{nD} \qquad \textbf{Eq. 5-5}$$

For the samples used in the experiments, the i_{corr} values most likely correspond to the first stage of the corrosion of galvanized steel where only the zinc coating is corroding because the i_{corr} is obtained from PDP at potentials before an increase in the anodic reaction rates is induced. Under this consideration, the atomic weight of zinc (65.38 g/mol) and the density of zinc (7.14 g/cm^3) can be replaced in Eq. 5-5 to produce the plot in Figure 5-35 that presents graphically

the conversion between i_{corr} in $\mu A/cm^2$to penetration rates (r) in μm/yr. In this figure, various conversion points are indicated, that correspond to the highest corrosion rates produced by each organic.

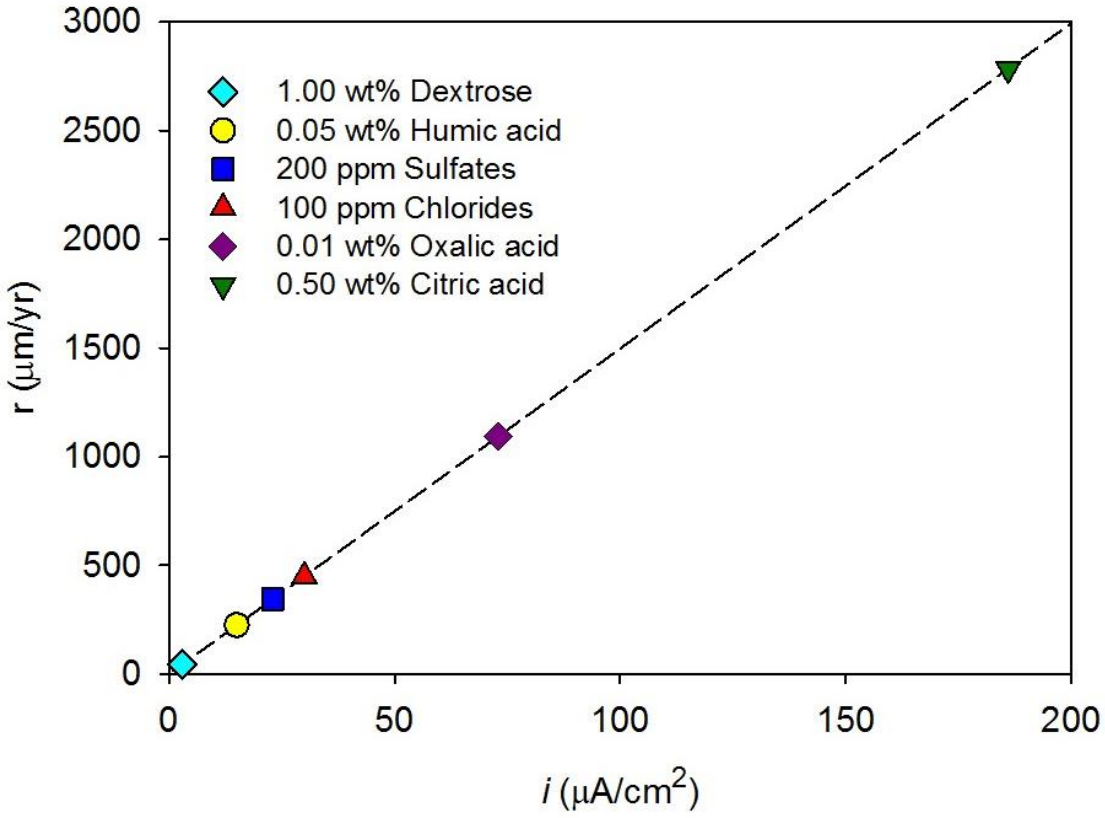

Figure 5-35: Conversion from i_{corr} values in $\mu A/cm^2$to penetration rates (r) in μm/yr.

Dextrose produced similar i_{corr} independently of concentration, with values close to 3 $\mu A/cm^2$, which corresponds to 45 µm/yr. The highest i_{corr} due to humic acid was 15 $\mu A/cm^2$, produced at concentration 0.05 wt%, is equivalent to 225 µm/yr. Similarly, i_{corr} of 23 and 30 $\mu A/cm^2$ due to 100ppm chlorides and 200ppm sulfates are equal to 344 and 449 µm/yr, respectively.

Likewise, the 73 $\mu A/cm^2$ obtained in 0.01 wt% solutions of oxalic acid, are equal to 1093 µm/yr and the 186 $\mu A/cm^2$ from 0.50 wt% citric acid solutions, to 2785 µm/yr.

A possible relationship between the corrosion current densities (i_{corr}) and the pH of the organic solutions was considered regardless of the concentration (Figure 5-36).

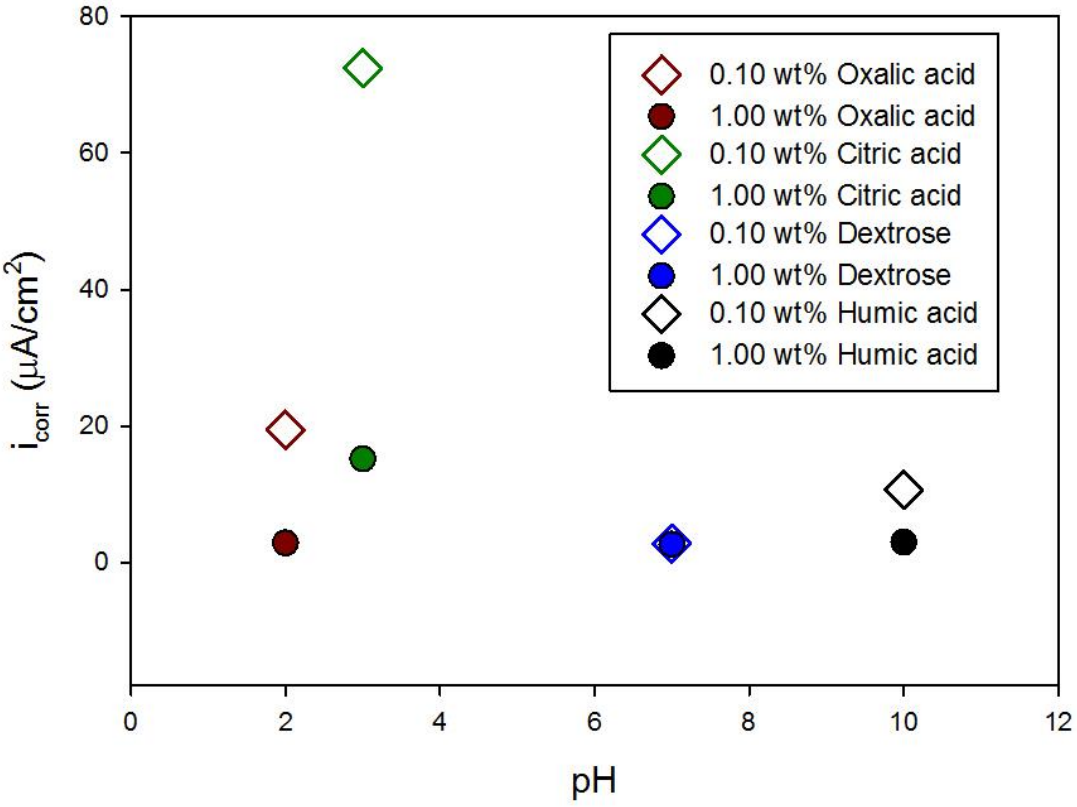

Figure 5-36: Corrosion current densities at different pH values.

The pH did not seem to have a significant impact on the i_{corr} values as is observed in Figure 5-36 by looking at the dots that represent the values obtained at concentration of 1.00 wt% for all organic species. Independently of the pH, the i_{corr} had values between 3 and 20 $\mu A/cm^2$. Considering the i_{corr} at different pH of the organics at concentration 0.10 wt% the

range of values becomes larger. However, taking the citric acid as example, it appears that the concentration has a higher effect on the i_{corr} than the pH.

Similarly, the possible relationship between current densities and conductivity was considered. In Figure 5-37 each of the four dots of each organic represents a different concentration but the values are not detailed because the objective of this plot is to focus solely on i_{corr} and σ.

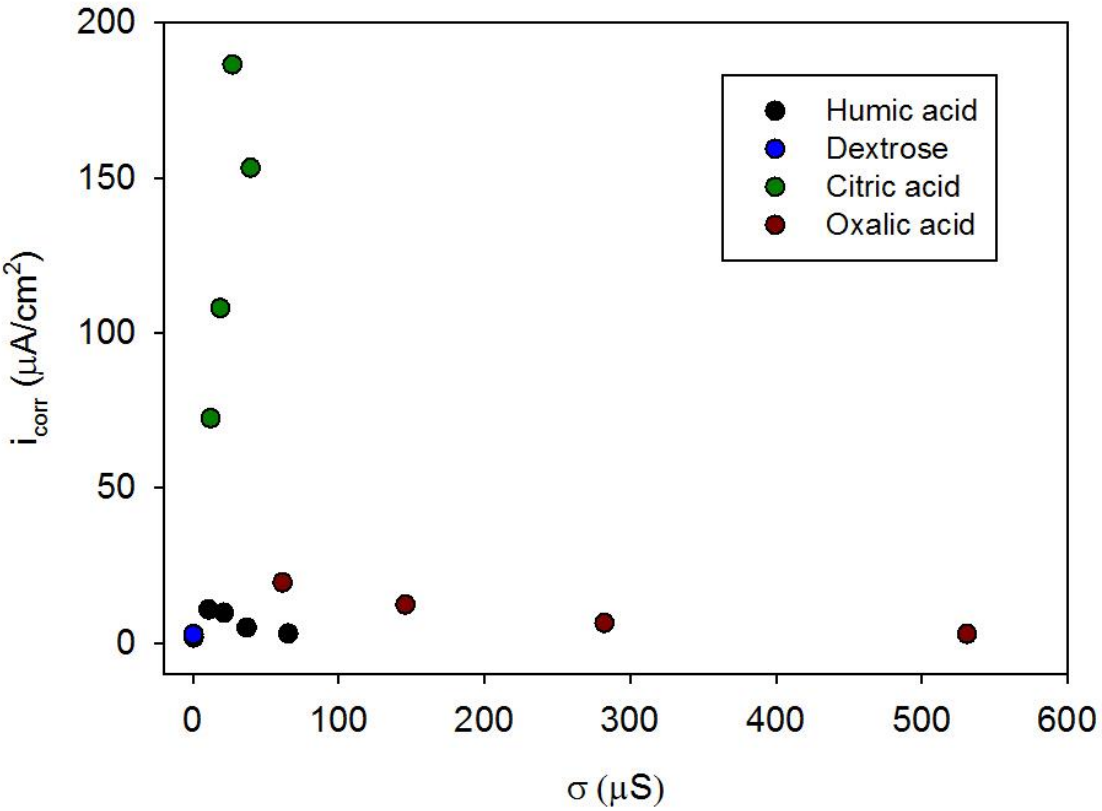

Figure 5-37: Corrosion current densities and conductivity of organic solutions.

It is observed that on one hand, while the conductivity of citric acid varies in a small range, from 12 to 39μS, the i_{corr} values increases from 72 to 186 $\mu A/cm^2$. On the other hand, while the conductivity of oxalic acid spans in a large range, from 61 to 531 μS, the variation of i_{corr} is relatively small, going from 19.5 to 3 $\mu A/cm^2$. Therefore, the trend of the citric and oxalic acid

demonstrate that the relationship between i_{corr} and conductivity is non-existent. So, even though the conductivity measurements may provide an indication of the aggressiveness of the electrolyte, it does not provide sufficient information to predict the corrosion behavior of a material.

5.9 Summary

The corrosion potential (E_{corr}) and the current densities (i_{corr}) of galvanized steel in four organic solutions were obtained for concentrations ranging from 0.1 wt% to 1.0 wt%, from the potentiodynamic polarization curves. The increase of concentration of citric acid in solution was accompanied by an increase of current densities, while the opposite effect was observed for oxalic acid and humic acid, for which, as the concentration increased, the current densities decreased. This trend was not expected for oxalic acid because higher concentrations of it produced a higher conductivity. However, oxalic acid promoted the formation of a protective layer of zinc corrosion. In the case of glucose, the concentration did not seem to have an effect on the corrosion rates.

The comparison of the maximum current densities produced by each organic in the range 0.01 wt% to 1.0 wt% allows to classify their aggressiveness on galvanized steel in the following order: citric acid > oxalic acid > humic acid > glucose.

Chapter 6: Corrosion behavior of galvanized steel in solutions of simulated soil organic matter

In this chapter, the results from PDP, LPR and EIS electrochemical tests and surface analysis performed on galvanized steel in 0.25, 0.5, 0.75, and 0.91 wt% solutions of Simulated Soil Organic Matter (SSOM) are presented. The composition of SSOM is described in chapter 4. The focus of the results is to find the polarization resistance of galvanized steel by the different methods.

6.1 pH and conductivity

The pH and the conductivity of the solutions were measured prior to performing the electrochemical tests. Both parameters increased as the SSOM concentration was increased as shown in Figure 6-1. The pH moved towards from near neutral to more alkaline values. The pH values measured for 0.25, 0.5, 0.75, and 0.91 wt% concentrations were, 6±0.2, 7.2±0.1, 8.3±0.1, and 8.8±0.3. In the same range of concentration, the conductivity also increased following this order: 15.7 ± 0.6 μS at 0.25 wt%; 26.8 ± 0.7 μS at 0.5 wt%; 37.3 ± 43.1 μS at 0.5 wt%; and 43 ± 0.5 μS at 0.91 wt%.

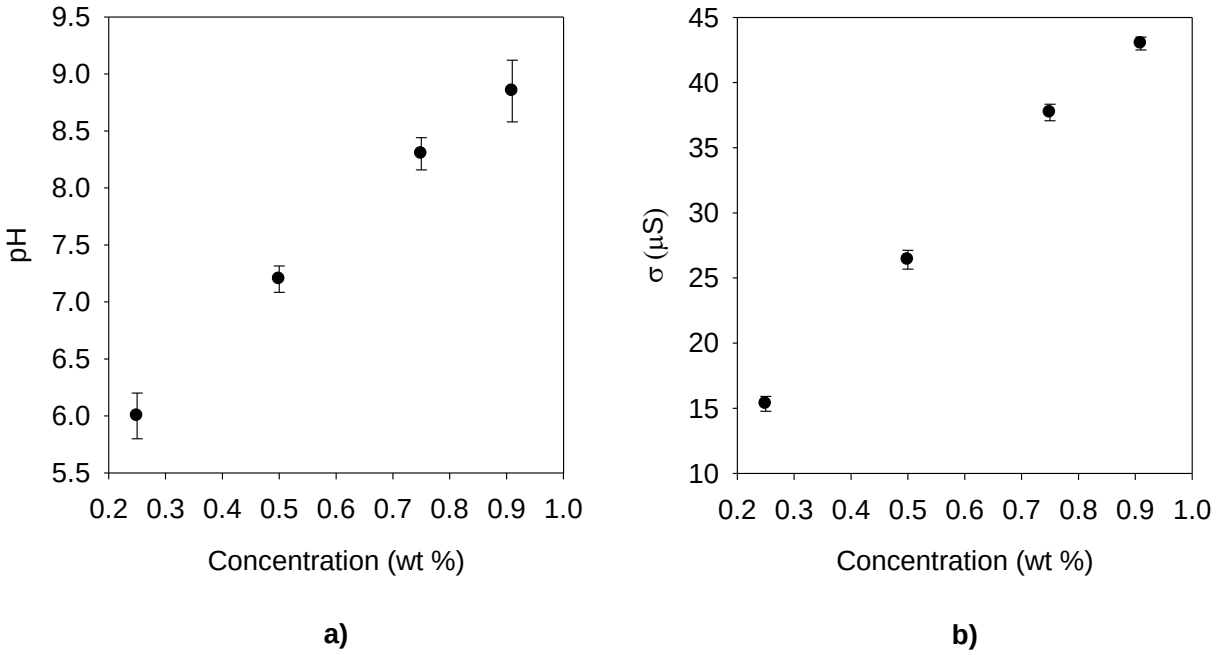

Figure 6-1: Parameters of the SSOM solutions as a function of concentration at 25°C: a) pH, b) conductivity

6.2 Electrochemical measurements

Figure 6-2 presents the PDP curves obtained. The cathodic process appeared controlled by diffusion at all concentrations with limiting current densities between 10^{-5} and 10^{-4} A/cm^2. The anodic branched of GS in solutions with 0.25, 0.5, and 0.75 wt% SSOM were very similar in shape among them, showing active dissolution of the material. However, at 0.91 wt%, the shape of the curve changed. In the anodic branch, two inflections were observed at potentials near -0.9 V and -0.3 V. These potentials correspond approximately to the standard potentials of the dissolution of zinc and iron. Moreover, at this concentration the pH was close to 9. For both metals, at this pH value, the thermodynamics favor the formation of oxides. Thus it is possible

that the decrease in the current densities at this potential was due to the formation of zinc and iron corrosion products, respectively.

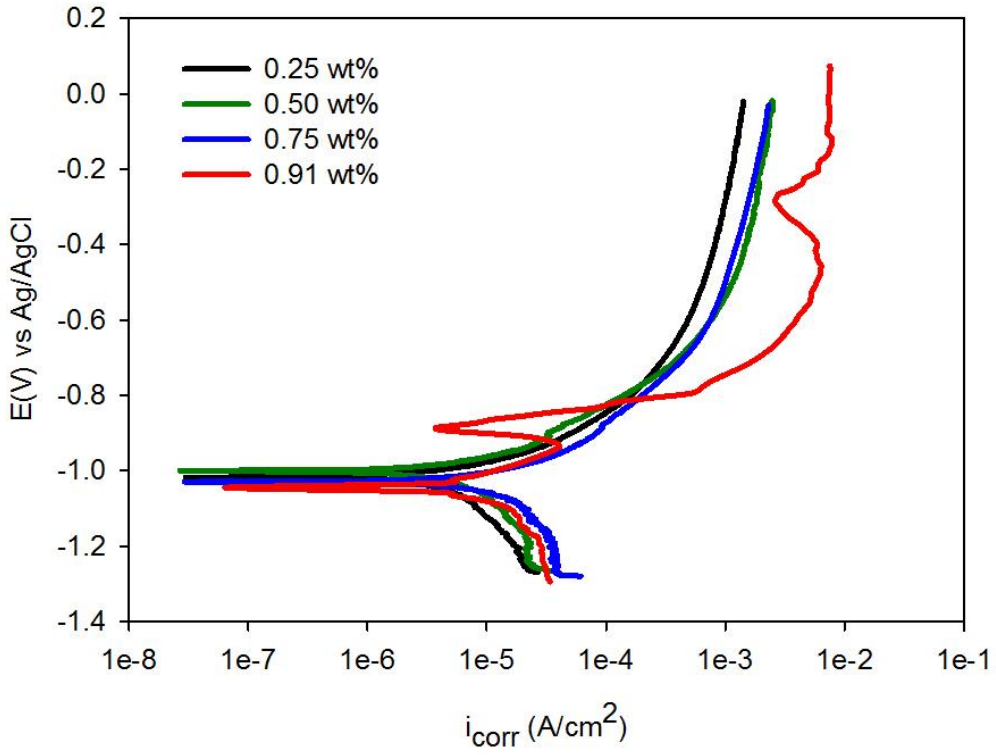

Figure 6-2: Potentiodynamic curves of galvanized steel immersed in solutions with different concentrations of a combination of organics that simulate the typical composition of soil organic matter

The corrosion potential values at each concentration are presented in Table 6-1. It can be considered that the corrosion potential was not affected by the additions of SSOM and remained close to -1015 mV. Comparing with the results presented in chapter 5, it appears that the minute additions of citric acid dragged the corrosion potential of the SSOM system to the same E_{corr} values of pure citric acid solutions.

Table 6-1: Kinetic parameters obtained from PDP curves of SSOM solutions at 25°C and concentrations from 0.25 wt% to 1.0 wt%

wt%	E_{corr} (mV)	i_{corr} ($\mu A/cm^2$)	$R_P(k\Omega)$
0.25	-1011 ± 8	28 ± 23	2.11 ± 1.11
0.50	-998 ± 3	43 ± 10	1.59 ± 0.90
0.75	-1021 ± 13	84 ± 98	1.33 ± 0.92
0.91	-1041 ± 4	81 ± 95	1.18 ± 0.56

The calculated current densities increased as the concentration increased. To put these values in perspective, the mean i_{corr} values produced by the individual organics presented in the previous chapter are reproduced here in graphic form in the concentration range between 0.25 and 1.0 wt% together with the mean i_{corr} values of SSOM presented in the table above (Figure 6-3).

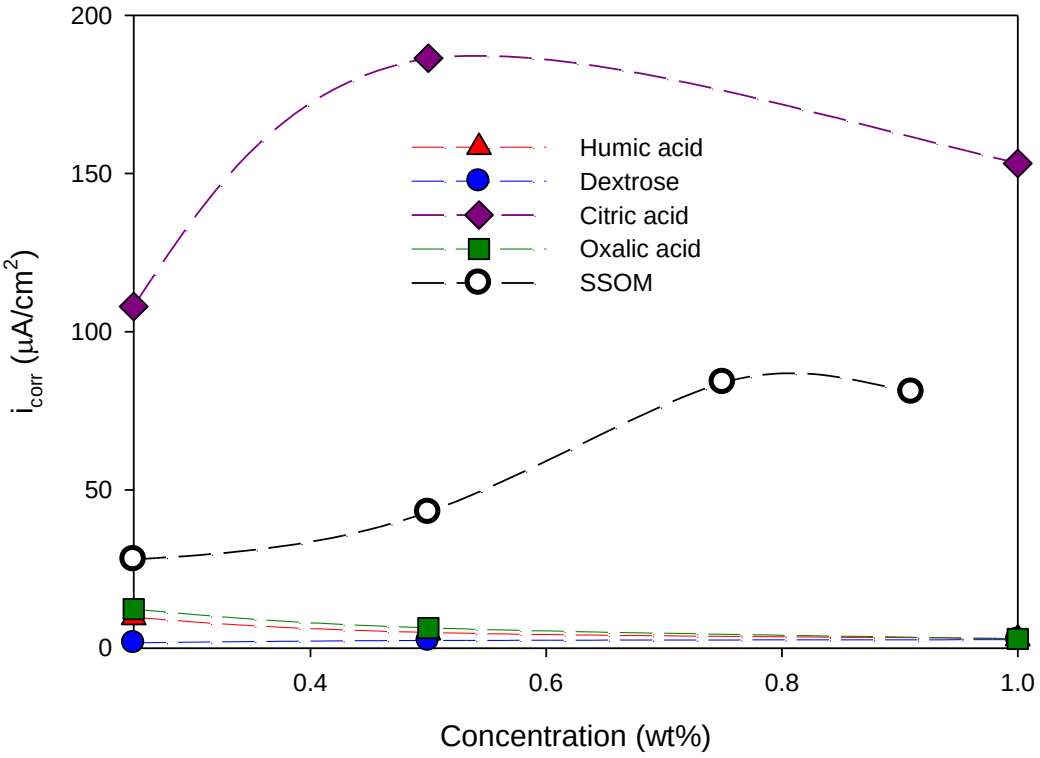

Figure 6-3: Graphic comparison of the current densities produces by individual organics and by the combination of them in SSOM solutions at 25°C

It can be seen that the i_{corr} produced by SSOM were, at all concentrations, higher than those produced by individual solutions of dextrose, humic acid and oxalic acid, but lower than those produced by individual solutions of citric acid. Moreover, at concentrations of 0.25 and 0.5 wt%, the i_{corr} was higher than the values obtained in solutions with 100 ppm chlorides and 200 ppm sulfates, indicating that under the experimental conditions, SSOM can be more aggressive to galvanized steel than chlorides and sulfates.

The high standard deviation in the i_{corr} at concentrations of 0.75 wt% and 0.91 wt% puts in evidence that it became difficult to find reproducibility of the results. At the time of performing the experiments no explanation could be found for the poor repeatability. However, it was later retrieved that the dissolution rates of humic acid particles can be increased up to 30 times in the presence of monocarboxylic acids (Brigante *et al.*, 2008). Although in these experiments the organic acids used were di and tricarboxylic acids, a possibility exist that they exhibit a similar effect on humic acid and that an incomplete dissolution of humic acid particles could have affected the results at 0.75 wt% and 0.91 wt% concentrations.

The polarization resistance (R_P) of galvanized steel in SSOM solutions was obtained from PDP results by means of Eq. 6-1:

$$i_{corr} = \frac{B}{R_P} \qquad \textbf{Eq. 6-1}$$

Where

$$B = \frac{\beta_a \cdot \beta_c}{2.3(\beta_a + \beta_c)} \qquad \textbf{Eq. 6-2}$$

The polarization resistance values were also obtained from LPR measurements by using the principle of Ohm's law.

Table 6-2: Polarization resistance at different concentrations of combined organics

wt%	R_P (kΩ)
0.25	9.0 ± 0.7
0.50	9.9 ± 0.5
0.75	7.6 ± 1.6
0.91	5.5 ± 1.2

The R_P was also obtained from EIP results. Again, good repeatability was found at SSOM concentrations of 0.25 wt% and 0.5 wt%. The measurements correspond to samples in 0.5 wt% SSOM solutions. Similarly than in PDP results, repeatability was not observed at concentrations 0.75 wt% and 0.91 wt%. One representative Nyquist plot for each concentration of SSOM solution is shown in Figure 6-4.

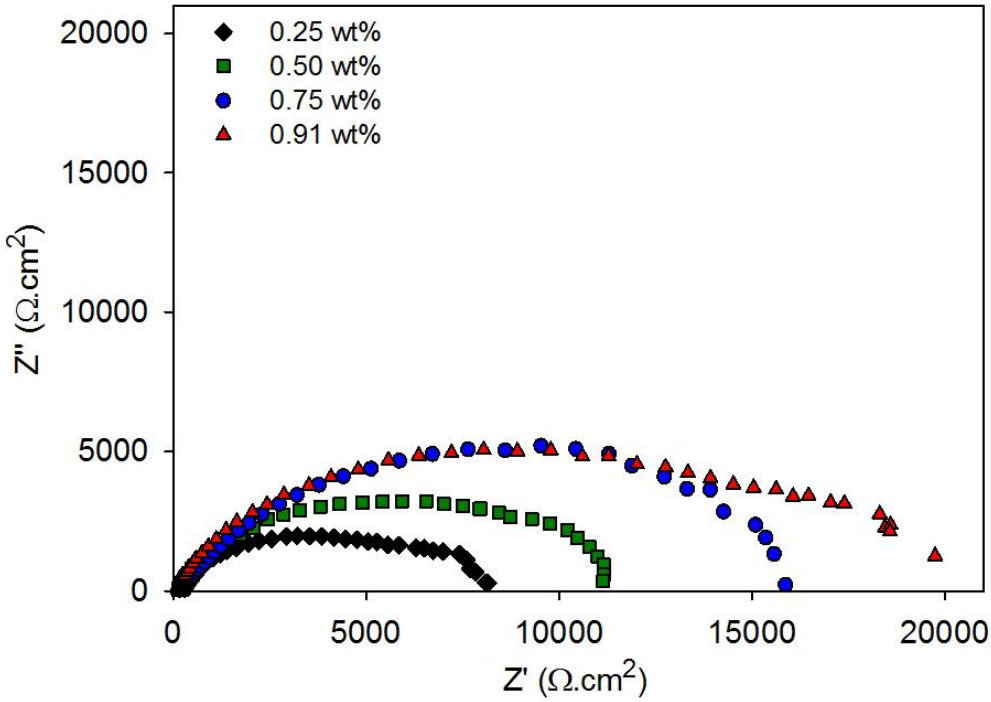

Figure 6-4: Nyquist plots of galvanized steel in SSOM solutions at different concentrations at 25°C.

It was determined that at all concentrations the data was best fitted by the response of the equivalent electronic circuit shown in Figure 6-5, with which the chi square values were in the order of 10^{-4}. This circuit represents the response of a porous layer, where Rs is the solution resistance, Re is the resistance of the electrolyte in the pore and Rp is the polarization resistance, Q1 is the capacitance due to the porous layer and Q2 is the capacitance of the double layer (ECS, 2008).

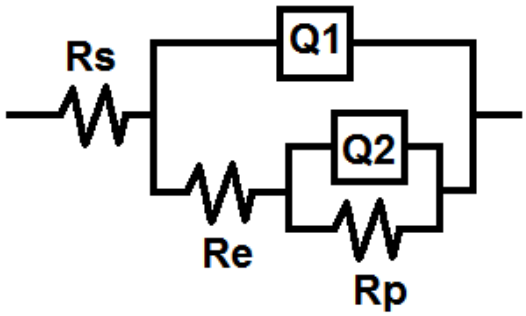

Figure 6-5: Equivalent circuit to EIS response

The parameters of the equivalent system are presented in the table below for the one test at each concentration.

Table 6-3: Parameters of the components of the equivalent circuit that simulates the frequency response of galvanized steel in SSOM solutions at 25°C

wt%	Rs (Ω)	Q1 (S.sec^n)	f power, n	Re (kΩ)	Q2 (S.sec^n)	f power, n	Rp (kΩ)	Chsq
0.25	631.000	7.365E-06	0.713	14.580	4.445E-05	1.000	2.351	5.47E-04
0.50	118.200	3.000E-06	0.800	8.190	2.366E-05	0.800	3.232	3.23E-04
0.75	252.500	4.973E-06	0.786	0.843	7.670E-06	0.517	7.699	1.22E-04
0.91	133.700	3.094E-06	0.822	8.270	1.061E-05	0.870	4.009	3.64E-04

6.3 Polarization resistance trend as a function of SSOM concentration in solution

The polarization resistance of galvanized steel obtained from three electrochemical methods (PDP, LPR and EIS) is presented graphically in Figure 6-6. The trend of the R_P calculated from PDP and LPR measurements is similar, however the values of R_P obtained from LPR are higher than the ones obtained by PDP. At concentrations of 0.25 wt% and 0.5 wt%, the values of R_P calculated from EIS were similar to R_P calculated by PDP results. At concentrations of 0.5 wt% and 0.91 wt%, the mean values of EIS were more similar to R_P obtained by LPR.

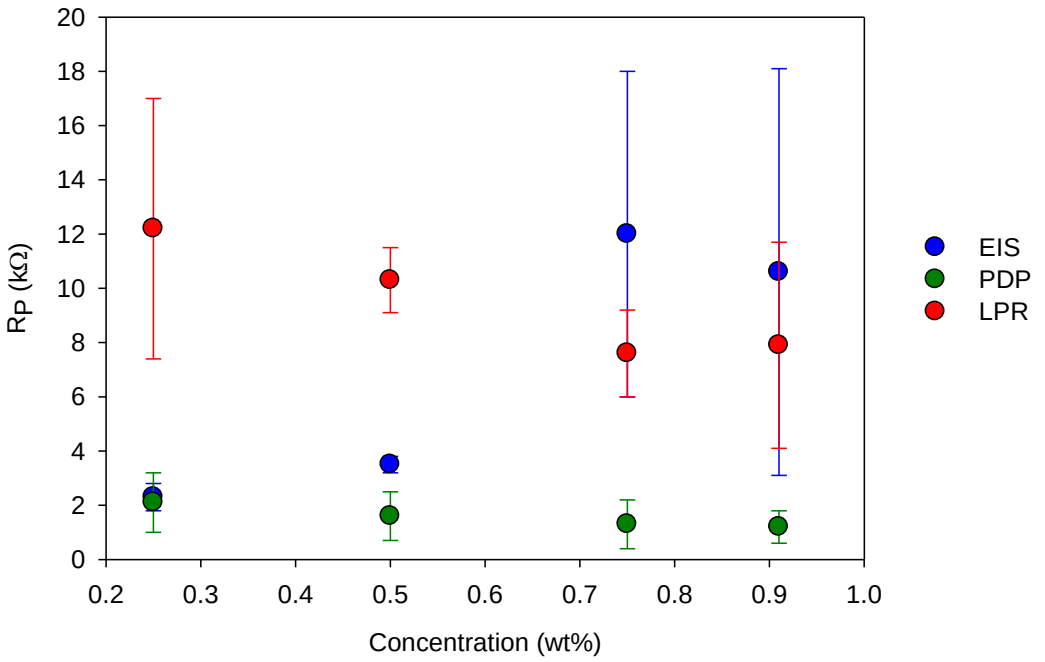

Figure 6-6: Polarization Resistance (RP) obtained by three methods with error bar plots of standard deviation

6.4 Surface characterization

By performing visual inspection of the galvanized steel samples after PDP tests at the different concentrations of SSOM, four distinct colors could be observed on the surface: dark gray, white, brown, and rusty red. These products were non-uniformly distributed on the surface of all samples exposed to SSOM concentrations of 0.25, 0.5, 0.75, and 0.91 wt% in solution. An example of the random distribution of deposits is given in Figure 6-7 where the different shades correspond to a different composition of the products formed in the presence of 0.5 wt% SSOM.

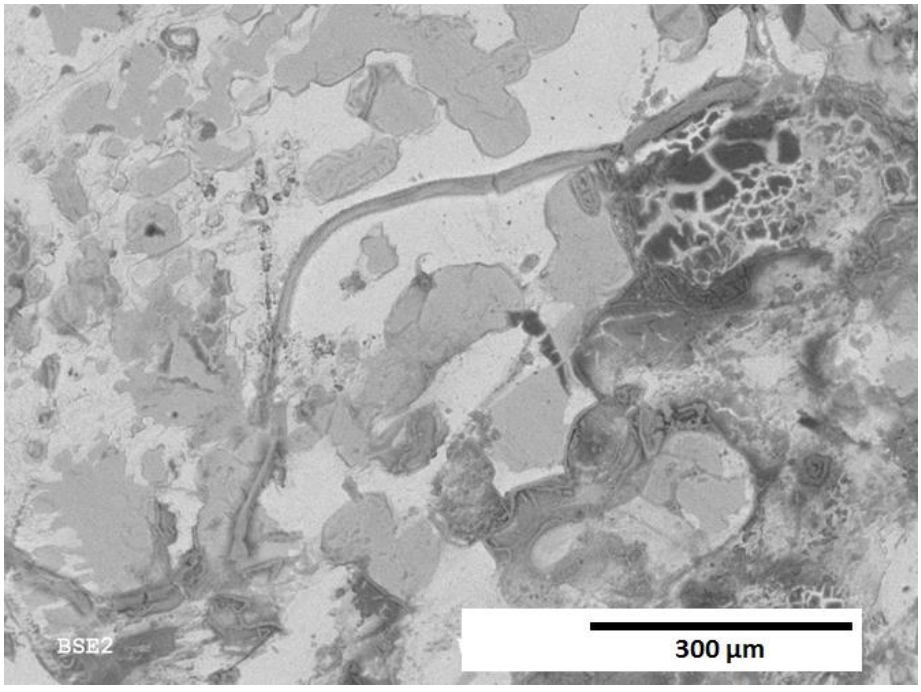

Figure 6-7: SEM image of galvanized steel after PDP in 0.50 wt% SSOM solution at 25°C

Further EDX analysis was required to identify the composition of the different types of products. For instance, in Figure 6-8, that shows another area of the surface of the sample immersed in

0.50 wt% SSOM, two different regions were identified and labeled with numbers 1 and 2. As per EDX results (Figure 6-9), the higher counts in region 1 were of zinc, showing that, in this specific area, the sample was still protected by the zinc coating. On the other hand, in region 2, the zinc coating had been completely corroded and the base steel was exposed (Figure 6-10). The absence of oxygen indicated that corrosion products were not formed.

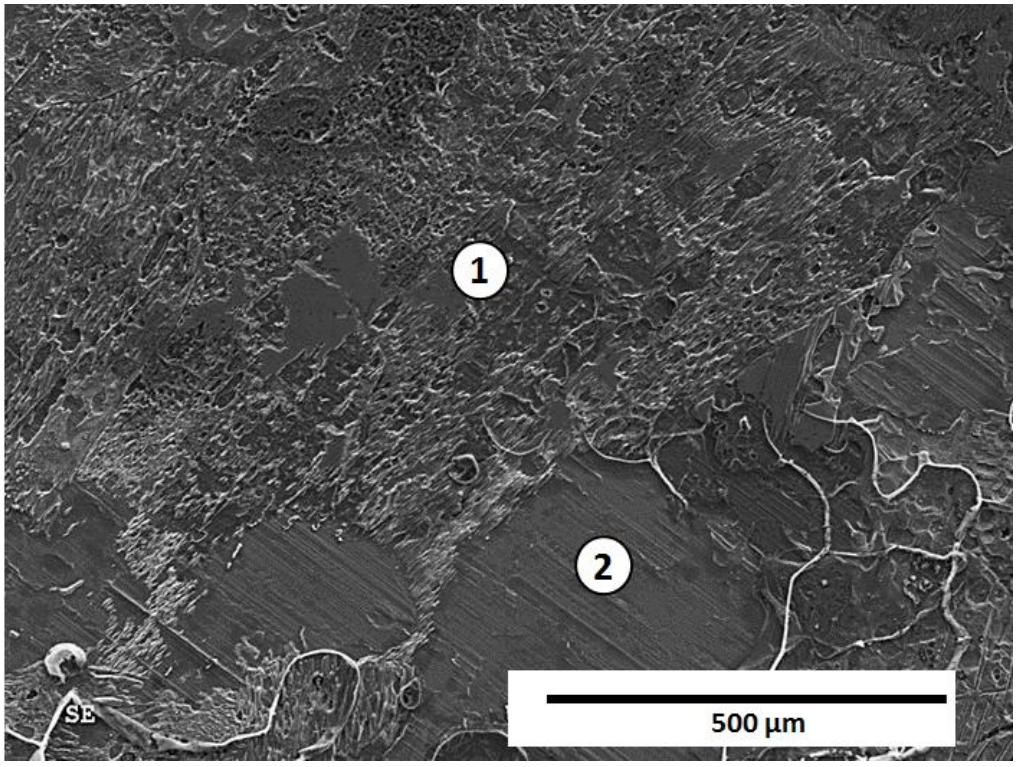

Figure 6-8: SEM image of GS sample after PDP immersed in solutions with 0.5 wt% SSOM

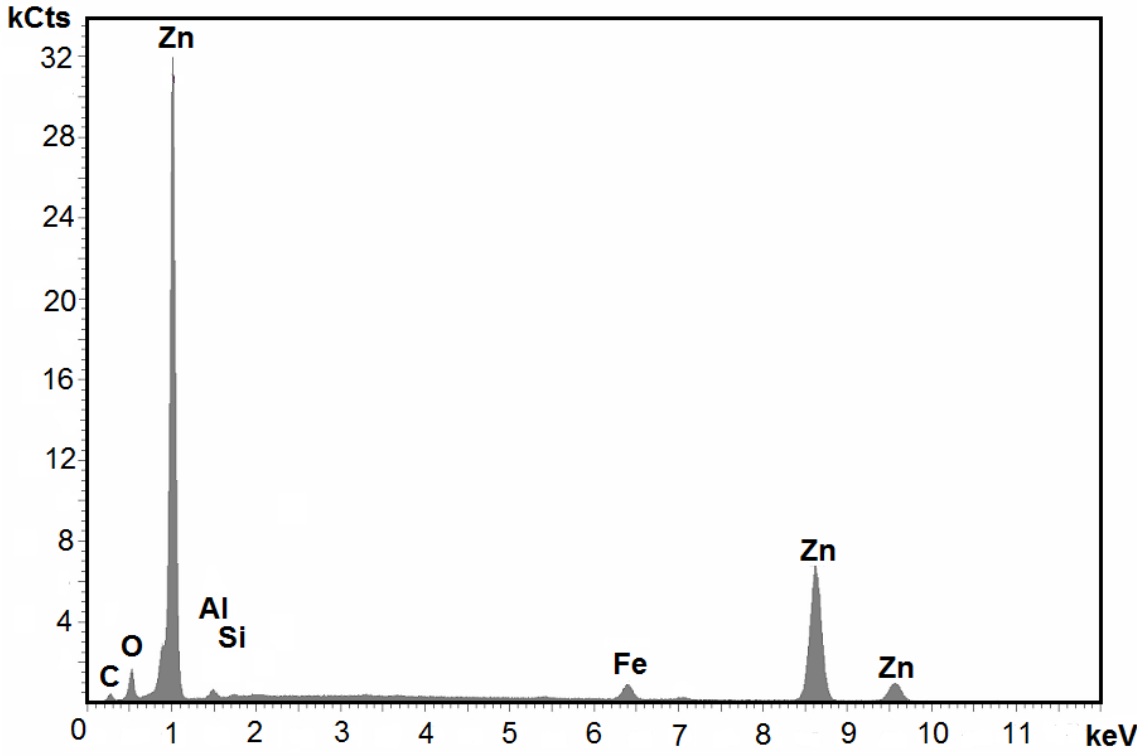

Figure 6-9: EDX analysis of region 1 from Figure 6-8

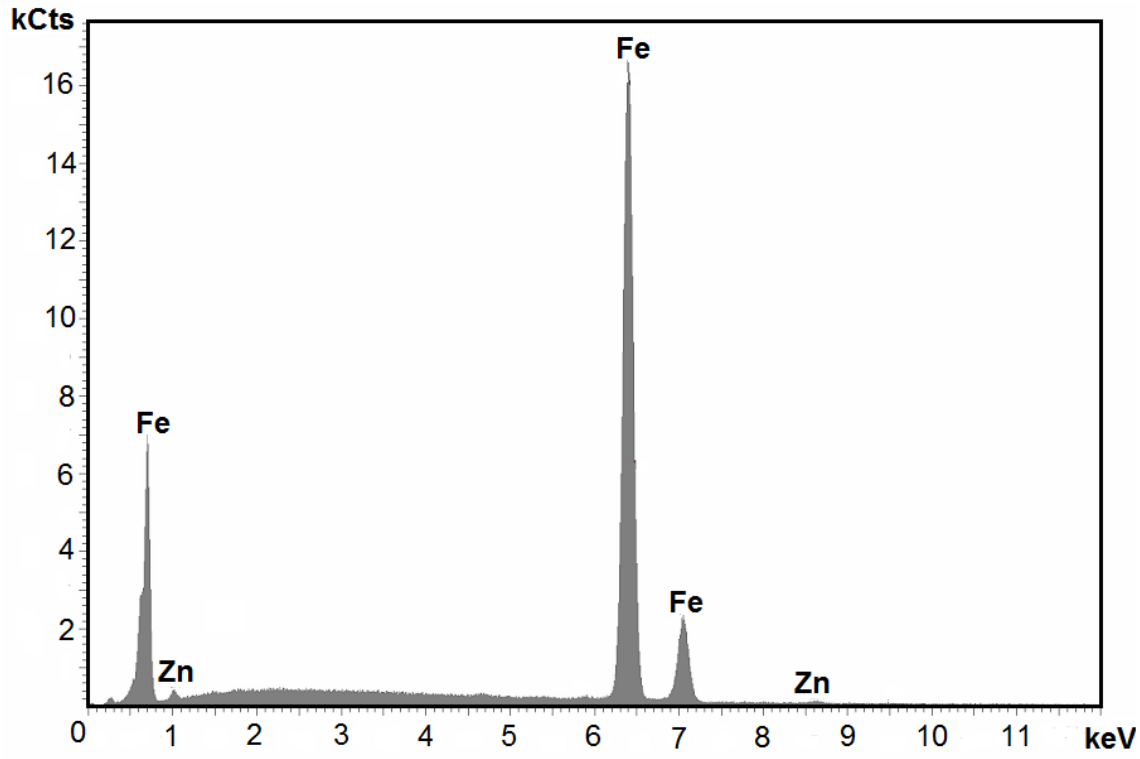

Figure 6-10: EDX analysis of region 2 from Figure 6-8

At 0.91 wt% SSOM concentration, two other regions were identified, labeled with numbers 1 and 2 in Figure 6-11. Figure 6-12 is a magnification of region 1 from Figure 6-11, where well-defined grains were observed. EDX results showed that they correspond to base steel that was exposed (Figure 6-13).

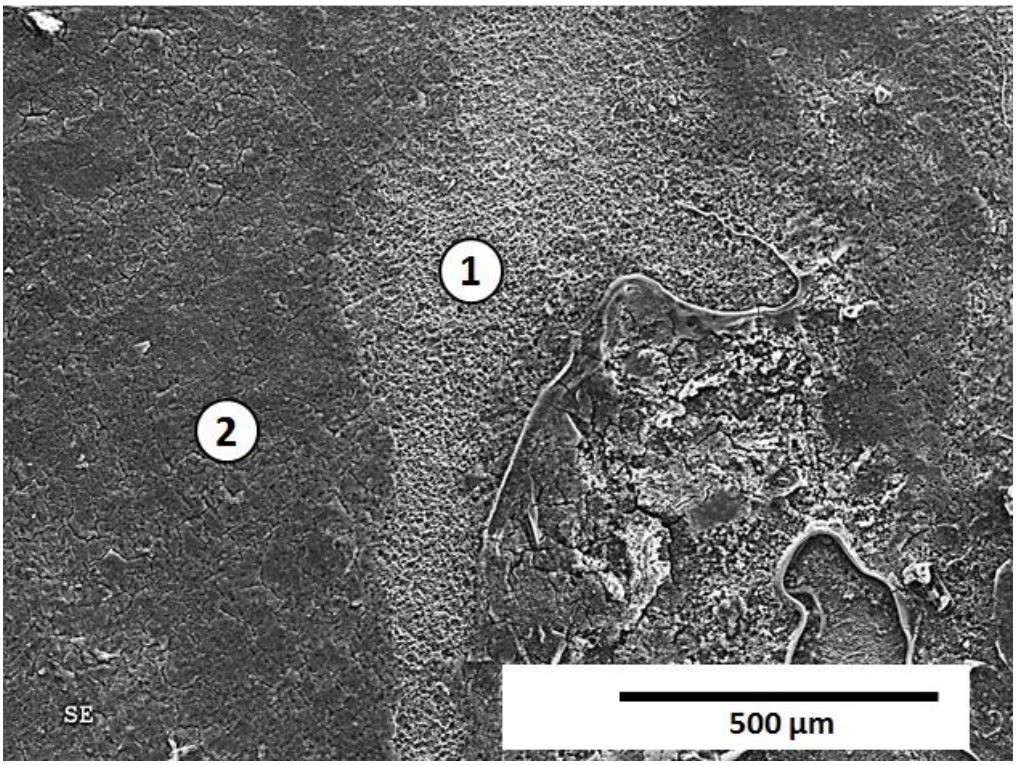

Figure 6-11: SEM image of galvanized steel sample after PDP in 0.91 wt% SSOM solution

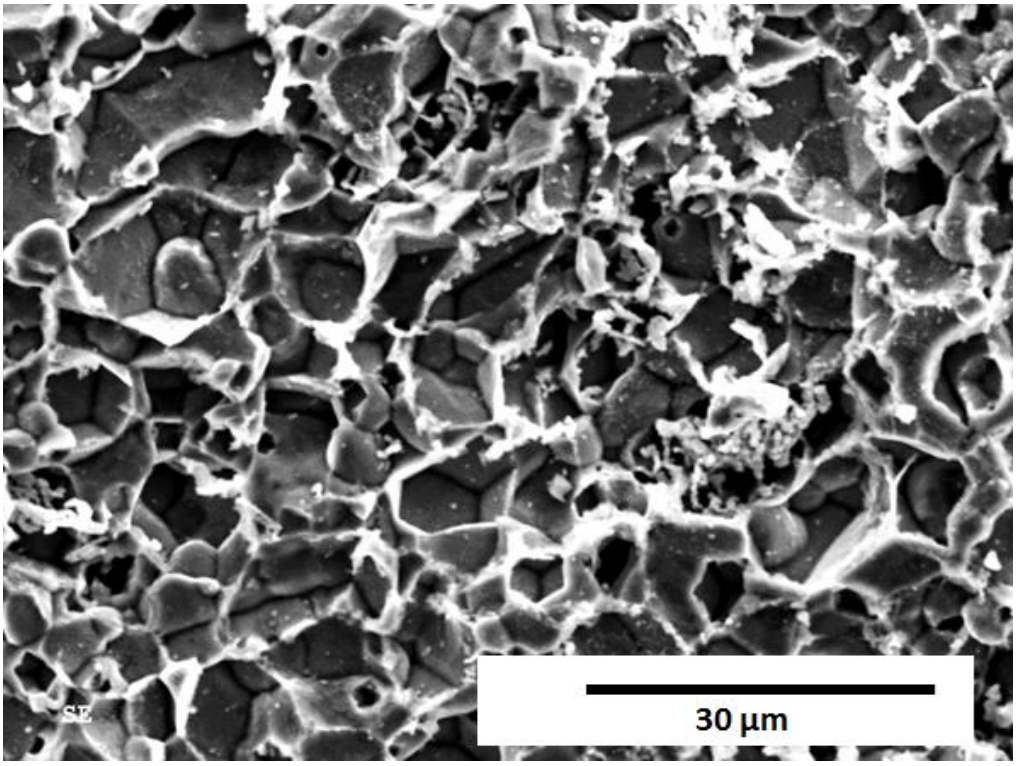

Figure 6-12: SEM image of region labeled as 1 in Figure 6-11 (0.91 wt% SSOM)

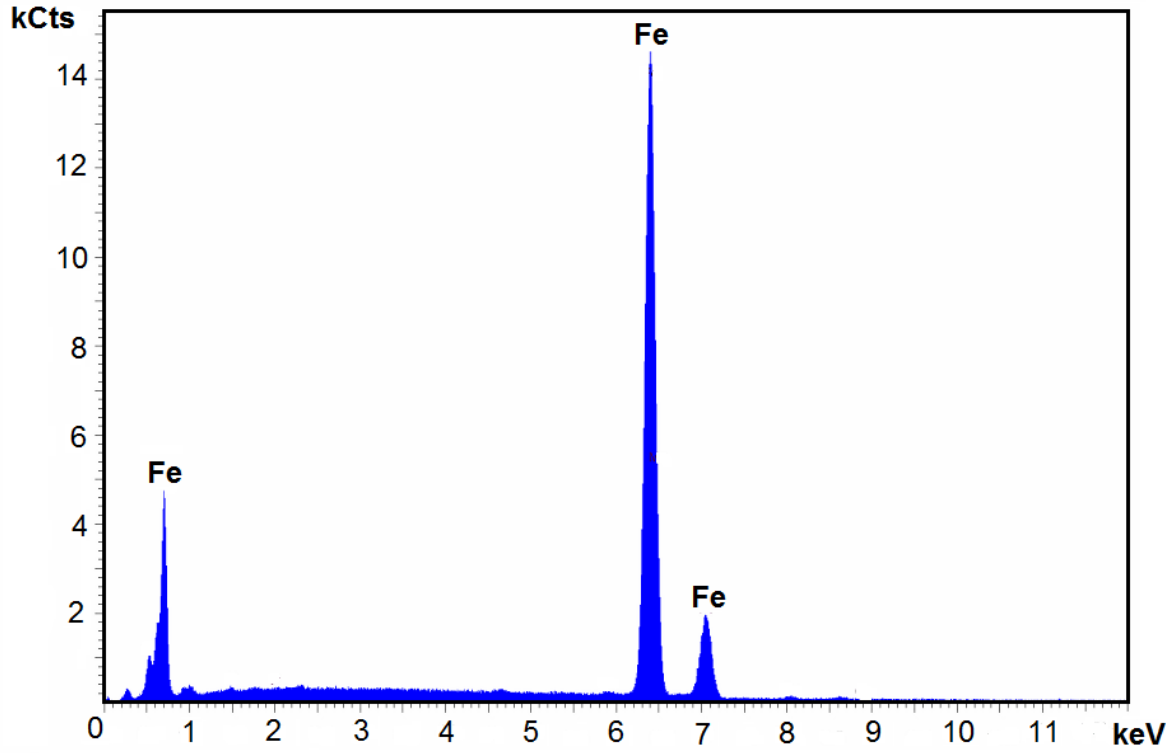

Figure 6-13: EDX analysis of region 1 of Figure 6-11

In Figure 6-14, a magnification of region 2 from Figure 6-11 is observed, in which, deposits without defined shape were observed that formed a porous layer on the surface. EDX analysis of this area (Figure 6-15) revealed that the elemental composition was iron, oxygen, and carbon.

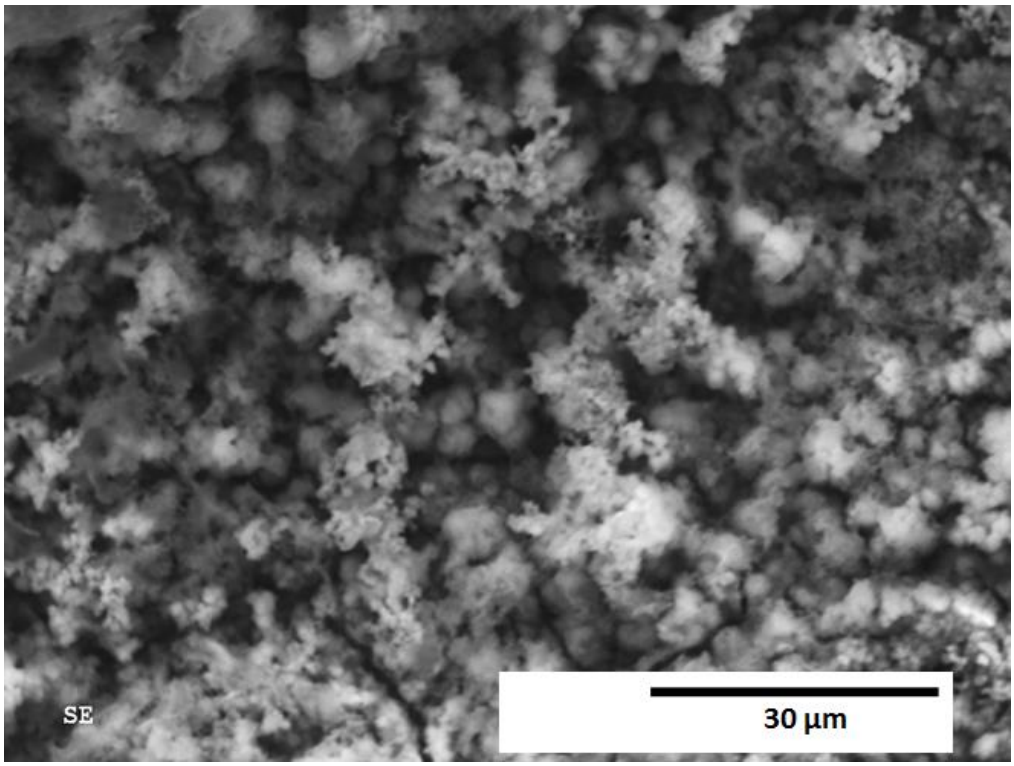

Figure 6-14: SEM image of region 2 of Figure 6-11 (0.91 wt% SSOM)

In this particular case, because the color of this area was dark brown rather than rusty red, it is speculated that the presence of iron and oxygen could correspond to the formation of metal organic complexes. For example, the formation of the metal oxalate complex $[Fe(C_2O_4)_3]^{3-}$ has been clearly identified for ferritic stainless steel in oxalic acid solutions (Sekine *et al.*, 1990).

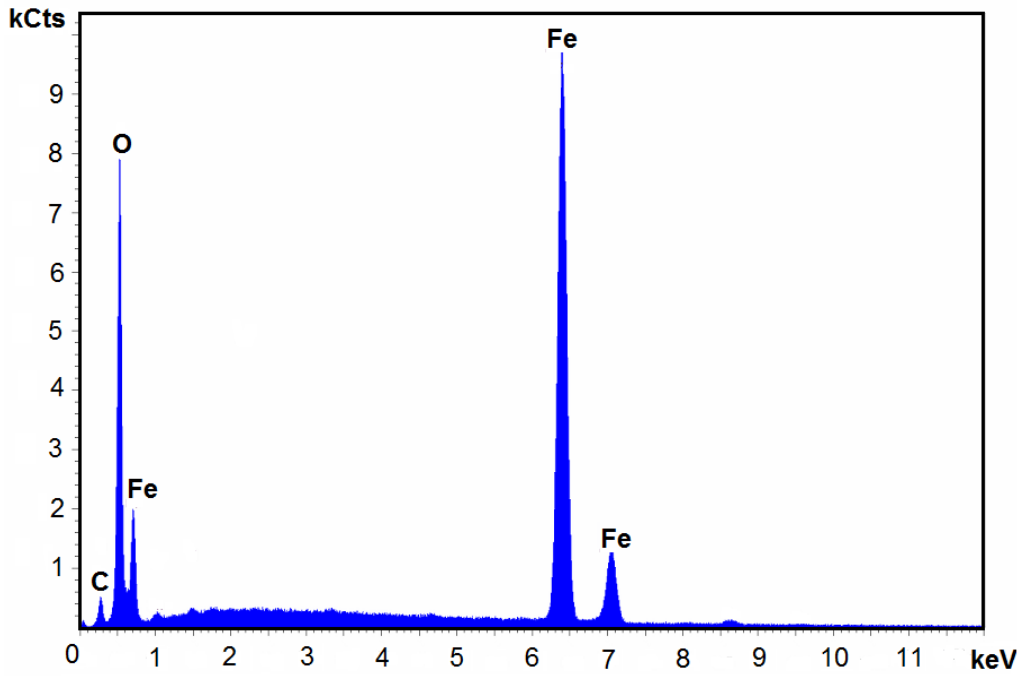

Figure 6-15: EDX analysis of region labeled as 2 in Figure 6-11

6.5 Summary

In summary, solutions with concentrations inferior to 1.0 wt% of the proposed system that simulates the typical composition of soil organic matter are capable to corrode the zinc coating and the base steel. The polarization resistance was calculated from electrochemical data obtained by PDP, LPR and EIS. A relationship between the polarization resistance of galvanized steel and the concentration of soil organics cannot be established with the given results.

Chapter 7: Conclusions

The results of the electrochemical test and the analysis presented in this thesis lead to the following conclusions:

- The corrosion behavior of galvanized steel in organic solutions at 25°C in concentrations lower than 1.00 wt% depends on the composition of the organics.
- The highest corrosion current density produced by each organic is reached at a concentration that is specific for each type of organic.
- At concentrations below 1.00 wt% of solutions of individual organics, the comparison of the highest current density produced by each organic, allows to range their aggressiveness on galvanized steel in the following order: citric acid > oxalic acid > humic acid > dextrose.
- Oxalic acid enhances the formation of a compact layer of zinc corrosion products that isolates galvanized steel from the environment and blocks the anodic reactions.
- A system of organics (SSOM) that simulates the typical composition of soil organic matter is proposed to study the corrosion behavior of galvanized steel by electrochemical techniques
- The system of combined organics produces higher corrosion rates than the individual organics at concentrations lower than 1.00 wt%
- SEM analysis and EIS results confirm the formation of a non-protective porous layer in SSOM solutions at concentrations lower than 1.00 wt%.

Chapter 8: Future work

- Perform further experiments in dextrose solutions, to confirm if the results found in this thesis correspond or not to the exchange current density of dextrose.
- Increase the concentration range of SSOM solutions and improve the repeatability of the results in order to identify a trend in the polarization resistance as a function of concentration that can be used in the form of an equation that can be incorporated in the numerical model that has been previously developed to estimate the remaining service life of MSE walls.
- Focus the next part of the investigation of the role of organics on the effect that they may produce on iron only to complement the results from this thesis, which focused mostly on the effect produced on zinc.
- Analyze the organic composition of backfill soil used in the construction of MSE walls to validate that the proposed Simulated Soil Organic Matter is a suitable system to conduct experiments to characterize the corrosion behavior of galvanized steel in the presence of soil organics.
- Conduct long-term corrosion tests of galvanized steel reinforcements in soil samples with controlled content of Simulated Soil Organic Matter.

Bibliography

AASHTO (Ed.). (2002). *Standard specifications for highway bridges* (17th ed.). Washington, DC: American Association of State Highway and Transportation Officials.

AASHTO (Ed.). (2010). *LRFD bridge design specifications* (5th ed.). Washington, DC: American Association of State Highway and Transportation Officials.

Abdel Rehim, S. S., Sayyah, S. M. & El Deeb, M. M. (2003). Corrosion of tin in citric acid solution and the effect of some inorganic anions. *Materials Chemistry and Physics, 80*(3), 696-703. doi:10.1016/S0254-0584(03)00128-7

Anderson, P. L., Gladstone, R. A., & Sankey, J. E. (2012). State of the practice of MSE wall design for highway structures. *Geotechnical Engineering State of the Art and Practice: Keynote Lectures from GeoCongress 2012,* 443-463.

Anderson, P. L., & Brabant, K. (2010). Increased use of MSE abutments. Retrieved September, 2012, from http://www.amsewalls.org/wp-content/uploads/2013/06/Increased_Use_of_MSE_Abutments.pdf

Andrade, C., Alonso, C. & Sarra, J. (2002). Corrosion rate evolution in concrete structures exposed to the atmosphere. *Cement and Concrete Composites, 24*(1), 55-64. doi:10.1016/S0958-9465(01)00026-9

Asgari, H., Toroghinejad, M. R. & Golozar, M. A. (2009). Effect of coating thickness on modifying the texture and corrosion performance of hot-dip galvanized coatings. *Current Applied Physics, 9*(1), 59-66. doi:10.1016/j.cap.2007.10.090

Baah, C. A. & Baah, J. I. (2000). Inhibition effect of oxalic acid on copper corrosion. *Anti-Corrosion Methods and Materials, 47*(2), 105-108. doi:10.1108/00035590010317790

Baker, H. & Khalili, F. (2005). A study of complexation thermodynamic of humic acid with cadmium (II) and zinc (II) by schubert's ion-exchange method. *Analytica Chimica Acta, 542*(2), 240-248. doi:10.1016/j.aca.2005.04.008

Bohn, H. L., McNeal, B. L. & O'Connor, G. A. (2001). *Soil chemistry*. New York: Wiley.

Borghi, E. B., Ali, S. P., Morando, P. J. & Blesa, M. A. (1996). Cleaning of stainless steel surfaces and oxide dissolution by malonic and oxalic acids. *Journal of Nuclear Materials, 229*(1), 115-123. doi:10.1016/0022-3115(95)00201-4

Brigante, M., Zanini, G. & Avena, M. (2008). On the dissolution kinetics of humic acid particles. effect of monocarboxylic acids. *Chemosphere, 71*(11), 2076-2081. doi:10.1016/j.chemosphere.2008.01.038

Campbell, R. B., Bower, C. A. & Richards, L. A. (1948). Change of electrical conductivity with temperature and the relation of osmotic pressure to electrical conductivity and ion concentration for soil extracts. *Soil Sci. Soc. Am. Proc. 13,* 66-69.

Chen, Y. (2000). Practical analysis and design of mechanically-stabilized earth walls - I. design philosophies and procedures. *Engineering Structures, 22*(7), 793-808. doi:10.1016/S0141-0296(99)00021-8

CSA. (2006). *CAN/CSA-S6-06, Canadian highway bridge design code* (10th ed.). Mississauga, ON.: CSA.

Darbin, M., Jailloux, J. M. & Montuelle, J. (1986). Durability of reinforced earth structures: Results of experiments of long duration on galvanized steel. *Bulletin De Liaison Des Laboratoires Des Ponts Et Chaussees,* (141), 21-35.

Dick, L. F. P. & Rodrigues, L. M. (2006). Influence of humic substances on the corrosion of the API 5LX65 steel. *Corrosion, 62*(1), 35-43.

ECS. (2008). In Orazem M. E., Tribollet B. (Eds.), *Electrochemical impedance spectroscopy* John Wiley & Sons, Inc.

Elias, V., Fishman, K. L., Christopher, B. R. & Berg, R. R. (1990). Corrosion/Degradation of soil reinforcements for mechanically stabilized earth walls and reinforced soil slopes.(FHWA-NHI-09-087)

El-Mahdy, G. A., Nishikata, A. & Tsuru, T. (2000). Electrochemical corrosion monitoring of galvanized steel under cyclic wet-dry conditions. *Corrosion Science, 42*(1), 183-194. doi:10.1016/S0010-938X(99)00057-8

El-Maksoud, S. A. A. (2008). The effect of organic compounds on the electrochemical behaviour of steel in acidic media. A review. *International Journal of Electrochemical Science, 3*(5), 528-555.

El-Sherbini, E., Wahaab, S. M. A. & Deyab, M. (2005). Ethoxylated fatty acids as inhibitors for the corrosion of zinc in acid media. *Materials Chemistry and Physics, 89*(2-3), 183-191. doi:10.1016/j.matchemphys.2003.09.055

Gerber, T. M. (2012). *NCHRP synthesis 437 - assessing the long-term performance of mechanically stabilized earth walls*. Washington, D.C.: TRB.

Gerber, T. M. & Billings, D. A. (2010). *Assessing corrosion of MSE wall reinforcement.* (No. UT-10.20).Utah Department of Transportation.

Giacomelli, C., Giacomelli, F. C., Baptista, J. A. A. & Spinelli, A. (2004). The effect of oxalic acid on the corrosion of carbon steel. *Anti-Corrosion Methods and Materials, 51*(2), 105-111. doi:10.1108/00035590410523193

Gladstone, R. A., Anderson, P. L., Fishman, K. L. & Withiam, J. L. (2006). Durability of galvanized soil reinforcement: More than 30 years of experience with mechanically stabilized earth. *Transportation Research Record: Journal of the Transportation Research Board, 1975*(-1), 49-59.

Gladstone, R. A., Fishman, K. L. & Langill, T. J. (2008). Sustainable design concepts and galvanized MSE reinforcements. *GeoCongress 2008: Geosustainability and Geohazard Mitigation, March 9, 2008 - March 12,* (178) 968-975. doi:10.1061/40971(310)121

Gouda, V. K., Abd El Wahaab, S. M. & Ibrahim, E. M. (1980). The corrosion behaviour in organic acid solutions—II. A steel electrode. *Corrosion Science, 20*(10), 1091-1099. doi: http://dx.doi.org/10.1016/0010-938X(80)90139-0

Gouda, V. K., Rizkalla, E. N., Abd-El-Wahab, S. & Ibrahim, E. M. (1981). Corrosion behaviour in organic acid solutions—I. tin electrode. *Corrosion Science, 21*(1), 1-15. doi:http://dx.doi.org/10.1016/0010-938X(81)90058-5

Graedel, T. E., McCrory-Joy, C. & Franey, J. P. (1986). POTENTIAL CORROSION OF METALS BY ATMOSPHERIC ORGANIC ACIDS. *Journal of the Electrochemical Society, 133*(2), 452-453.

Gungor, E. B. & Let, M. (2010). Zinc release by humic and fulvic acid as influenced by pH, complexation and DOC sorption. *Geoderma, 159*(1-2), 131-138. doi:10.1016/j.geoderma.2010.07.004

Heitz, E. (1974). Corrosion of metals in organic solvents. *Advances in corrosion science and technology* (pp. 149-243) Springer.

Holtz, R. D., Christopher, B. R. & Berg, R. R. (1995). *Geosynthetic design and construction guidelines - participants notebook* (revised April 1998 ed.) Publication No. FHWA-AS-96-071.

Huang, P. T., Patel, M., Santagata, M. C. & Bobet, A. (2009). *Classification of organic soils. Publication FHWA/IN/JTRP-2008/02.* Indiana: Joint Transportation Research

Program, Indiana Department of Transportation and Purdue University. doi:10.5703/1288284314328

Jafarian, M., Gobal, F., Danaee, I., Biabani, R. & Mahjani, M. G. (2008). Electrochemical studies of the pitting corrosion of tin in citric acid solution containing cl-. *Electrochimica Acta, 53*(13), 4528-4536. doi:10.1016/j.electacta.2008.01.051

Jiang, L., Mao, X., Yu, J. & Gan, F. (2008). Effect of humic acid on the corrosion behavior of carbon steel in natural freshwaters. *Anti-Corrosion Methods and Materials, 55*(4), 204-207. doi:10.1108/00035590810887709

Kim, J. O., Lee, Y. W. & Chung, J. (2013). The role of organic acids in the mobilization of heavy metals from soil. *KSCE Journal of Civil Engineering, 17*(7), 1596-1602. doi:10.1007/s12205-013-0323-z

Korshin, G. V., Benjamin, M. M. & Sletten, R. S. (1997). Adsorption of natural organic matter (NOM) on iron oxide: Effects on NOM composition and formation of organo-halide compounds during chlorination. *Water Research, 31*(7), 1643-1650. doi:http://dx.doi.org/10.1016/S0043-1354(97)00007-9

LCPC -SETRA. (1979). *Les ouvrages en terre armée, recommendations et règles de l'art* Bulletin des Laboratoires des Ponts et Chausses.

Li, X., Deng, S., Xie, X. & Fu, H. (2014). Inhibition effect of bamboo leaves' extract on steel and zinc in citric acid solution. *Corrosion Science, 87*, 15. doi:10.1016/j.corsci.2014.05.013

Li, Y., Yue, Q. & Gao, B. (2010). Adsorption kinetics and desorption of cu(II) and zn(II) from aqueous solution onto humic acid. *Journal of Hazardous Materials, 178*(1-3), 455-461. doi:10.1016/j.jhazmat.2010.01.103

Livens, F. R. (1991). Chemical reactions of metals with humic material. *Environmental Pollution, 70*(3), 183-208. doi:http://dx.doi.org/10.1016/0269-7491(91)90009-L

Marder, A. R. (2000). Metallurgy of zinc-coated steel. *Progress in Materials Science, 45*(3), 191-271. doi:10.1016/S0079-6425(98)00006-1

Markham, E. R. (1913). *Steel: Its selection, annealing, hardening and tempering*. New York: Henley.

McLaren, A. D. & Peterson, G. H. (1967). *Soil biochemistry*. New York: M. Dekker.

Padilla, V. (2013). *Soil corrosion behavior of hot-dipped galvanized steel in infrastructure applications.* (Unpublished PhD). University of British Columbia,

Padilla, V. & Alfantazi, A. (2013). Corrosion performance of galvanized steel in Na2SO4 and NaCl solutions at subfreezing temperatures. *Corrosion, 69*(2), 174-185. doi:10.5006/0645

Padilla, V., Ghods, P. & Alfantazi, A. (2013a). Effect of de-icing salts on the corrosion performance of galvanized steel in sulphate contaminated soil. *Construction and Building Materials, 40*, 908-918. doi:10.1016/j.conbuildmat.2012.09.077

Padilla, V., Ghods, P. & Alfantazi, A. (2013b). Practical model for three-stage corrosion behavior of galvanized steel reinforcement in soil. *Corrosion, 69*(5), 509-521. doi:10.5006/0622E

Pantazopoulou, S. & Papoulia, K. (2001). Modeling cover-cracking due to reinforcement corrosion in RC structures. *Journal of Engineering Mechanics, 127*(4), 342-351.

Pertusatti, J. & Prado, A. G. S. (2007). Buffer capacity of humic acid: Thermodynamic approach. *Journal of Colloid and Interface Science, 314*(2), 484-489. doi:10.1016/j.jcis.2007.06.006

Prado, A. G. S. Torres, J. D., Martins, P. C., Pertusatti, J., Bolzon, L. B., & Faria, E. A. (2006). Studies on copper(II)- and zinc(II)-mixed ligand complexes of humic acid. *Journal of Hazardous Materials, 136*(3), 585-588. doi:10.1016/j.jhazmat.2005.12.035

RECo. (2011). Reinforced earth 40th anniversary brochure. Retrieved September, 2012, from http://www.reinforcedearth.com/sites/default/files/40th_anniversary_brochure_0.pdf

Renella, G., Landi, L. & Nannipieri, P. (2004). Degradation of low molecular weight organic acids complexed with heavy metals in soil. , *122*(2-4) 311-315. doi:10.1016/j.geoderma.2004.01.018

Romanoff, M. (1957). *Underground corrosion*. Washington, DC: National Bureau of Standards.

Samouelian, A., Cousin, I., Tabbagh, A., Bruand, A. & Richard, G. (2005). Electrical resistivity survey in soil science: A review. *Soil and Tillage Research, 83*(2), 173-193. doi:10.1016/j.still.2004.10.004

Schnitzer, M. & Khan, S. U. (1978). *Soil organic matter*. Amsterdam; New York: Elsevier Scientific Pub. Co.

Schulten, H. R. & Schnitzer, M. (1993). A state-of-the-art structural concept for humic substances. *Naturwissenschaften, 80*(1), 29-30. doi:10.1007/BF01139754

Schwab, A. P. Zhu, D. S., & Banks, M. K. (2008). Influence of organic acids on the transport of heavy metals in soil. *Chemosphere, 72*(6), 986-994. doi:10.1016/j.chemosphere.2008.02.047

Sekine, I., Okano, C. & Yuasa, M. (1990). Corrosion behaviour of ferritic stainless steel in oxalic acid solutions. *Corrosion Science, 30*(4-5), 351-366.

Sekine, I. & Senoo, K. (1984). Corrosion behavior of SS 41 steel in formic and acetic acids. *Corrosion Science, 24*(5), 439-448. doi:10.1016/0010-938X(84)90069-6

Sekine, I. Okano, C. & Yuasa, M. (1990). The corrosion behavior of ferritic stainless steel in oxalic acid solutions. *Corrosion science, 30*(4/5), 351-366.

Sekine, I. & Okano, C. (1989). Corrosion behavior of mild steel and ferritic stainless steels in oxalic acid solution. *Corrosion, 45*(11), 924-932.

Soil Classification Working Group. (1998). *The canadian system of soil classification* (3rd ed.). Ottawa, ON: Agriculture and Agri-Food Canada Publication.

Soil Survey Division Staff. (1993). In Soil Conservation Service. U.S. (Ed.), *Soil survey manual.* U.S. Department of Agriculture Handbook 18.

Stevenson, F. J. (1994). *Humus chemistry: Genesis, composition, reactions*. New York: Wiley.

Struyk, Z. & Sposito, G. (2001). Redox properties of standard humic acids. *Geoderma, 102*(3–4), 329-346. doi:http://dx.doi.org/10.1016/S0016-7061(01)00040-4

Szilagyi, M. (1971). Reduction of Fe3+ ion by humic acid preparations. *Soil Science, 111*(4), 233-235.

Sziraki, L., Szocs, E., Pilbath, Z., Papp, K. & Kalman, E. (2001). Study of the initial stage of white rust formation on zinc single crystal by EIS, STM/AFM and SEM/EDS techniques. *Electrochimica Acta, 46*(24-25), 3743-3754. doi:10.1016/S0013-4686(01)00656-9

Thebault, F., Vuillemin, B., Oltra, R., Allely, C. & Ogle, K. (2011). Protective mechanisms occurring on zinc coated steel cut-edges in immersion conditions. *Electrochimica Acta, 56*(24), 8347-8357. doi:10.1016/j.electacta.2011.07.016

Thebault, F., Vuillemin, B., Oltra, R., Allely, C., Ogle, K. & Tada, E. (2008). Investigations of cut-edge corrosion of galvanized steels by coupling local electrochemical methods and computational modeling. *High Resolution Characterization of Corrosion Processes - 212th ECS Meeting, October 7, 2007 - October 12, , 11*(22) 91-105. doi:10.1149/1.2925266

Thebault, F., Vuillemin, B., Oltra, R., Ogle, K. & Allely, C. (2008). Investigation of self-healing mechanism on galvanized steels cut edges by coupling SVET and numerical modeling. *Electrochimica Acta, 53*(16), 5226-5234. doi:10.1016/j.electacta.2008.02.066

Thornley, J. D. & Siddharthan, R. V. (2010). Effects of corrosion aggressiveness on MSE wall stability in Nevada. *2010 Earth Retention Conference - Earth Retention Conference 3, August 1, 2010 - August 4, , 384*(208) 539-547. doi:10.1061/41128(384)54

Thornley, J. D., Siddharthan, R. V., Luke, B. & Salazar, J. M. (2010). Investigation and implications of mechanically stabilized earth wall corrosion in Nevada. *Transportation Research Record,* (2186), 154-160. doi:10.3141/2186-17

Uhlig, H. H. & Revie, R. W. (2000). *Uhlig's corrosion handbook* (2nd ed.). New York: Wiley.

Weissenrieder, J., Kleber, C., Schreiner, M. & Leygraf, C. (2004). In situ studies of sulfate nest formation on iron. *Journal of the Electrochemical Society*, *151*(9), B497-B504.

Yadav, A. P., Nishikata, A. & Tsuru, T. (2004a). Degradation mechanism of galvanized steel in wet-dry cyclic environment containing chloride ions. *Corrosion Science, 46*(2), 361-376. doi:10.1016/S0010-938X(03)00153-7

Yadav, A. P., Nishikata, A. & Tsuru, T. (2004b). Electrochemical impedance study on galvanized steel corrosion under cyclic wet–dry conditions—influence of time of wetness. *Corrosion Science*, *46*(1), 169-181. doi:10.1016/S0010-938X(03)00130-6

Yang, R. & Van, D. B. (2009). Metal complexation by humic substances in seawater. *Environmental Science and Technology, 43*(19), 7192-7197. doi:10.1021/es900173w

Yasakau, K. A., Weber, C. R., Rodrigues, L. M., Zheludkevich, M., Ferreira, M. G. S. & Dick, L. F. P. (2008). AFM study of the corrosion of pipeline steel in organic compounds

extracted from soil. *High Resolution Characterization of Corrosion Processes - 212th ECS Meeting, October 7, 2007 - October 12, , 11*(22) 107-119. doi:10.1149/1.2925267

Ying, L., Haitao, F., Yifan, Z. & Wuji, W. (2003). Study on the inhibiting behavior of AMT on bronze in 5% citric acid solution. *Journal of Materials Science, 38*(3), 407-411. doi:10.1023/A:1021803211415

Yip, T. C. M., Yan, D. Y. S., Yui, M. M. T., Tsang, D. C. W. & Lo, I. M. C. (2010). Heavy metal extraction from an artificially contaminated sandy soil under EDDS deficiency: Significance of humic acid and chelant mixture. *Chemosphere, 80,* 416. doi:10.1016/j.chemosphere.2010.03.033

Zaleckas, E., Paulauskas, V. & Sendzikiene, E. (2013). Fractionation of heavy metals in sewage sludge and their removal using low-molecular-weight organic acids. *Journal of Environmental Engineering and Landscape Management, 21*(3), 189-198. doi:10.3846/16486897.2012.695734

Zerfaoui, M., Oudda, H., Hammouti, B., Kertit, S. & Benkaddour, M. (2004). Inhibition of corrosion of iron in citric acid media by aminoacids. *Progress in Organic Coatings, 51*(2), 134-138. doi:10.1016/j.porgcoat.2004.05.005

Zhang, X. G. (1996). *Corrosion and electrochemistry of zinc*. New York, U.S.: Plenum Press. doi:10.1007/978-1-4757-9877-7